



Figure 43 110 kV 4 circuits line

At the transmission site, the digital-to-analog converted signal is immediately feeded into a Dimat ad-hoc built amplifier. From 50 kHz to 1.4 MHz, this 37.5 dB gain amplifier can deliver up to 160 W of PEP. When amplified, the signal gets the coupling device that, taking into account the coupler capacitance, matches the 75 Ω amplifier output impedance with the line access impedance. Once the signal is in the power line, the line trap prevents it from entering the substation premises and it propagates toward the receiver site. When decoupled and before the acquisition, the signal is amplitude limited and noise and antialias low pass filtered at 6 MHz. In the sequel, the channel is considered to be between the amplifier output and the transient limiter input, other devices will be properly compensated.

A deepest explanation of the measurement set-up, as well as the measurements, symbol design and results can be found in Appendix A.4 and in Appendix A.6.

In the next Sections, the channel measurements as well as the symbol design and test concerning the short link will be given. Since the same procedure has been followed for the long link study, the most important details concerning that link can be seen in Appendix A.4 and in Appendix A.6.

5.4. MEASUREMENTS AND RESULTS

In this section, the measurement procedures as well as their outcomes will be shown. First, the attenuation characteristic will show the power line transmission capabilities and its long term variations. Then, in order to get knowledge of the short term variations and the channel delay and Doppler spread, a Pseudo-Noise (PN) sequence based sounding will be carried out. From these measurements, the channel coherence time and coherence bandwidth will be deduced in order to properly design the MC symbol.

5.4.1. ATTENUATION CHARACTERISTICS

The attenuation characteristic of the link under study has been taken by means of a five days measurement: one tone sweep every 20 minutes from 10 kHz to 2 MHz in 10 kHz steps. Each step consists of 10 averaged acquisitions in a 2 seconds window. In Figure 44 all the 360 sweeps can be seen overimposed.

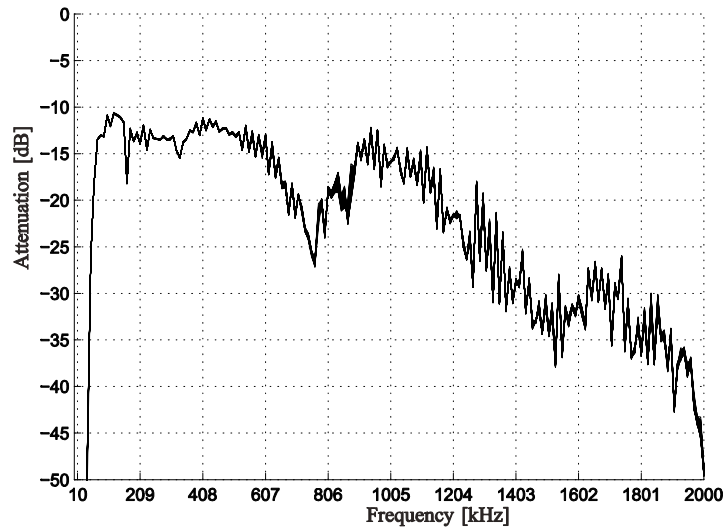


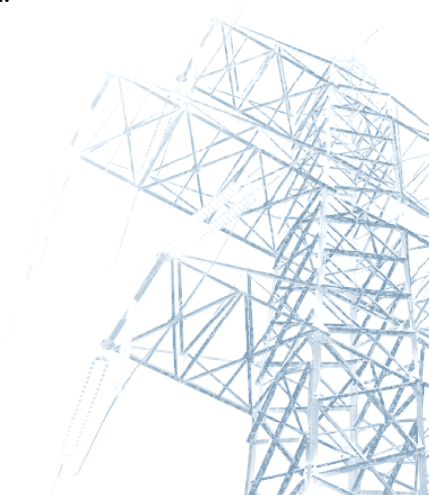
Figure 44 Link attenuation

The channel attenuation characteristic shows a pass band behavior. The low cut-off frequency (40 kHz) is due to the coupling capacitor and coupling device combined frequency response, and the high one is due to the same devices plus the line attenuation. The ripple at the pass band is due to the multipath effect, as it will be shown later, while the fading from 610 kHz to 880 kHz is due to the coupling devices impedance mismatching. The perfect match among the 360 sweeps means that both propagation and coupling performances remained constant for one week.

5.4.2. BACKGROUND NOISE

In this Section, a closer look will be given to the noise scenario, specifically, to background noise. This type of noise is a broadband permanent interference with relatively high level and mainly caused by corona effect and other leakage or discharge events. Background noise PSD is time and frequency variant (colored noise). Due to climatic dependences, corona noise power fluctuations up to tens of dB may be expected. Moreover, stationary, low-power periodical and synchronous with the mains power frequency impulse events can also be considered background noise. These kinds of impulses are caused by discharges on insulators and other electrical substation devices. Narrowband interferences such as coupled broadcast emissions or other communications equipment, due to its slow variability, can be considered background noise too [4].

Figure 45 shows the background noise and the received OFDM overimposed PSDs at the receiver site. Two noise regions can be clearly identified, i.e., from the lower frequencies up to 500 kHz and from 500 kHz on. The former band is colored noise limited, while the latter is narrowband interference limited.



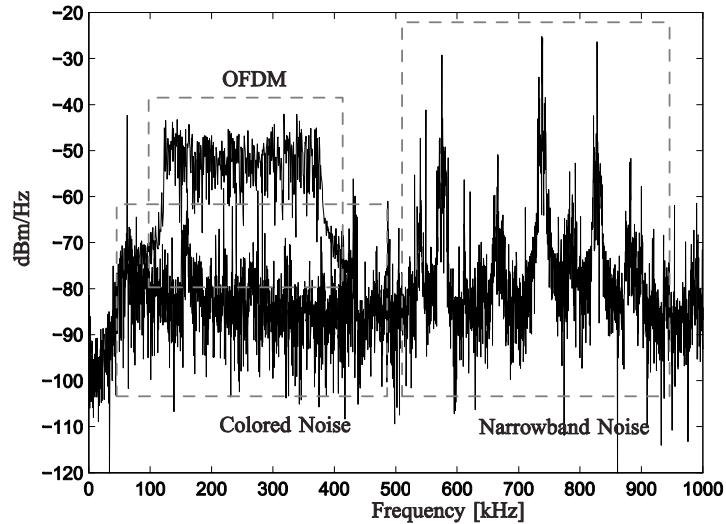


Figure 45 Background noise

Figure 46 depicts the maximum, the minimum and the mean PSD values (three upper black lines) from 40 kHz to 1 MHz, during a 4 days observation period. Although this behavior can be considered slow variant, large differences in time show up. This scenario shows a highly dynamic background noise in frequency domain, since maximum variations up to 40 dB have been measured, with standard deviations (STD) around 10 dBm/Hz, in the whole frequency range. Larger differences between maximum and minimum, as well as larger STD values, can be found in the frequencies where coupled signals from other equipment are located, e.g., around 160 kHz and 320 kHz. Since no adaptive scheme will be used, this background noise study will not directly affect the MCM symbol design, but the obtained results claim again for a power and bit-loading adaptive MCM physical layer [16].

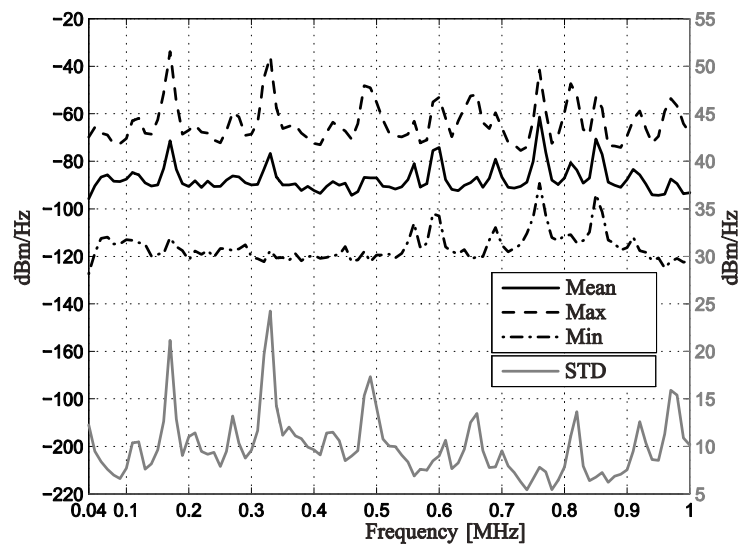


Figure 46 Background noise statistics

5.4.3. TIME SPREAD AND FREQUENCY SPREAD

From the measurements of previous section, it has been shown that there is not long term variation in the link transfer function. In this section, by means of PN sequences, short term channel variation as well as time spreading will be studied.

The delay and frequency spread has been measured by means of correlating a local pattern and through-channel received PN sequences. 2047 chips PN sequences have been transmitted at 600 kcps, centered at 600 kHz with 0.99 MHz bandwidth (symbol filter roll off factor of 0.65).

The received delay profile, $h(\tau)$, (Figure 47) shows the first and most powerful path, which is the direct one, followed by a negative exponential spreading of 20 μs . This decreasing spreading may be caused by network elements non idealities. That first path is followed by a second one, 47 μs after. This second path is due to the reflection of the first incoming signal at the receiving substation, its propagation back again to the transmitter site and its second reflection to the original destination. The same can be told about the third path [72][73].

Since no short term variations can be seen in the overimposed channel impulse responses, a frequency or Doppler spread tending to 0 Hz is also shown, i.e., a coherence time (Δt_0) tending to infinity. This means that no restrictions have to be fulfilled regarding pilot separation in time domain (N_t).

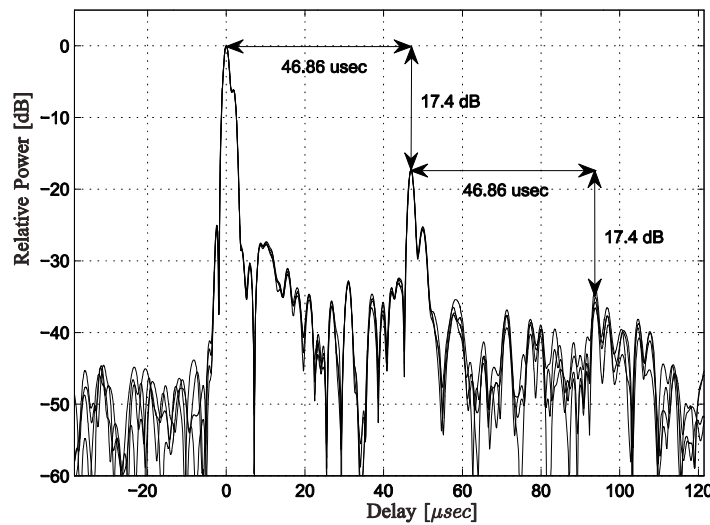


Figure 47 Channel delay profile

From $h(\tau)$, the transfer function $H(f)$ can be obtained by means of the Fourier Transform. Let's examine the frequency autocorrelation function in order to get the coherence bandwidth (Δf_0) of the channel under study. Since we can suppose a Wide Sense Stationary Uncorrelated Scattering (WSSUS) channel, the frequency autocorrelation function is defined as (5.1).

$$R(\Delta f) = \frac{E\{H(f) \cdot H^*(f + \Delta f)\}}{E\{H(f)\}} \quad (5.1)$$

In this work, the Δf_0 is calculated for a 0.9 correlation. The Figure 48 shows that the Δf_0 is 70 kHz. Taking this frequency correlation measure into account, the channel sampling theorem has to be fulfilled in the frequency domain [77][78]. This means that the frequency pilot separation (N_f) has to follow, according to the subcarrier bandwidth (Δf), the channel variations in frequency domain [16].

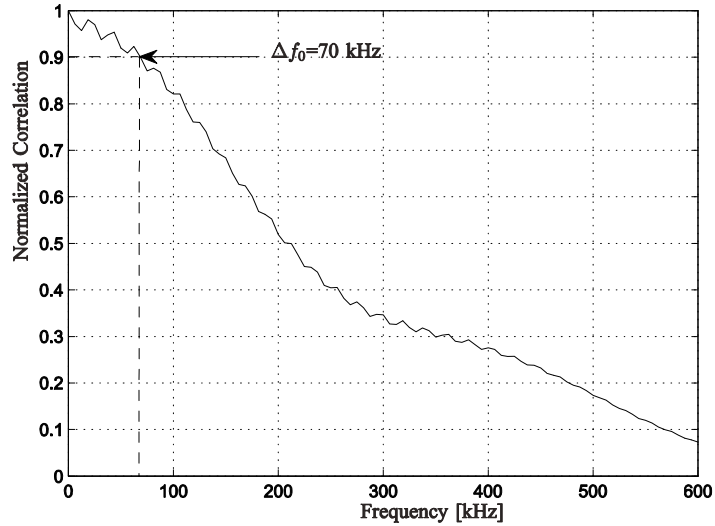


Figure 48 Frequency autocorrelation function

5.4.4. MCM DESIGN AND TEST: SHORT LINK

SYMBOL DESIGN

In this section, based on the measurements previously presented, the MCM symbol design will be presented, as well as the delivered performance for the three tested physical layer schemes: OFDM and two combinations of OFDM and code division multiple access (CDMA), generally known as MC-SS techniques. According how different streams share the spectrum, two typical schemes arise under the concept of MC-SS: multicarrier- code division multiple access (MC-CDMA) and multicarrier - direct sequence - code division multiple access (MC-DS-CDMA) [82][83].

Before designing the frame format, the determination of the OFDM symbol has to be done. The guard interval duration (T_g) is in charge of avoiding ISI (and consequently, ICI). This guard interval has to be greater than the maximum delay spread (T_{max}) [16].

Transmitted power will be chosen in order to get a BER of approximately 10^{-2} before decoding. If using 16-QAM as a mapping scheme, 256 kHz of occupied bandwidth and 9 dBm of transmitted mean power, about 20 dB of SNR is expected at the receiver site. Taking into account this ratio and the impulse response in Figure 47, the second path (at 46.86 μ s) and a security margin, yielding to a $T_g = 80 \mu$ s.

Once fixed the guard interval length, the symbol length will be chosen while trying to maximize the cyclic prefix efficiency (5.2), that is, the ratio between the useful symbol time (T_u) and the symbol time (T_s), where $T_s = T_u + T_g$.

$$\rho_{CP} = \frac{T_u}{T_u + T_g} \quad (5.2)$$

If a minimum efficiency of 0.9 is desired as a lower bound, a useful symbol time of 1 msec will fulfill this constraint ($\rho_{CP} = 0.926$). The maximum symbol time is restricted by the Δf_0 and practical issues as the Δf (5.3), since a minimum Δf is needed in order to avoid the effect of ICI for a given frequency offset.

$$\Delta f = \frac{1}{T_u} \quad (5.3)$$

Finally, a 1080 μ s MC symbol of $N_{SC} = 256$ subcarriers will be used. With $\Delta f = 1$ kHz per subcarrier, an overall symbol bandwidth of 256 kHz is achieved.

Once Δf has been determined, the pilot distance in time domain, N_f , can be found by satisfying the Nyquist sampling theorem in the frequency domain. There are some rule of thumbs that states that a channel oversampling of 2x is recommended [74][75][76], so following (5.4) and (5.5), where Δf_{N_f} and $\lceil \cdot \rceil$ are the frequency separation between pilot subcarriers and the next integer respectively, N_f can be found.

$$\Delta f_{N_f} = \frac{1}{2} \frac{\Delta f_0}{2} = \frac{1}{2} \frac{70\text{kHz}}{2} = 17.5\text{kHz} \quad (5.4)$$

$$N_f = \left\lceil \frac{\Delta f_{N_f}}{\Delta f} \right\rceil = 18 \quad (5.5)$$

In order to avoid the channel estimation having to perform channel prediction at the first and the last subcarrier, which is more unreliable than interpolation, instead of using a N_f of 18 subcarriers, a separation of 16 subcarriers will be used.

The number of MC symbols in one frame is upper limited by the receiving equipment digitizer memory, so a limitation of 16 (+1 pilot symbol) symbols has to be respected.

There is no restriction regarding the pilot separation in time domain but the same issue regarding avoiding channel prediction has to be taken into account in time domain. Equation (5.6) shows the pilot density related efficiency.

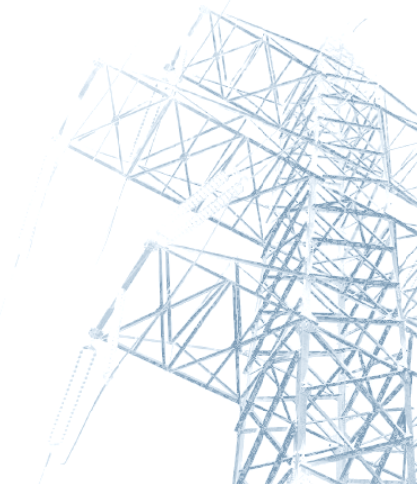
$$\rho_{PD} = \frac{N_f \cdot N_t - 1}{N_f \cdot N_t} \quad (5.6)$$

If a $N_f = 16$ is chosen, the efficiency is 0.996. On the other hand, if we reduce the pilot distance down to $N_f = 4$, the efficiency is reduced only by a 1.2 %, yielding to the overall system performance shown in Equation (5.7).

$$\rho_{CP} \cdot \rho_{PD} = 0.911 \quad (5.7)$$

Finally, the OFDM frame and its parameters can be seen in Figure 49. While trying to simplify the receiver complexity, least squares channel estimation and 1D+1D lineal channel interpolation have been carried out before equalization, moreover, a PN based pilot symbol for FFT windowing has also been used [16].

In order to have a fair comparison between the OFDM and the MC-SS schemes, a Walsh-Hadamard fully loaded MC-CDMA and MC-DS-CDMA will be considered (Figure 49, Table 8 and Table 9). The interleaving carried out in OFDM yields to an increase of both frequency and time diversity at symbol level. In the MC-SS modulations, a chip level interleaving in frequency and time will be carried out in MC-CDMA and MC-DS-CDMA, respectively. A single user detection scheme will be used for despreading [16].



| Parameter | Value |
|---|--|
| Bandwidth | $BW = 256$ kHz |
| Carrier frequency | $f_c = 250$ kHz |
| OFDM frame duration | $T_f = 17.28$ msec |
| OFDM symbols per OFDM frame | $N_s = 16$ |
| OFDM symbol duration | $T_s = 1.08$ msec |
| Cyclic prefix duration | $T_g = 0.08$ msec |
| Subcarrier spacing | $\Delta f = 1$ kHz |
| Number of subcarriers | $N_{sc} = 256$ |
| Pilot distance in frequency domain | $N_f = 16$ |
| Pilot distance in time domain | $N_t = 4$ |
| Mapping | 16-QAM |
| Coding | $1/2$ convolutional code, constraint length 7 and trace-back length 35 with 120 depth interleaving |
| Channel estimation method | Least squares |
| Interpolation method | 1-D + 1-D |
| Gross bitrate | $R_{bg} = 930$ kbps |
| User bitrate | $R_{bu} = 465$ kbps |
| Mean transmission power | $P_{tx} = 8.9$ dBm |
| Peak transmission power | $P'_{tx} = 21.7$ dBm |

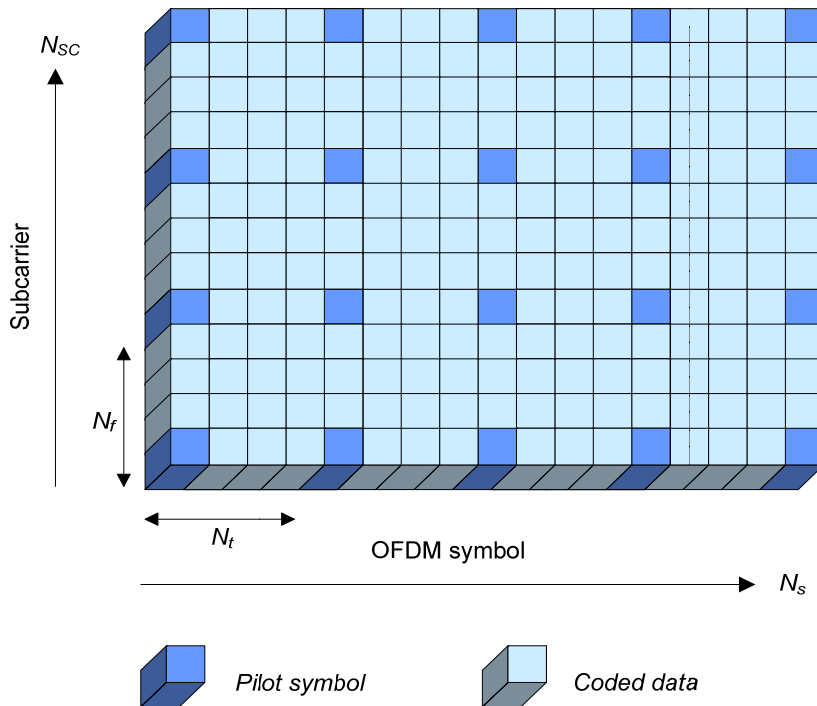


Figure 49 OFDM frame and symbol parameters

| Parameter | Value |
|---------------------------|--------------------------------------|
| Spreading sequence | Walsh-Hadamard |
| Spreading factor | 8, with chip interleaving depth of 8 |
| Multuser detection | Single user |
| Number of streams | 8, fully loaded |

Table 8 MC-CDMA parameters

| Parameter | Value |
|--------------------|--------------------------------------|
| Spreading sequence | Walsh-Hadamard |
| Spreading factor | 8, with chip interleaving depth of 8 |
| Multuser detection | Single user |
| Number of streams | 8, fully loaded |

Table 9 MC-DS-CDMA parameters

SYSTEM PERFORMANCE

The BER performance of the pure OFDM scheme is depicted in Figure 50. The continuous line represents the modulation BER, i.e., without decoding, and the dashed line represents the BER after decoding, for a user bit rate of 465 kbps. Those lines show the day-by-day averaged performance.

The modulation BER showed a constant behavior, around $2 \cdot 10^{-2}$, while the performance after decoding yielded to a BER of $4.4 \cdot 10^{-6}$. The fifth day shows no line for the BER after decoding. During this interval, all the modulation errors were successfully corrected by the code, so a BER better than 10^{-7} was observed.

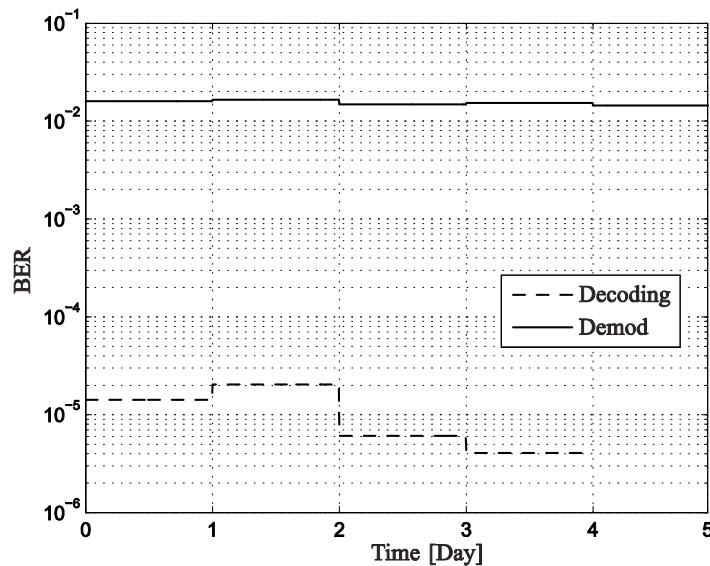
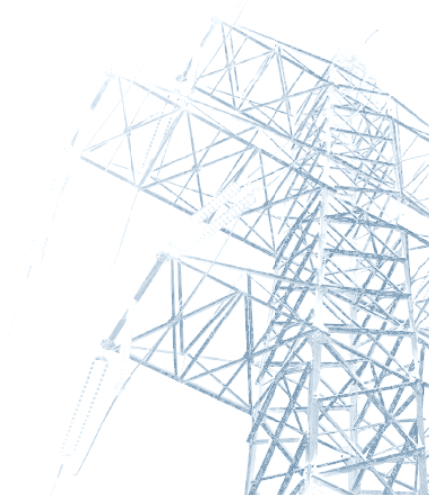


Figure 50 OFDM performance

The MC-SS scheme performance is depicted in Figure 51. Again, the continuous lines represent the modulation BER and the dashed lines represent the BER after decoding, for a user bit rate of 465 kbps. Since a higher level of channel diversity is obtained with spreading, both MC-SS schemes outperform the pure OFDM approach. Specifically, the MC-CDMA scheme delivers the best performance, i.e., $3.1 \cdot 10^{-7}$ of decoded BER (again, no errors during the fifth day). This is due to the fact that the channel we are dealing with presents a higher level of frequency selectivity rather than time selectivity. This selective behavior is most probably due to the noise scenario (colored spectrum in frequency domain and asynchronous impulses in time domain) rather than to the multipath effect.



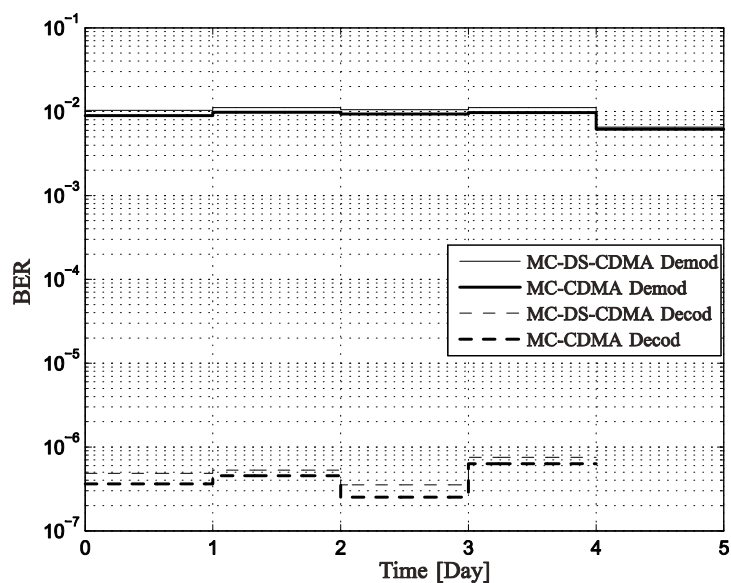


Figure 51 MC-SS performance

Table 10 summarizes the performance of the three tested schemes.

| Gross bitrate = 930 kbps | |
|--------------------------|---------------------|
| Scheme | Gross BER |
| OFDM | $2 \cdot 10^{-2}$ |
| MC-DS-CDMA | $9.9 \cdot 10^{-3}$ |
| MC-CDMA | $8.7 \cdot 10^{-3}$ |
| User bitrate = 465 kbps | |
| Scheme | Gross BER |
| OFDM | $4.4 \cdot 10^{-6}$ |
| MC-DS-CDMA | $4.2 \cdot 10^{-7}$ |
| MC-CDMA | $3.1 \cdot 10^{-7}$ |

Table 10 Short link system performance

5.4.5. MCM DESIGN AND TEST: LONG LINK

Previous sections have been focused on the channel study and symbol design for a low power MCM symbol. Only 7.7 mW of average power have been used in order to deliver the system performance shown in Table 11.

Now, by means of the same channel study and symbol design methodologies, both MC-CDMA and MC-DS-CDMA schemes have been tested. In this scenario, the system performance has been measured by using a similar peak envelope power (PEP) that other commercial systems use: 40 W, in a 27 km link.

With illustrative purposes only, Figure 52 and Figure 53 show the link attenuation and the delay spread, respectively. In the former, the lowest cut-off frequency is again caused by the coupling devices and the ripple in the pass band region by the multipath shown in the latter.

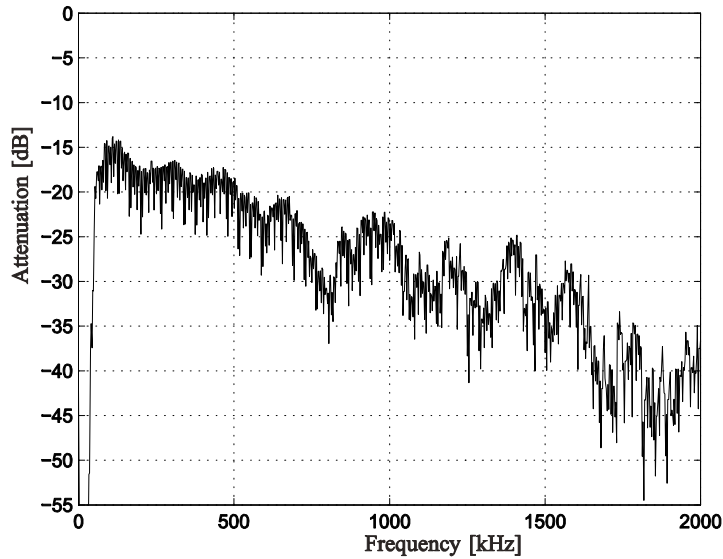


Figure 52 Long link attenuation characteristic

As expected, the attenuation characteristic is more severe and the channel delay is longer than the ones found in the 6.85 km link, Figure 53 shows the first path followed by two reflected paths 19.8 dB below and 188 μs after their predecessor. As the link length increases, the time distance between reflections increases, as well as their relative power. In order to be efficient in terms of cyclic prefix duration, an adaptive guard interval length is also welcomed in this channel invariant scenario.

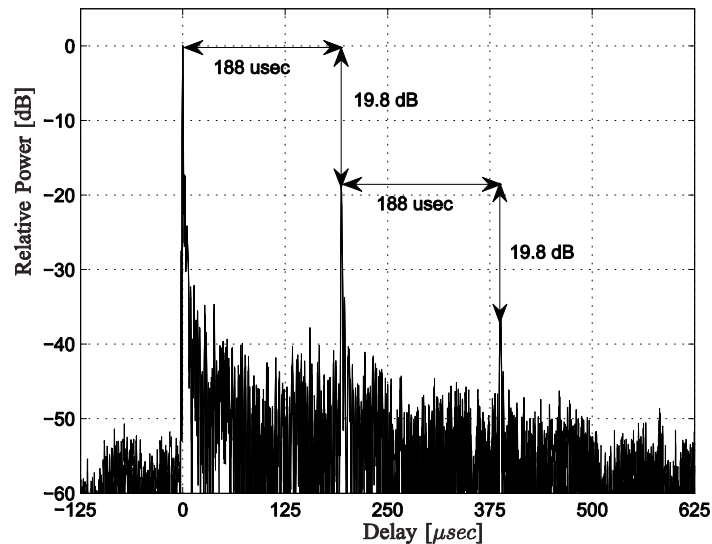


Figure 53 Long link delay spread

From the obtained results in the short link, only the MC-SS schemes, not the pure OFDM, have been tested. In this scenario, taking into account a PEP of 40 W and 12 dB of peak to average power ratio (PAPR), since no PAPR reduction technique has been implemented, an average power of 2.5 W will be injected into the channel. The test results are shown in Table 11. Again, taking profit of the noise scenario frequency selectivity, the spreading in frequency outperforms the spreading in time. In some situations, by means of power and bit-loading techniques, the achieved performance (465 kbps with $8 \cdot 10^{-8}$ BER) may be desired to be converted into a less demanding figure (less bit rate and/or higher BER) by reducing the average power

and transmitted PSD. Moreover, it is also possible that for some applications a BER of, e.g., $1 \cdot 10^{-3}$, may be enough, so higher bit rates could be achieved using the same transmitted power.

| Gross bitrate = 930 kbps | |
|--------------------------|-------------------|
| Scheme | Gross BER |
| MC-DS-CDMA | $4 \cdot 10^{-3}$ |
| MC-CDMA | $3 \cdot 10^{-3}$ |
| User bitrate = 465 kbps | |
| Scheme | Gross BER |
| MC-DS-CDMA | $1 \cdot 10^{-7}$ |
| MC-CDMA | $8 \cdot 10^{-8}$ |

Table 11 Long link system performance

5.5. OUTCOMES AND CONCLUSIONS

In this work, a first step towards a new wideband physical layer on HV lines has been presented. The needed channel measurements to carry out a MCM symbol design have been fulfilled, and the performance of the proposed system has been tested in a real scenario.

A properly designed OFDM allows an easy equalization and detection while avoiding ISI. OFDM splits the selective signal bandwidth into several flat subchannels, however, an efficiency loss has to be paid due to the cyclic prefix. In order to minimize that loss, a short cyclic prefix is desired, so, if received SNR is low enough, less channel delay spread will have to be considered. In this work, only the first reflected path was needed to be avoided. Moreover, it has been shown that high rates can be achieved by increasing bandwidth instead of signal power. This low-PSD minimizes undesired emissions and signal coupling into other systems or other MV-PLC links. The spectral granularity delivered by MCM can be also exploited in terms of spectral notching, that is a desirable characteristic in PLC modulations when trying to completely avoid the emission in certain frequencies.

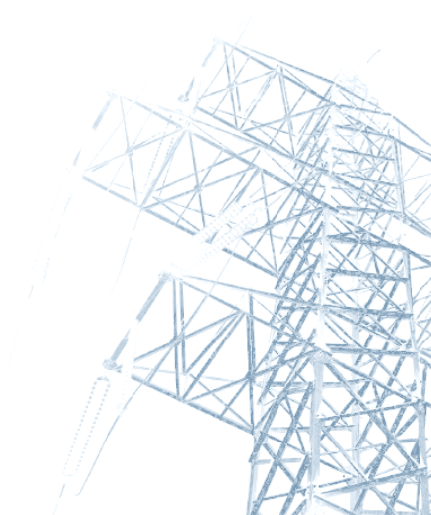
Regarding channel time domain behavior, it has been found that channel transfer function and access impedance can be considered constant, revealing neither short time nor long time variations. This friendly behavior in time domain suggests the use of an adaptive modulation for efficient channel capacity exploitation. Thus, without wasting power or increasing BER, a higher link spectral efficiency can be achieved by taking advantage of the OFDM subbands flat fading through adaptation [66]. On the other hand, background noise does vary in time domain (up to 40 dB in certain bands), but its slow variability does not present a serious impairment for an adaptive approach. Moreover, special attention should be given to this particular noise scenario: variable and colored background noise regarding frequency domain selectivity, and asynchronous impulse events regarding both frequency and time domain selectivity; when designing noise aware adaptive schemes.

Although channel diversity is exploited at bit level by means of coding and interleaving, it has been shown that better performance can be obtained by exploiting diversity at chip level when using MC-SS schemes. Specifically, the MC-CDMA scheme is able to take profit of the noise scenario frequency selective behavior (colored spectrum) delivering the best performance of the three tested schemes, i.e., 465 kbps with $8 \cdot 10^{-8}$ of BER with 2.5 W of average power in a 27 km link.

Moreover, measurements have revealed that transmission is possible beyond the licensed HV-PLC band. The next spectrum band is licensed to broadcast systems, but, as it has been shown, an easily exploitable narrowband interference limited noise region characterizes the spectrum from 500 kHz and on. MCM access methods and CR techniques offer a good possibility to increase HV-PLC channel bandwidth and minimize interferences between HV-PLC neighboring equipment [68].

Future work points to the test of MC-SS signals with PAPR reduction techniques, different detectors, and hybrid MC-SS approaches like orthogonal frequency and code division multiplexing (VSF-OFCDM, MCM with variable spreading in both dimensions) [16][84]. This kind of hybrid schemes offer a great level of

granularity and adaptation capabilities, being able to offer several quality of service levels in one single frame architecture simultaneously.



CHAPTER 6

6. CONCLUSIONS AND FUTURE WORK

6.1. CONCLUSIONS

PLC communications is now experimenting a great evolution, especially in the field of broadband PLC (access and in-home applications). Other PLC fields like utility oriented low frequency LV-PLC are still trying to cope with the new EUs requirements: high speed and low cost. Having a closest look to the AMR related applications, there are five main manufacturers involved on AMR EN50065 compliant systems with gross bitrates ranging from 1200 to 4800 bps. Three of them are using narrowband modulations, while Yitran is using a chirp-based SS technique. The frequency diversity of the latter is implicit in its SS nature, while no “real” frequency diversity is obtained by the narrowband implementations.

The SS implementation by Yitran uses chirp sequences to transmit data, which is transported in the relative shift of that chirp sequence. Since a chirp sequence always uses the same spectrum, independently of the modulated data, its frequency diversity cannot be optimized for each scenario, and interference cannot be always avoided. This problem can be overcome by using the most adaptable modulation, i.e., MCM. MCM are suitable when dealing with channel and noise frequency selectivity. The main drawback of a MCM is its sensitiveness to synchronization errors, so relatively complex receivers are needed. Complex receivers means costly equipment, and this issue is a problem that an EU installing millions of meters has to take care of. A low complexity MC proposal with mains zero-crossings based synchronization has been proposed, obtaining an easily adaptable MC scheme, designed to cope with channel and other equipment interferences. This approach has been found to be really interesting, and other research groups like the one in Karlsruhe University are also working in this field.

MV voltage channel is typically used for telecontrol and teleprotection, but since the deregulation of the telecommunications and the energy market, EUs want to make it a real uplink from the customer to the backhaul and to send the metering data to the processing center (e.g. Enel). The first step before going to the physical layer design is to have a proper channel model.

Current MV channel topology model proposals deal with particular issues or are based on behavioral characterization (multipath models), providing a non complete or an imprecise channel behavior model. For this kind of scenario, the approximation that best suits this channel is a combination of deterministic and stochastic modeling for the channel transfer function and the noise scenario, respectively. Focusing on channel transfer function, a scattering parameters based structural characterization of network devices has been fulfilled, yielding to the deterministic modeling of an arbitrary network topology, i.e., any kind of topology with any type of components. This is a very powerful approach, since the model can be exported to different regions where different topologies and/or network devices are used while obtaining precise channel transfer functions. Moreover, the structural parameters can be set by statistical values, in order to get the channel behavior for a certain network topology subset or group.

Although HV-PLC modems are still tied to legacy standards, there are some SCM-QAM based reaching a net bit rate of up to approximately 80 kbps in a 16 kHz bandwidth with BER equal or below 10^{-6} . Moreover, MCM begins to play an important role in HV-PLC due to its inherent robustness against multipath effects and narrowband interferers and its high spectral efficiency. This is making OFDM the choice for manufacturer's next generation HV-PLC equipment. This work has shown that the evolution of HV-PLC should point to exploiting the whole (or all the available) HV-PLC licensed bandwidth, enhancing the link capacity (exploiting bandwidth instead of increasing power) and keeping the PSD low (reducing interference to other power line carriers systems), two of the main handicaps in the current HV-PLC implementations. Moreover, the combination of MC modulations with SS techniques has shown good performance, beating all the current systems and delivering high adaptive and quality of service capabilities.

6.2. NEXT STEPS

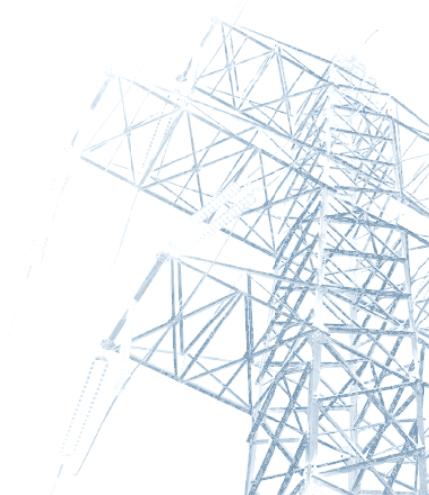
In this thesis, the state of the art of utility oriented PLC has been presented, especially in the fields of AMR and HV-PLC. Beside MV channel measurements, two different ways, both MC based, have been identified as a good choice for the CENELEC LV-PLC and for HV-PLC, on one hand, due to its frequency diversity, robustness against interferences and low complexity, and, on the other, due to its low PSD, high robustness against channel and noise frequency selectivity and interference, respectively.

Following the three research lines done so far, some aspects have appeared as especially interesting to be further investigated. Regarding LV-PLC, the use of MC modulation with mains-zero crossings based synchronization has proved a good trade-off between performance and complexity. Once the basic modulation parameters have been identified, there are others that have to be studied:

- Frame detection, and the minimization of false alarms, is a key point concerning the physical layer performance. Robust headers or preambles are needed in order to efficiently detect the beginning of the frame.
- The noise cyclostationary behavior demand a well designed frame format and coding scheme. Both issues are tightly related and apart of coping with channel impairments, they have to be designed to satisfy medium access control layer requirements too.
- Related to coding, the use of spreading in time can enhance the system time diversity in cyclostationary scenarios, while spreading in frequency, improves frequency diversity and helps avoiding interference. As well as in other scenarios, the study of the trade-off between spreading and coding will worth the effort.
- Coding, spreading and frame configuration will determine physical layer performance, and this performance has to be tested in a complete scenario, including several users in a LV cell and MAC layer functionality.

Focusing on the MV model, in order to properly design a valid channel simulator, more measurements should be done: in one hand, the S parameters characterization of more cable and coupler types and, on the other, more noise scenario measurements in several locations in order to improve the statistic consistence. Then, once the model is considered valid, the simulation of the model will allow the design and comparison of different physical and access methods, in order to exploit the MV channel capacity.

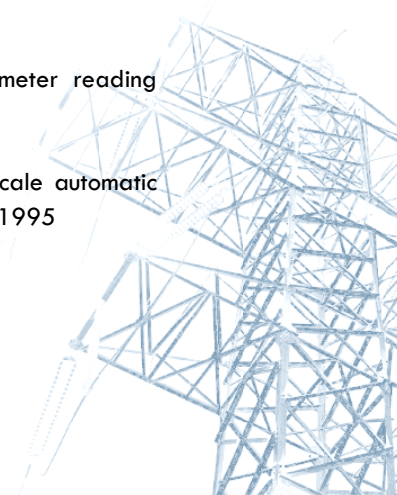
Endesa Network Factory has shown to be very confident with the obtained results in the MC-SS field tests, and the next step is the implementation of a real time version of the proposed physical layer, including the adaptive and cognitive techniques. This new project has just begun and will show the real performance of the system proposed when adaptive techniques are deployed. Two software radio platforms, based on digital signal processors and field programmable gate arrays are used for developing.



7. REFERENCES

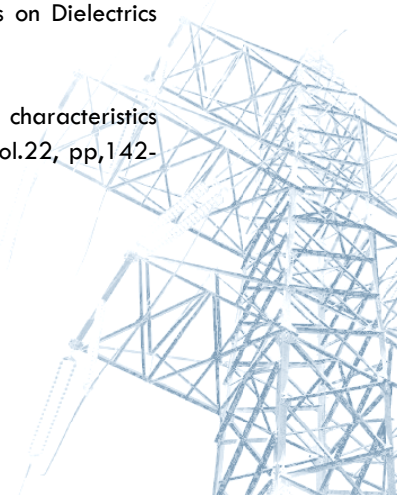
- [1] R. Aquilué, P. Bergadà, I. Gutiérrez, J.L. Pijoan, "Channel Estimation for Long Distance HF Communications based on OFDM Pilot Symbols", in Proc. IET Ionospheric Radio Systems and Techniques (IRST 2006), London, England, 2006
- [2] C. Fetter, Patent No. 1607668, United States, 1924
- [3] R. Honaman, Patent No. 1672940, United States, 1924
- [4] K. Dostert, "Powerline Communications", Prentice Hall, 2001
- [5] International Electrotechnical Commission, "IEC/TR 60663: Planning of (single-sideband) power line carrier systems", 1980
- [6] International Electrotechnical Commission, "IEC/TR 60495: Single sideband power-line carrier terminals", 1993
- [7] Dimat S.A., "OPD-1 Digital Power-Line Carrier Terminal", Datasheet, 2004
- [8] ABB Switzerland Ltd., "ETL600 Universal Digital Power Line Carrier", Datasheet, 2006
- [9] R. Napolitano, "Communications over HV-MV-LV Power Lines: Europe Standards and Regulations overview", IEEE International Symposium on Power Line Communications and its Applications 2007 (ISPLC2007), p.33-33, Italy, 2007
- [10] OPERA, "D45 – Specification of PLC system requirements", 2005
- [11] OPERA, "D 89 – Reports and presentations about relevant results related to regulatory issues", 2005
- [12] OPERA, "D 58 – Report on the progress of PLC standardization", 2006
- [13] CENELEC, "EN 50065-1:2001: Signalling on low-voltage electrical installations in the frequency range 3 khz to 148,5 khz – part 1: General requirements, frequency bands and electromagnetic disturbances,", 2001
- [14] S.Rogai, "Telegestore Project Progresses And Results", IEEE International Symposium on Power Line Communications and its Applications 2007 (ISPLC2007), Italy, 2007
- [15] R.Aquilue, M. Deumal, J.L. Pijoan and L. Corbeira, "A low complexity multicarrier proposal for medium rate automatic meter reading systems", IEEE International Symposium on Power Line Communications and its Applications 2007 (ISPLC2007), Italy, 2007
- [16] K. Fazel and S. Kaiser, "Multi-Carrier and Spread Spectrum Systems", John Wiley & Sons, 2003
- [17] C.E. Shannon, "A mathematical theory of communication", Bell System Technical Journal, vol. 27, pp. 379-423 and 623-656, July and October, 1948
- [18] R. W. Chang, "Synthesis of band-limited orthogonal signals for multi-channel data transmission", Bell System Technical Journal 46, 1996, pp.1775-1796

- [19] S. B. Weinstein and P. M. Ebert, "Data transmission by frequency division multiplexing using the discreet Fourier transform", *IEEE Transactions on Communication Technology*, vol.19, pp.628-634, 1971
- [20] C. Wong, R. Cheng, K. Letaief and R. Murch, "Multiuser OFDM with adaptive subcarrier, bit and power allocation", *IEEE Journal on Selected Areas in Communications*, vol. 17, pp. 1747-1758, Oct. 1999
- [21] F. Kiessling, P. Nefzger, J. F. Nolasco, and U. Kaintzyk "Overhead Power Lines: Planning, Design, Construction", Springer, 2003
- [22] OPERA, "D44 – Report presenting the architecture of PLC system, the electricity network topologies, the operating modes and the equipment over which PLC access system will be installed", 2005
- [23] N. Suljanovic, A. Mujcic, M. Zajc, and J.F. Tasic, "Computation of high-frequency and time characteristics of corona noise on HV power line", *IEEE Transactions on Power Delivery*, vol.20, pp.71-79, 2005
- [24] M. Zimmermann and K. Dostert, "Analysis and modeling of impulsive noise in broad-band powerline communications", *IEEE Transactions on Electromagnetic Compatibility*, vol.44, pp.249-258, 2002
- [25] M. Zimmermann and K. Dostert, "A multipath model for the powerline channel", *IEEE Transactions on Communications*, vol.50, pp.553-559, 2002
- [26] A. Mujcic, N. Suljanovic, M. Zajc, and J. F. Tasic, "Power line noise model appropriate for investigation of channel coding methods", *IEEE EUROCON 2003*, vol.1, pp.299-303, 2003
- [27] Dimat S.A. "Coupling unit for PLC equipment over medium voltage lines", Datasheet, 2005
- [28] OPERA, "D05 - Pathloss as a function of frequency, distance and network topology for various LV and MV European powerline networks", 2005
- [29] R. C. Hemminger, L. J. Gale, F. Amoura and J. B. O'Neal, "The Effect of Distribution Transformers on Distribution Line Carrier Signals", *IEEE Transactions on Power Delivery*, vol.2, pp.36-40, 1987
- [30] B. Gustavsen, "Wideband modeling of power transformers", *IEEE Transactions on Power Delivery*, vol.19, pp.414-422, 2004
- [31] M. Gotz, M. Rapp and K. Dostert, "Power line channel characteristics and their effect on communication system design", *IEEE Communications Magazine*, vol.42, pp.78-86, 2004
- [32] J. W. Hohn and J. A. Zipp, "Power Line Carrier Practices and Experiences", *IEEE Transactions on Power Delivery*, vol.10, pp.639-647, 1995
- [33] D. Sabolic, "Influence on the transmission medium quality on the automatic meter reading capacity", *IEEE Transactions on Power Delivery*, vol.18, pp.725-728, 2003
- [34] S. Mark and D. Radford, "Design considerations for implementation of large scale automatic meter reading systems", *IEEE Transactions on Power Delivery*, vol.10, pp.97-113, 1995



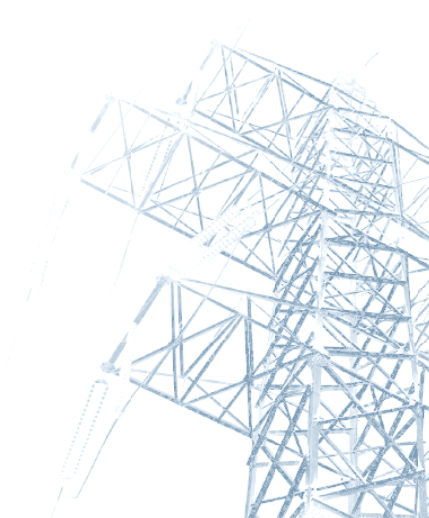
- [35] M. Karl and K. Dostert, "Selection of the optimal modulation scheme for digital communications over low voltage power lines", IEEE International Symposium on Spread Spectrum Techniques and Applications, vol.3, pp.1087-1091, 1996
- [36] I. H. Cadvar, "Performance analysis of FSK power line communications systems over the time-varying channels: measurements and modeling", IEEE Transactions on Power Delivery, vol.19, pp.111-117, 2004
- [37] K. Dostert, "Frequency-hopping spread-spectrum modulation for digital communications over electrical power lines", IEEE Journal on Selected Areas in Communications", vol.8, pp.700-710, 1990
- [38] E. Biglieri, "Coding and modulation for a horrible channel", IEEE Communications Magazine, 2003
- [39] I. H. Cadvar, "A solution to remote detection of illegal electricity usage via power line communications", IEEE Transactions on Power Delivery, vol.19, pp.1663-1667, 2004
- [40] H. C. Ferreira, H. M. Grove, O. Hooijen and A. J. Han Vinck, "Power line communications: an overview", IEEE Africon, vol.2, pp.558-563, 1996
- [41] M. Götz, M. Rapp and K. Dostert, "Power line channel characteristics and their effect on communication system design", IEEE Communications Magazine, 2004
- [42] J G. Proakis, "Digital Communications", McGraw-Hill, 2000
- [43] R. Aquilué, "COM-ENDESA_DE_P01_TR01_V020 ENDESA Distribución Eléctrica (RPF – Servicios Profesionales PLC-BE) Nivel Físico", Endesa Distribución Eléctrica Technical Report, 2005
- [44] R. Aquilué, "COM-ENDESA_DE_P01_TR02_V045 ENDESA Distribución Eléctrica (RPF – Professional Services PLC-BE) Physical Layer Specification", Endesa Distribución Eléctrica Technical Report, 2006
- [45] STMicroelectronics, "ST7538 FSK power line transceiver", Datasheet, 2005
- [46] Echlon Corp., "PL3120 and PL3150 power line smart transceivers", Datasheet, 2005
- [47] AMI Semiconductor, "AMIS-30585 S-FSK plc modem", Datasheet, 2005
- [48] Yitran. Communications Ltd., "IT800-DS-016-R1.2", Datasheet
- [49] J. Bausch, T. Kistner, M. Babic and K. Dostert, "Characteristics of indoor power line in the frequency range 50-500 kHz", IEEE International Symposium on Power Line Communications and its Applications 2006 (ISPLC2006), USA, 2006
- [50] OPERA, "D14 – Report on MV backbone system", 2005
- [51] H. Philipps, "Performance measurements of powerline channels at high frequencies", IEEE International Symposium on Power Line Communications and its Applications 1998 (ISPLC1998), Japan, 1998
- [52] D. Liu, E. Flint, B. Gaucher and Y. Kwark, "Wide band AC power line characterization", IEEE Transactions on Consumer Electronics, vol.45, pp.1087-1097, 1999

- [53] H. Philipps, "Modelling of powerline communication channels", IEEE International Symposium on Power Line Communications and its Applications 1999 (ISPLC1999), UK, 1999
- [54] I. C. Papaleonidopoulos, C. N. Capsalis, C. G. Karagiannopoulos, and N. J. Theodorou, "Statistical analysis and simulation of indoor single-phase low voltage power-line communication channels on the basis of multipath propagation", IEEE Transactions on Consumer Electronics, vol.49, pp.89-99, 2003
- [55] F. J. Cañete, J. A. C. Arrabal, L. D. del Rio, and J. T. E. Muñoz, "Analysis of the cyclic short-term variation of indoor power line channels", IEEE Journal on Selected Areas in Communications, vol.24, pp.1327-1338, 2006
- [56] S. Galli and T. C. Banwell, "A deterministic frequency-domain model for the indoor power line transfer function", IEEE Journal on Selected Areas in Communications, vol.24, pp. 1304-1316, 2006
- [57] P. Steaner and P. Delogne, "Deterministic modeling of the (shielded) outdoor power line channel based on the multiconductor transmission line equations", IEEE Journal on Selected Areas in Communications, vol.24, pp. 1277-1291, 2006
- [58] T. Esmailian, F. R. Kschischang, and P. G. Gulak, "An in-building power line channel simulator", IEEE International Symposium on Power Line Communications and its Applications 2002 (ISPLC2002), Athens, 2002
- [59] F. J. Cañete, "Power line channels: frequency and time selective Part 1.-Response of indoor PLC channels", IEEE International Symposium on Power Line Communications and its Applications 2007 (ISPLC2007), Italy, 2007
- [60] S. Sancha, F. J. Cañete, L. Díez and J.T. Entrambasaguas "A channel simulator for indoor power-line communications", IEEE International Symposium on Power Line Communications and its Applications 2007 (ISPLC2007), Italy, 2007
- [61] C. Hensen, W. Schulz and S. Schwarze, "Characterization, measurement and modeling of medium-voltage power line cables for high data rate communication", IEEE International Symposium on Power Line Communications and its Applications 1999 (ISPLC1999), UK, 1999
- [62] P. Amirshahi and M. Kavehrad, "Medium voltage overhead power-line broadband communications: transmission capacity and electromagnetic interference", IEEE International Symposium on Power Line Communications and its Applications 2005 (ISPLC2005), USA, 2005
- [63] R. Papayzan and R. Eriksson, "Calibration for time domain propagation constant measurements on power cables", IEEE Transactions on Instrumentation and Measurements, vol.52, pp.415-418, 2003
- [64] R. Papayzan, P. Pettersson, H. Edin, R. Eriksson and U. Gäfvert, "Extraction of high frequency power cable characteristics from S-parameter measurements", IEEE Transactions on Dielectrics and Electrical Insulation, vol.11, pp.461-470, 2004
- [65] Z. Tao, Y. Xiaoxian, Z. Bahoui, C. Jian, Y. Zhi and T. Zhihong, "Research of noise characteristics for 10-kV medium-voltage power lines", IEEE Transactions on Power Delivery, vol.22, pp,142-150, 2007



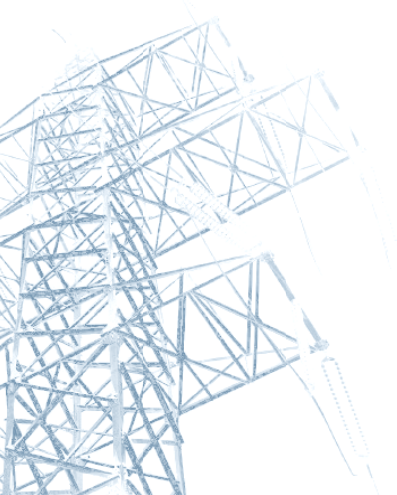
- [66] S. Taek and A. J. Goldsmith, "Degrees of freedom in adaptive modulation: an unified view", *IEEE Transactions on Communications*, vol.49, pp.1561-1571, 2001
- [67] S. Kaiser, "Trade-off between channel coding and spreading in multi-carrier CDMA systems", *IEEE International Symposium on Spread Spectrum Techniques and Applications*, 1996
- [68] S. Srinivasa and S. A. Jafar, "The throughput potential of cognitive radio: a theoretical perspective", *IEEE Communications Magazine*, 2007
- [69] National Instruments, "NI-660x specifications", Datasheet, 2006
- [70] National Instruments, "NI PXI-5441 specifications, 100 msp/s, 16-bit arbitrary waveform generator with onboard signal processing", Datasheet, 2005
- [71] National Instruments, "NI PXI-5142 specifications, 14-bit 100 ms/s digitizer with onboard signal processing", Datasheet, 2006
- [72] R. Aquilué, P. Bergadà, I. Gutiérrez, J.L. Pijoan, "Channel Estimation for Long Distance HF Communications based on OFDM Pilot Symbols", in *Proc. IET Ionospheric Radio Systems and Techniques (IRST 2006)*, England, 2006
- [73] R. Aquilué, P. Bergadà, M. Deumal, J.L. Pijoan, "Multicarrier Symbol Design for HF Transmissions from Antarctica Based on Real Channel Measurements", in *Proc. IEEE Military Communications Conference (MILCOM2006)*, USA, 2006
- [74] P. Hoeher, S. Kaiser, and P. Robertson, "Pilot-symbol-aided channel estimation in time and frequency", *International Workshop Multi-Carrier Spread-Spectrum*, 1997
- [75] M. Hsieh and C. Wei, "Channel estimation for OFDM systems based on comb-type pilot arrangement in frequency selective fading channels", *IEEE Transactions on Consumer Electronics*, Vol.44, pp.217-225, 1998
- [76] Morelli and Mengali, "A comparison of pilot-aided channel estimation methods for OFDM systems", *IEEE Transactions on Signal Processing*, Vol.49, pp.3065-3073, 2001
- [77] P. Hoeher, S. Kaiser, and P. Robertson, "Two-dimensional pilot-symbol aided channel estimation by Wiener filtering", *IEEE International Conference on Acoustics, Speech, and Signal Processing 1997 (ICASSP1997)*, 1997
- [78] F. Sanzi and J. Speidel, "An adaptive two-dimensional channel estimator for wireless OFDM with application to mobile DVB-T", *IEEE Transactions on Broadcasting*, vol.46, pp. 128-133, 2000
- [79] Y. Xiaoxian, Z. Tao, Z. Baohui, Y. Fengchun, D. Jiandong and S. Minghui, "Research of Impedance characteristics for medium-voltage power line networks", *IEEE Transactions on Power Delivery*, vol.22, pp,870-878, 2007
- [80] Y. Xiaoxian, Z. Tao, Z. Baohui, N. H. Xu, W. Goujun and D. Jiandong, "Investigation on transmission properties on 10-kV medium voltage power lines – part I: general properties ", *IEEE Transactions on Power Delivery*, vol.22, pp,1446-1454, 2007
- [81] T. Tran-Anh, P. Auriol and T. Tran-Quoc, "High frequency power transformer modeling for Power Line Communications applications", *IEEE Power Systems Conference and Exposition*, 2006

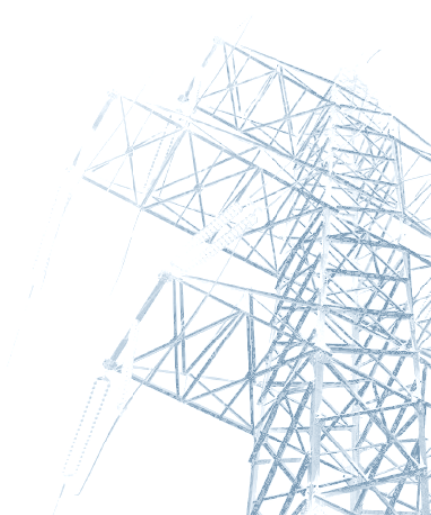
- [82] S. Kondo and L. B. Milstein, "On the use of multicarrier direct sequence spread spectrum systems", IEEE Military Communications Conference, 1993
- [83] A. Chouly A. Brajal and S. Jourdan, "Orthogonal multicarrier techniques applied to direct sequence spread spectrum CDMA systems", IEEE Global Telecommunications Conference, 1993
- [84] N. Maeda, Y. Kishiyama, K. Higuchi, H. Atarashi and M. Sawahashi, "Experimental evaluation of throughput performance in broadband packet wireless access based on VSF-OFCDM and VSF-CDMA", IEEE International Symposium on Personal, Indoor and Mobile Radio Communications, 2003
- [85] T. Kistner, M. Bauer, A. Hetzer and K. Dostert, "Analysis of Zero Crossing Synchronization for OFDM-Based AMR Systems", in Proc. IEEE Symposium on Power Line Communications and its Applications (ISPLC2008), Jeju, South Korea, 2008
- [86] M. Karl and K. Dostert, "Selection of an Optimal Modulation Scheme for Digital Communications over Low Voltage Power Lines", in Proc. IEEE International Symposium on Spread Spectrum Techniques and Applications, 1996



8. APPENDIX A. INCLUDED PAPERS

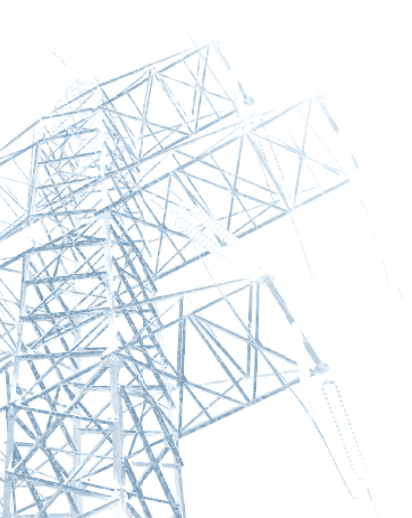
1. R. Aquilué, P. Bergadà, M. Deumal, J.L. Pijoan, "Multicarrier Symbol Design for HF Transmissions from Antarctica Based on Real Channel Measurements", in Proc. IEEE Military Communications Conference (MILCOM2006), Washington, United States, 2006.
2. R. Aquilué, M. Deumal, J.L. Pijoan, L. Corbeira, "A Low Complexity Multicarrier Proposal for Medium Rate Demanding Automatic Meter Reading Systems", in Proc. IEEE Symposium on Power Line Communications and its Applications (ISPLC2007), Pisa, Italy, 2007.
3. R. Aquilué, M. Ribó, J.R. Regué, J.L. Pijoan, G. Sánchez, "Urban Underground Medium Voltage Channel Measurements and Characterization", in Proc. IEEE Symposium on Power Line Communications and its Applications (ISPLC2008), Jeju, South Korea, 2008.
4. R. Aquilué, J.L. Pijoan, G. Sánchez, "High Voltage Channel Measurements and Field Test of a Low Power OFDM System", in Proc. IEEE Symposium on Power Line Communications and its Applications (ISPLC2008), Jeju, South Korea, 2008.
5. R. Aquilué, M. Ribó, J.R. Regué, J.L. Pijoan, G. Sánchez, "Scattering Parameters Based Underground Medium Voltage Power Line Communications Channel Measurements, Characterization and Modeling", accepted for publication in IEEE Transactions on Power Delivery, June 2008.
6. R. Aquilué, I. Gutiérrez, J.L. Pijoan, G. Sánchez, "High Voltage Multicarrier Spread Spectrum Field Test", accepted for publication in IEEE Transactions on Power Delivery, May 2008.

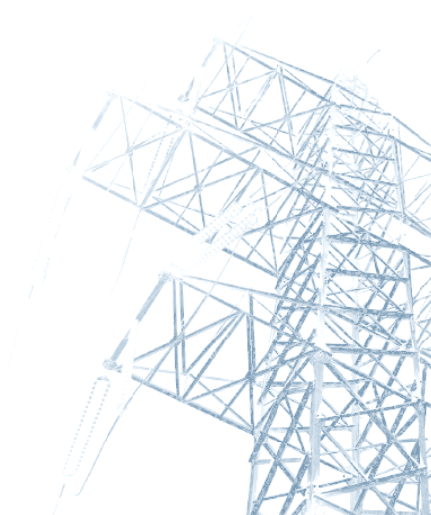




8.1. APPENDIX A.1

R. Aquilué, P. Bergadà, M. Deumal, J.L. Pijoan, "Multicarrier Symbol Design for HF Transmissions from Antarctica Based on Real Channel Measurements", in Proc. IEEE Military Communications Conference (MILCOM2006), Washington, United States, 2006.





MULTICARRIER SYMBOL DESIGN FOR HF TRANSMISSIONS FROM THE ANTARCTICA BASED ON REAL CHANNEL MEASUREMENTS

Ricard Aquilué

Pau Bergadà

Marc Deumal

and

J.L. Pijoan

Dept. of Communications and Signal Theory

La Salle Engineering, Ramon Llull University

Pg. Bonanova 8, Barcelona, Spain

ABSTRACT

Last fifteen years improvements in HF digital systems have made ionospheric communications a true alternative to low bit rate, long distance links, especially in the polar caps where alignment with geostationary satellites is not always possible. Our previous research efforts were focused on using pseudo-noise (PN) sequences and Orthogonal Frequency Division Multiplexing (OFDM) pilot symbols to evaluate the 7900 miles link from the Spanish Antarctic Base Juan Carlos I to Spain, crossing the equatorial belt. In this paper we face the problem of designing the OFDM physical layer. Two multicarrier transmission schemes are proposed and compared based on channel measured transfer functions and noise plus interference records. Special attention is paid to pilot pattern design in order to maximize the system performance while assuring high power and bandwidth efficiency. The quality and throughput in real transmissions from the Antarctica, as well as the evolution of BER in front of interferences, are studied.

INTRODUCTION

Data communications from the Antarctica is mainly achieved via satellite. However, since communication with geostationary satellites is not always possible from the poles, skywave ionospheric radiocommunications have become a good and inexpensive alternative. The Research Group in Electromagnetism and Communications from La Salle School of Engineering, Ramon Llull University, is working on the design of a robust unidirectional system for very long distance HF communications. The transmitter is located at the Spanish Antarctic Base (SAB) in Livingston Island (62.6°S, 60.4°W) and the receiver is located at the Ebre Observatory (EO) in Spain (40.8°N, 0.5°E).

As a first step towards the implementation of the radiomodem the significant parameters of the ionospheric

link between the Antarctica and Spain were measured. In that sense a sounding system, named SANDICOM (Sounding System for Antarctic Digital Communications), was designed. SANDICOM is based on a digital platform with high speed A/D/A converters and FPGA devices. The signal is fully processed digitally and, as a result, only amplification and some filtering are performed in the analog domain [1,2].

Although channel measurements are still being done to obtain sufficient statistics of the channel, current work is mainly focused on the preliminary design of the system for data transmissions. Two major advanced modulation techniques are being evaluated: Direct-Sequence Spread-Spectrum (DS-SS) Signaling [3] and Orthogonal Frequency Division Multiplexing (OFDM) [4]. In this paper we will focus on the design and evaluation of OFDM as a system candidate. In an OFDM system the data are transmitted over a number of parallel frequency channels, modulated by a baseband PSK symbol. The advantage of this technique is that it has an intrinsic robustness against multipath fading channels and narrowband interference.

In [4] we presented a preliminary OFDM system that was used to evaluate the success of multicarrier modulations in long distance data communications. The work was focused on evaluating the channel estimation capabilities in long-distance low-SNR HF link. In this paper, the channel measurements from the link between the Antarctica and Spain are used to find the optimum parameters of the OFDM physical layer, from theoretical analysis and exhaustive simulations. Subsequently, a physical layer technique that reduces the effect of interferences is evaluated. Simulation results with recorded interferences at the receiver site are used to evaluate the performance improvement capabilities of an OFDM system exploiting this technique compared to a conventional OFDM system.

SYSTEM ARCHITECTURE

The system that was designed for channel sounding (SANDICOM) is also used for preliminary data transmissions. One of the major considerations to be considered for the design of the physical layer is the strict power consumption restrictions at the transmitter site. Since the SAB is only served by wind and solar power during 8 months per year, a power amplifier capable of transmitting at a maximum power of 250 watts is used.

As multiple frequencies in the HF band are used, a broadband antenna is required. A monopole and an antenna tuner have been employed both in the emitter and in the receiver because of the ease of installation and the acceptable performance they show in the frequency range from 4 to 18MHz.

Both, transmitted power and antenna restrictions, imply that low SNR will be obtained at the receiver site. For instance, when a transmission bandwidth of 300 Hz is used an average SNR at the receiver of 8 dB has been measured when the channel is available [5]. In the next campaign, a directive antenna will be used at the receiver site in order to increase the available SNR up to 10 dB in a 1 KHz. This is the condition assumed in the following design.

SYMBOL DESIGN

Channel state information prior to the demodulation stage is needed at the receiver in order to compensate the different attenuation and phase rotations of the subcarriers introduced by the channel. First, the pilot pattern has to be designed. We define the efficiency of an OFDM system as a function of the pilot density, and it can be approximated as:

$$\rho_{PD} \approx \frac{N_T \cdot N_F - 1}{N_T \cdot N_F} \quad (1)$$

Where N_T and N_F are the pilot spacing in the time and frequency directions, respectively. If the pilots are too close to each other, an oversampling of the channel will occur causing an unnecessary penalty of the system efficiency. On the other hand, if pilot spacing is too large, channel variations will go unnoticed, dramatically reducing the system performance. In order to get a good estimation of the channel, the pilot grid has to fulfill the two-dimensional sampling theorem [6-8]. This theorem restricts the pilot spacing in the time domain to fulfill the following expression:

$$\frac{1}{2 \cdot N_T \cdot T_S} \geq f_D \quad (2)$$

Where f_D is the maximum Doppler frequency and T_S is the OFDM symbol time. The pilot spacing in the frequency domain has to fulfill:

$$\frac{1}{N_F \cdot \Delta f} \geq \tau \quad (3)$$

Where τ is the maximum delay spread of the channel and Δf is the subcarrier separation.

Next, a cyclic prefix is added at the beginning of each OFDM symbol in order to assure that no inter symbol interference (ISI) occurs. Let T_{CP} be the length of the cyclic prefix and T_U the length of the useful part of the symbol. The total symbol time becomes $T_S = T_{CP} + T_U$. The efficiency of an OFDM system due to the cyclic prefix can be expressed as

$$\rho_{CP} = \frac{T_U}{T_U + T_{CP}} \quad (4)$$

Note that in order to increase both the spectral and power efficiency, large values of ρ_{CP} should be used, i.e. the useful symbol time should be much larger than the length of the cyclic prefix. Let us define the efficiency of the OFDM system from (1) and (4) as:

$$\rho = \rho_{PD} \cdot \rho_{CP} = \frac{N_T \cdot N_F - 1}{N_T \cdot N_F} \cdot \frac{T_U / T_{CP}}{T_U / T_{CP} + 1} \quad (5)$$

Figure 1 represents the efficiency of the system as defined in (5). It can be appreciated that for T_U / T_{CP} values over 16, efficiency improves slowly.

We recall from [5] that typical 10dB-delay spread of 2.5 msec and maximum 10dB-doppler frequency of 1.6 Hz have been observed during the sounding survey. In order to avoid ISI, the cyclic prefix is set to be $T_{CP} = 3$ milliseconds. From the sampling theorem introduced in (2) and (3), the maximum spacing between time and frequency pilots can be obtained.

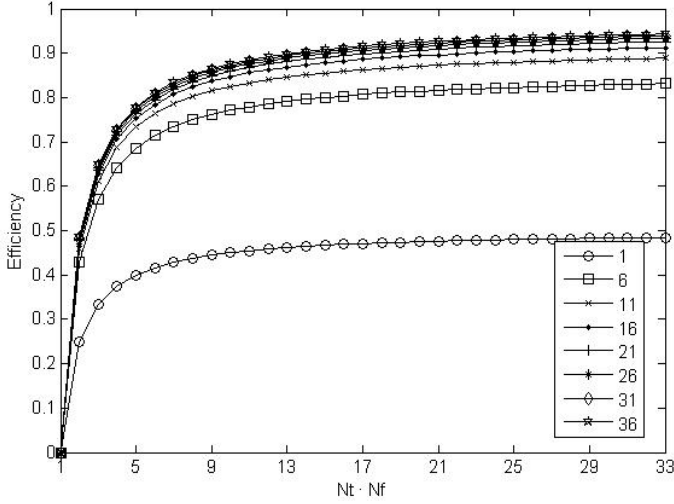


Figure 1. Efficiency of the system as a function of the pilot density and the ratio T_U/T_{CP}

Choosing a useful time in order to get a $\rho_{CP} > 0.95$, we have $T_U = 60$ milliseconds ($T_U/T_{CP} = 20$). If 60 milliseconds is used as the useful symbol time, we have:

$$N_F \leq \frac{1}{\tau \cdot \Delta f} = \left\lfloor \frac{1}{0.0025 \cdot \frac{1}{0.06}} \right\rfloor = 24 \quad (6)$$

$$N_T \leq \frac{1}{2 \cdot f_D \cdot T_s} = \left\lfloor \frac{1}{2 \cdot 1.5 \cdot 0.063} \right\rfloor = 5 \quad (7)$$

The sampling theorem assumes a frequency doppler caused by different celerity vectors between transmitter and receiver and a uniform power density of the channel scattering function [9]. Moreover, some “rule of thumbs” can be found in the literature [8,10,11] that suggest a minimum oversampling of 2x or even more exhaustive channel sampling. If we focus on the ionospheric channel, spreading values varies widely from one path to another, so it is possible that the strongest signal path is not affected by the fastest variations. If dealing with low SNR levels, the effects of the weakest paths will go unnoticed, so if we synchronize to the strongest path, there is no need to track other paths variability if their relative level is low enough, yielding a more relaxed design. In addition, the fastest ionospheric layers variance occurs during the sunrise and sunset periods. If the channel propagation is not favourable for an OFDM transmission, the effects of these periods should not be taken into account [5]. There are several combinations of $N_T T_s$, $N_F \Delta f$ and T_U that meet the sampling requirements shown in (1) and (2) respectively. Using channel measurements when

propagation has been favourable enough for an OFDM transmission, a global best solution will be fulfilled.

The maximum useful symbol time will be found using the simulation scheme of Figure 2. Random data is generated and after a serial to parallel conversion, data is mapped into a BPSK constellation space. Multipath ionospheric channel realizations taken from real measurements are applied in the frequency domain. The transfer function is directly extracted from the estimations of [4], so, no channel model is used. In order to find the maximum symbol time, white gaussian noise (AWGN) is added as the first approach. Beginning with an oversampled channel estimation, several pilot densities will be tested in order to search the optimum symbol time for this channel.

Table 1. Optimum symbol time – Initial search parameters

| | |
|--|---|
| SNR | 10 dB |
| T_{CP} | 3 msec |
| T_U | 5, 55, 105, 155, 205, 255, 305 and 355 msec |
| N_T | 2, 3, 4, 5, 6, 7 |
| N_F | 2, 3, 4, 5, 6, 7 |
| <i>Channel estimation method</i> | Least Squares |
| <i>Interpolation method</i> | Nearest pilot padding |
| <i>Runs for each T_U, N_T and N_F combination</i> | 1.000 |
| <i>Total runs</i> | 288,000 |

Table 1 shows the simulation parameters: Six values of N_T and of N_F are evaluated based on hexagonal pattern locations [4,12] among several useful symbol times ranging from 5 to 355 msec. In order to compensate for the channel effects with reduced complexity methods (real time operation oriented), the channel is estimated with the Least Squares method [13] and interpolated with the novel Nearest Pilot Padding method [14]. This interpolation technique offers similar performance than other more complex methods in low SNR scenarios.

When the pilots are close enough to each other, many values of the symbol time result in a good channel estimation. This circumstance is exposed Figure 3 ($N_T = 2$, $N_F = 2$), where the channel is sampled over the minimum sampling frequency and the BER will not improve even though the pilot density is increased.

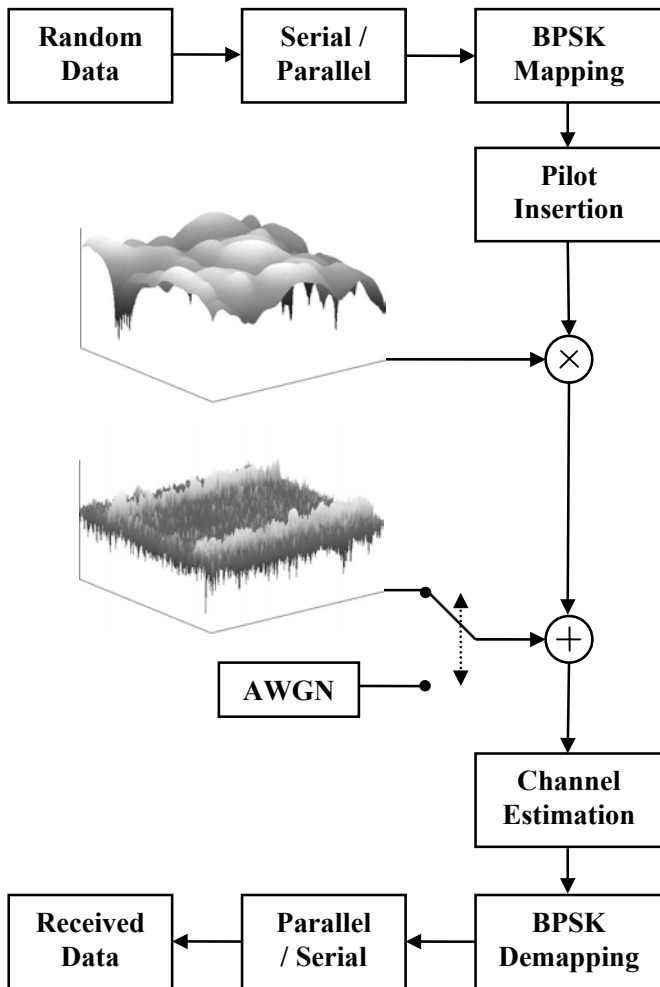


Figure 2. Simulation block diagram with real channel measurements

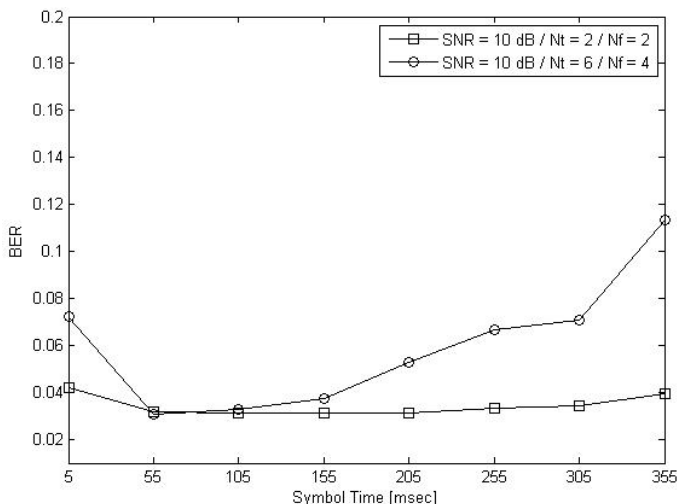


Figure 3. BER and useful symbol time ($N_T = N_F = 2$ and $N_T = 6$ $N_F = 4$)

As pilot spacing increase, BER levels begin to rise. However, there is an optimum symbol duration that exhibits the same BER than before. From Figure 3 ($N_T = 6$ $N_F = 4$), an optimal symbol time around 55 msec can be guessed.

A finest search is required, since a precision of 50 msec is not enough. The parameters used in order to find the exact value of the optimum symbol time are shown in Table 2.

Table 2. Optimum symbol time – Fine search parameters

| | |
|---|---|
| T_{CP} | 3 msec |
| T_U | 25, 30, 35, 40, 45, 50, 55, 60, 65, 70, 75, 80, 85, 90, 95, 105, 110 and 115 msec |
| N_T | 5, 6, 7 |
| N_F | 5, 6, 7 |
| Channel estimation method | Least Squares |
| Interpolation method | Nearest pilot padding |
| Runs for each T_U , N_T and N_F combination | 1.000 |
| Total runs | 153,000 |

From Figure 4 we can state that the maximum useful symbol time for low BER values is 75 msec. Once the symbol time is fixed, simulations for finding the optimum value for N_T and N_F are performed.

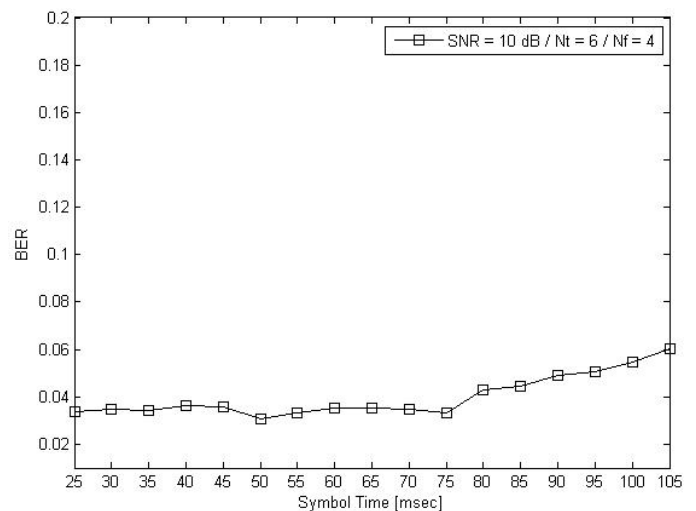


Figure 4. Detail of BER and symbol time ($N_T = 6$ $N_F = 4$)

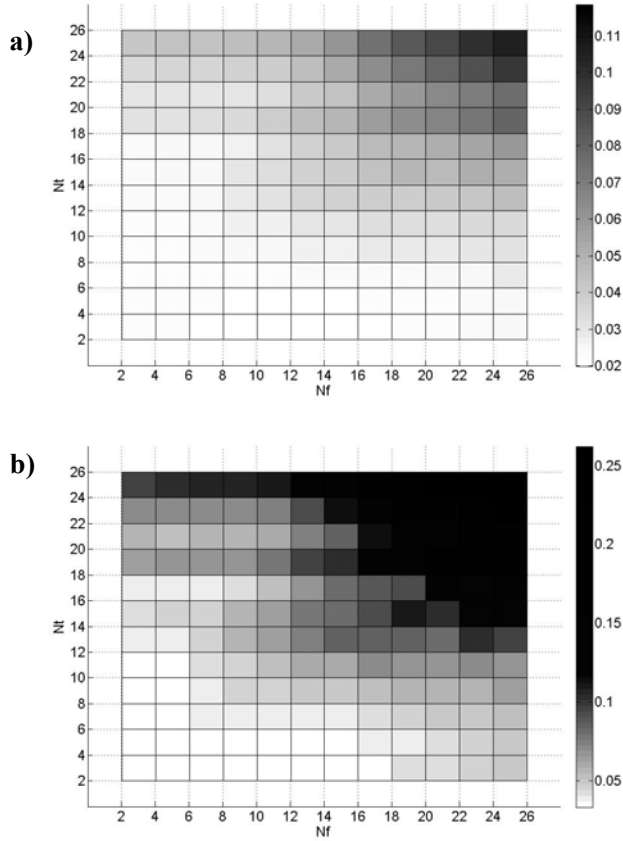


Figure 5. BER and pilot densities from $N_T = N_F = 2$ to $N_T = N_F = 26$ (a. average channel and b. worst channel)

In Figure 5, the study for the average and worst channel is shown. If focused on the worst case, the maximum pilot spacing in the time domain without BER degradation is $N_T = 12$ and $N_F = 18$ for the frequency domain. Taking into account the pilot number efficiency, the maximum expected SNR at the receiver and following the balanced design approach defined in [8], the selected values for the OFDM symbol are presented in Table 3:

Table 3. Frame and symbol parameters

| | |
|-------------|-----------------|
| T_{CP} | 3 milliseconds |
| T_U | 75 milliseconds |
| T_S | 78 milliseconds |
| Δf | 13.33 Hz |
| N_T | 6 |
| N_F | 12 |
| ρ_{CP} | 0.9615 |
| ρ_{PD} | 0.9861 |
| ρ | 0.9481 |
| N_{SC} | 73 |
| R_B | 948 bps |

Where N_{SC} is the number of subcarriers per OFDM symbol and R_B is the raw modulation bit rate.

INTERFERENCE EFFECTS

In HF channels, the level of interference is usually the limiting factor, more than SNR and multipath effects. In this section, measured interference records have been used to compute the robustness of two multicarrier modulations against interference.

First, a conventional OFDM modulation with the parameters shown in Table 3 will be tested under the measured multipath channel and AWGN (OFDM AvgNPI). Then, recorded noise plus interference (OFDM AvgNPI) samples will be used instead of AWGN and finally, OFDM performance will be evaluated under the worst interference conditions found during the sounding campaign (WstNPI). The OFDM AvgNPI simulation will show the average performance of the link. This is computed using the average interference found among all the situations during the sounding survey. Interferences in the HF band are usually slow variant, so they could be avoided if a feedback channel exists. In a simplex communication system, the interference location is unknown at the transmitter site, so the use of frequency diversity will guarantee the best average performance of the link.

Table 4. Interference effects – Simulation parameters

| | |
|---|--|
| <i>Num. subcarriers</i> | 73 |
| T_{CP} | 3 milliseconds |
| T_U | 75 milliseconds |
| T_S | 78 milliseconds |
| Δf | 13.33 Hz |
| <i>OFDM BW</i> | 1KHz |
| N_T | 6 |
| N_F | 12 |
| <i>Hopping rate (h_R)</i> | 0 Hz (hop every 0 symbols) 12.82 Hz (hop every 1 symbol) 1.83 Hz (hop every 7 symbols) 0.41 Hz (hop every 31 symbols) |
| <i>Hopping frequency</i> | 1KHz |
| <i>SNR</i> | 0 to 14 dB (1 dB step) |
| <i>Runs for each h_R and SNR combination</i> | 1.000 |
| <i>Total runs</i> | 60,000 |

OFDM has an intrinsic robustness against narrowband interference since the missing data of one subcarrier can be recovered if the information has been properly coded. This is only true when the interference bandwidth equals the subcarrier bandwidth and below. If interference

bandwidth is wide enough that equals the whole OFDM bandwidth, the multicarrier modulation sees the interference as a single carrier modulation would do, that is, as a global decrease of the SNR available at the receiver. In this situation, a frequency hopping approach with multicarrier modulation makes sense. Therefore, a frequency hopping OFDM modulation will be tested (Table 4) in order to approach the average performance of the conventional OFDM (OFDM AvgNPI).

In Figure 6, a conventional OFDM is compared with the results obtained by hopping the whole OFDM symbol by 1KHz frequency shift signal every 1,7 and 31 symbol times in order to evaluate the performance degradation due to the increase of the estimation error at the borders of the frequency / time matrix [9].

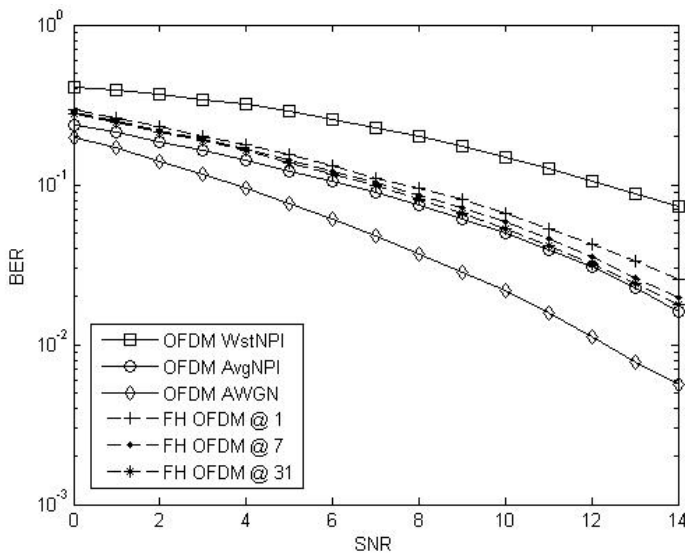


Figure 6. OFDM and FH-OFDM performances

There is a slightly decrease of the performance as the hopping rate increases. This is due to the fact that the area decreases faster than the perimeter of the frequency / time matrix and the ratio between the pilots located at the borders and the total number of pilots increases, yielding a decrease of the system performance. For hopping rates slower than 0.41 Hz, the performance almost equals the average performance of a standard OFDM.

Although slow hopping increases the estimation accuracy, fast hopping increases the diversity order, enhancing the correction capabilities of coding since errors are spread in time. However, this problem can be overcome by a deep interleaving, consequently the transmission delay will be penalised [15].

Interferences cause a serious impact on the system performance. From Figure 6, if we want to achieve the BER for the AWGN case, we are forced to reduce the number of active subcarriers in order to increase the SNR available at the receiver.

CONCLUSIONS

In this paper, the complete design of the most efficient useful symbol time and pilot density have been found for this trans-equatorial-belt 7900-miles-long ionospheric channel. On one hand, if the pilots are too close, the channel is oversampled and the efficiency is reduced without improving the estimation error. On the other hand, if the pilots are excessively spread along time and/or frequency dimension, the system performance will be dramatically reduced by channel aliasing. Although a generalized sampling theorem based on several mobile radio channel assumptions exists, a mismatch between the evaluation of that theorem and the exhaustive search for optimum symbol parameters has been exposed. In order to *a priori* properly estimate the pilot spacing requirements, several inputs are needed. First, an accurate path based channel sounding must be carried out in order to make the appropriate distinctions between path and multipath delay and doppler spread values. Second, without spreading gain, slightly high positive values of signal to noise ratio are needed in order to establish a reliable long distance link for low rate demanding applications. The OFDM has to be designed specifically for the time intervals where the propagation is good enough to transmit a non spread modulation.

Since a feedback channel is not available, frequency location information can not be known at the receiver. The risk of being jammed by a wideband interference can be overcome by hopping the OFDM signal among different carrier frequencies. Otherwise, if the carrier frequency is chosen based on link availability issues only, there is a risk of being jammed by wideband interference. The obtained results approach the average performance that we would get with a standard OFDM but without the risk of being continuously jammed.

In the next Antarctic campaign, an OFDM ionospheric link is expected to be established between SAB and OE based on the parameters found in this paper. The poor SNR available and the high interference level will constraint the maximum numbers of active subcarriers. A hexagonal pilot pattern with approximately 12 and 6 pilot spacing in frequency and time respectively will be used. Low complexity methods such Least Squares estimation and Nearest Pilot padding interpolation will be implemented

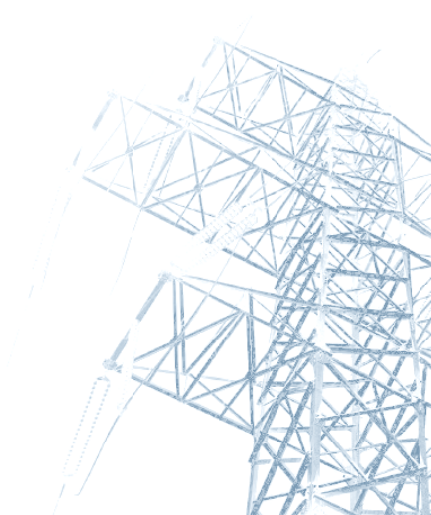
since a real-time FPGA based system is used for prototyping.

ACKNOWLEDGEMENTS

The aforementioned SANDICOM project has been developed in the framework of the research project REN2003-08376-C02-01 and the complementary action CGL2005-24213-E funded by the Spanish Government.

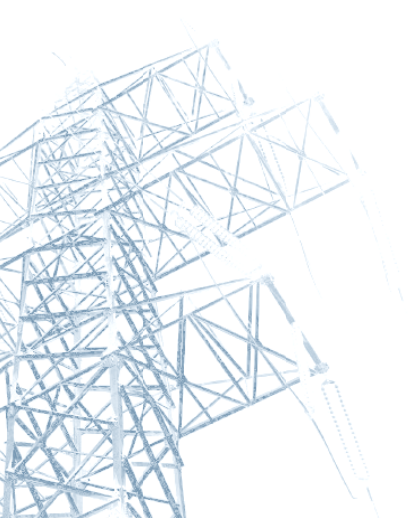
REFERENCES

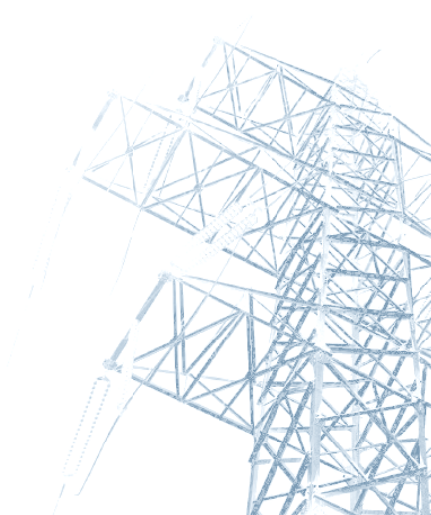
- [1] C. Vilella, J.C. Socoró, D. Miralles, J.L. Pijoan, P. Bergadà, "HF channel measurements for digital communications from Antarctica", 11th International ionospheric Effects Symposium IES 2005, May 2005.
- [2] C. Vilella, P. Bergadà, M. Deumal, J. L. Pijoan and R. Aquilué, "Transceiver Architecture and Digital Down Converter Design for Long Distance, Low Power HF Ionospheric Links", Proc. Ionospheric Radio Systems and Techniques, July 2006.
- [3] M. Deumal, C. Vilella, R. M. Alsina, J. L. Pijoan, "A DS-SS Signaling Based System Proposal for Low SNR HF Digital Communications", Proc. Ionospheric Radio Systems and Techniques, July 2006.
- [4] R. Aquilué, P. Bergadà, I. Gutiérrez, J.L. Pijoan, "Channel Estimation for Long Distance HF Communications based on OFDM Pilot Symbols", Proc. Ionospheric Radio Systems and Techniques, July 2006.
- [5] C. Vilella, J. Socoró, J. L. Pijoan, I. Gutiérrez and D. Altadill "An Antarctica to Spain HF Link. Oblique Sounding Results", Proc. Ionospheric Radio Systems and Techniques, July 2006.
- [6] P. Hoehner, S. Kaiser, and P. Robertson, "Two-dimensional pilot-symbol aided channel estimation by Wiener filtering", in Proc. ICASSP, Apr. 1997, pp. 1845–1848.
- [7] F. Sanzi and J. Speidel, "An adaptive two-dimensional channel estimator for wireless OFDM with application to mobile DVB-T", IEEE Trans. Broadcast., vol. 46, pp. 128–133, June 2000.
- [8] P. Hoehner, S. Kaiser, and P. Robertson, "Pilot-symbol-aided channel estimation in time and frequency", Proc. Int. Workshop Multi-Carrier Spread-Spectrum, Apr. 1997, pp. 169–178.
- [9] K. Fazel, S. Kaiser, Multi-Carrier and Spread Spectrum Systems, John Willey & Sons Ltd, 2003.
- [10] Meng-Han Hsieh, Che-Ho Wei, "Channel estimation for OFDM systems based on comb-type pilot arrangement in frequency selective fading channels", IEEE Transactions on Consumer Electronics, Volume 44, Issue 1, Feb. 1998 Page(s):217 – 225.
- [11] Morelli, Mengali, "A comparison of pilot-aided channel estimation methods for OFDM systems", IEEE Transactions on Signal Processing, Volume 49, Issue 12, Dec. 2001 Page(s):3065 – 3073.
- [12] M.J.F.-G. García, S. Zazo, J.M. Paez-Borrillo, "Pilot patterns for channel estimation in OFDM", IEEE Electronic Letters, Vol 36, 8 June 2000 Pages 1049-1050.
- [13] Van de Beek, Edfors, Sandell, Wilson, Borjesson, "On channel estimation in OFDM systems", Vehicular Technology Conference, 1995 IEEE 45th Volume 2, 25-28 July 1995 Page(s):815 - 819 vol.2.
- [14] I. Gutierrez, J.L. Pijoan, F. Bader , R. Aquilué, "New Channel Interpolation Method for OFDM Systems by Nearest Pilot Padding", in Proc. European Wireless 2006, March 2006.
- [15] L. Hanzo, S. X. Ng, T. Keller, W. Webb, "Quadrature Amplitude Modulation: From Basics to Adaptive Trellis-Coded, Turbo-Equalised and Space-Time Coded OFDM, CDMA and MC-CDMA Systems", John Wiley & Sons, Ltd. 2004.



8.2. APPENDIX A.2

R. Aquilué, M. Deumal, J.L. Pijoan, L. Corbeira, "A Low Complexity Multicarrier Proposal for Medium Rate Demanding Automatic Meter Reading Systems", in Proc. IEEE Symposium on Power Line Communications and its Applications (ISPLC2007), Pisa, Italy, 2007.





A Low Complexity Multicarrier Proposal for Medium Rate Demanding Automatic Meter Reading Systems

Ricard Aquilué*, Marc Deumal*, Joan Lluís Pijoan* and Laura Corbeira†

* Department of Communications and Signal Theory, La Salle Engineering, Ramon Llull University. Barcelona, Spain. Email: {raquilue,mdeumal,joanp}@salle.url.edu

† Endesa Network Factory, Centro Referencia Aplicaciones Tecnológicas. Barcelona, Spain.

Abstract—In Automatic Meter Reading (AMR) technology, electrical utilities (EUs) have been exploiting their own infrastructure to bill their customers in an efficient and economical way using Power Line Communications (PLC) technologies. Since the amount of data that has to be send is quite low related to the available time to perform this task, AMR applications have been demanding low bit rates. At this moment, EUs are exploring and demanding other services as load and alarm management, remote monitoring and disconnections, etc. In this context, the Low Voltage PLC modems should provide more throughput while keeping the cost of the hardware low. In this paper, a low complexity multicarrier modulation is proposed in order to exploit the CENELEC A Band.

I. INTRODUCTION

The power line network has not been originally designed to transmit data, but the large coverage of the low voltage (LV) network has become a great opportunity to electrical utilities (EUs) to offer a “last-mile” communication alternative [1]. Another major application for Power Line Communications (PLC) in the LV network is Automatic Meter Reading (AMR) technology [2]. This application is especially interesting to EUs due to the fact that they can bill the customer by exploiting their own network, while meaning a cost reduction and the opportunity of offering added-value services.

A lot of research has been made in the field of broadband PLC, but little documentation can be found regarding systems in the low frequency range (below 100 kHz), sometimes because few studies have been done, sometimes because of its confidentiality. This work will be focused on the CENELEC EN50065, which rules the frequency usage from 3 to 148.5 kHz , concretely, on the A band, reserved for EU [3]. This band ranges from 9 to 95 kHz and it is characterized by high noise power spectral densities at lower frequencies, up to several tens of kHz , and a dense concentration of narrowband interferences [4].

Several solutions have been found, among them, we can highlight the narrowband designs of ST (ST7538, FSK) [5] or Echelon (PL3120, BPSK) [6] and the ones of AMIS (AMIS-30585, S-FSK) [7] and Yitran (IT800, DCSK) [8]. Another versatile solution based on DSP is offered by Texas Instruments [9].

The EUs are demanding new applications to the typical AMR system, e.g. dynamic node discovery capabilities, power consumption profiles, load connections and disconnections, alarm management... These new applications need an increase of the system performance in order to cope with the higher demanded throughput, without compromising the cost of the equipment, since the deployment and exploitation of the technology has to be profitable. The aim of this paper is to propose a low complexity physical layer approach, overcoming the rate limitation of the existing solutions, while keeping the complexity of the modulation technique reduced and the hardware costs low.

Reducing the complexity of the equipment means reducing the cost of the synchronization stages. We can distinguish three synchronization stages: time, phase and frequency. These are the approaches that we will follow in this work:

- *Time Synchronization*: Symbol windowing will be carried out by means of the zero crossings of the mains voltage carrier [10]. In order to cope with the drawbacks of this time reference, a multicarrier (MC) approach will be proposed.
- *Frequency Synchronization*: It is well known that frequency synchronization is a critical point of MC modulations. Since no frequency synchronization will be performed, the MC design and subcarrier separation have to cope with the possible deviations between the transmitter and the receiver clocks.
- *Phase Synchronization*: In order to avoid the phase recovery stage, a differential modulation will be proposed.

This paper is organized as follows: In Section II the advantages and the problems of windowing the symbol by using the mains voltage zero-crossing will be discussed. In this section the impact in the performance of the jitter of the zero-crossings will be theoretically analyzed and the use of a (MC) modulation will be justified. In Section III, an adjustment of the MC symbol will be carried out in order to cope with the frequency offset caused by the non idealities of the transmitter and receiver clocks, and finally, concluding remarks will be summarized in Section IV.

TABLE I
ZERO-CROSSING JITTER PARAMETERS

| | |
|--------------------|-----------------------------------|
| Propagation Speed | $0.577 \cdot c_0$ |
| DOWNLINK | |
| Mean | $\mu = 0$ |
| Standard Deviation | $STD \in (30, 100)\mu sec$ |
| UPLINK | |
| Mean | $\mu = 11.55 \frac{\mu sec}{K m}$ |
| Standard Deviation | $STD \in (30, 100)\mu sec$ |

II. TIME SYNCHRONIZATION

In AMR systems, time synchronization methods carried out by means of mains voltage zero-crossing are preferred in order to develop low cost modems. This time reference is not a fully reliable reference, since the crossing moments are affected by a jitter [10]. In this Section, we will assume a zero crossing rate of 100 Hz, as well as a BPSK single carrier modulation as a first approach of modulation scheme.

A. Time Reference

From [10], the zero-crossing can be characterized as a Gaussian random process as can be seen in Table I. When information is sent from the Transformation Center (TC)¹ to the customer site, the data and the time reference propagate in the same direction. Otherwise, if data is sent from the customer modem to the TS, the data and time reference propagate in opposite directions. In this case, a distance dependent delay between the data and the time reference occurs. The uncertainty of the zero-crossings around the mean is up to $STD = 100 \mu sec$ in the worst case. This variance will be used in the sequel.

B. Performance Degradation due to the Jitter

Next, the degradation of the system performance due to a time misalignment for a narrowband BPSK approach will be deduced. In Fig. 1, the received signal $r_i(t)$ is the sum of the transmitted symbols $s_i(t)$ and the Additive White Gaussian Noise (AWGN) $n(t)$, where $s_0(t) = A\pi\left(\frac{t-T}{T}\right)$ and $s_1(t) = -A\pi\left(\frac{t-T}{T}\right)$ are the two possible BPSK symbols. The matched filter $h(t)$ is matched to the difference signal defined as $c(t) = s_0(t) - s_1(t)$. Then, after the receiving filter, we have $z_i(t)$ that is the sum of the signal $a_i(t)$ and AGN noise $n_c(t)$, and finally, the sampled signal z_i that will be tested against the decision threshold γ . Let us define T as the bit time, T' as the symbol time (with BPSK $T = T'$), $d \in (0, 1)$ as the ratio between the time misalignment and T' .

First, we will suppose that we have no adjacent symbols, that is, there will be no signal energy in the time interval $d \cdot T$. We define the sampled signal at the output of the correlator as a_0 and a_1 when $s_0(t)$ and $s_1(t)$ are received respectively ((1) and (2)).

¹The TC is where the low voltage transformer is located and where the connection point that aggregates the PLC clients of that TC is coupled.

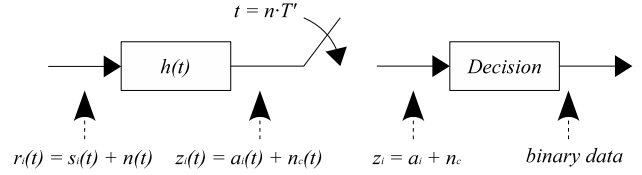


Fig. 1. Receiver block diagram

$$a_0 = s_0(t) * h(t) \Big|_{t=n \cdot T'} = 2A^2T(1-d) \quad (1)$$

$$a_1 = s_1(t) * h(t) \Big|_{t=n \cdot T'} = -2A^2T(1-d) \quad (2)$$

The system error probability is given in (3), where $p_e(e/s_0(t))$ and $p_e(e/s_1(t))$ are the conditional probabilities and $p(s_0(t))$ and $p(s_1(t))$ the probability of transmitting $s_0(t)$ and $s_1(t)$ respectively.

$$p_e(e) = p(s_0(t)) \cdot p_e(e/s_0(t)) + p(s_1(t)) \cdot p_e(e/s_1(t)) \quad (3)$$

Assuming equiprobable symbols, (3) yields to (4), where σ_c^2 is the noise power after the correlator. The expression of this power is given in (5), where $\frac{N_0}{2} \left[\frac{W}{Hz}\right]$ is the noise power density at the input of the receiver.

$$p_e(e) = Q\left(\frac{2A^2T(1-d)}{\sigma_c}\right) \quad (4)$$

$$\sigma_c^2 = \frac{N_0}{2} \int_{-\infty}^{\infty} |h(t)|^2 dt = 2N_0A^2T \quad (5)$$

If we substitute the bit energy $E_b = A^2T$ and (5) in (4), we finally obtain the probability of error due to a windowing misalignment without the presence of an adjacent symbol in (6).

$$p_e(e) = Q\left(\sqrt{\frac{2E_b(1-d)^2}{N_0}}\right) \quad (6)$$

Only at the beginning or at the end of a frame we could have no interference from adjacent symbols. In the other cases, if a windowing misalignment occurs, we will be feeding the correlator with energy of another symbol, causing intersymbol interference (ISI) [11].

When the same symbols are transmitted, the correlator will give the same output as if we had no interference. In this case, the performance of the system can be obtained from (6) with $d = 0$. Maintaining the condition of equiprobability between $s_0(t)$ and $s_1(t)$, interfered and interfering will be the same with a probability of 0.5. Otherwise, if adjacent symbols are

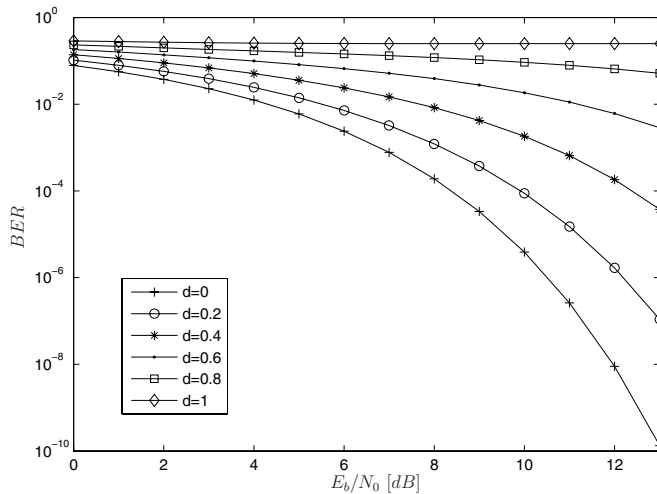


Fig. 2. BPSK Performance as a function of the parameter d

different, and the interference lasts for a period of $d \cdot T$ seconds, a decrease of the available energy for the detection stage will be caused, leading to a degradation of the performance given by (6) with $d' = 2d$.

$$p_{e,d,T}(e) = 0.5 \cdot Q\left(\sqrt{\frac{2E_b}{N_0}}\right) + 0.5 \cdot Q\left(\sqrt{\frac{2E_b(1-2d)^2}{N_0}}\right) \quad (7)$$

where

$$E_b = \int_0^T |s_0(t)|^2 dt \quad (8)$$

Finally, the probability of error that we will use is shown in (7) and Fig. 2, where, on one hand, performance is dramatically reduced as long as d increases, and, on the other hand, as the symbol rate is reduced, the ratio d decreases and the performance of the system increases. There is a trade off between rate and quality. This problem can be overcome by splitting the high rate data stream into several low rate subchannels, leading to a MC approach.

C. Multicarrier Proposal

A MC symbol is given by the complex modulation sequence shown in (9), where $s(t)$ is the time domain signal representation, N_{SC} is the number of substreams or the number of subcarriers, $b_n \in \{-1, 1\}$ are the BPSK modulated symbols, Δf is the minimum intercarrier spacing necessary to keep those subcarriers orthogonal, $m\Delta f$ is the real intercarrier separation and n is the subcarrier number where $n = 0, 1, 2, \dots, N_{SC}-1$ [12].

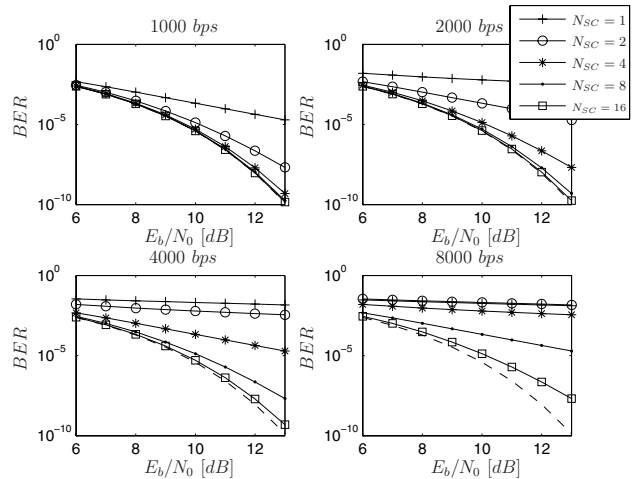


Fig. 3. System Performance ($p_{e,T'}(e)$) as a function of N_{SC}

$$s(t) = \sum_{n=0}^{N_{SC}-1} b_n e^{j2\pi(f+nm\Delta f)t} \cdot \Pi\left(\frac{t}{T'}\right) \quad (9)$$

where

$$T' = T \cdot N_{SC} \quad (10)$$

In Fig. 3 and (11), the influence of the probability distribution of the jitter is applied using a normal distribution ($p_j(j)$) with mean $\mu = 0$ and standard deviation $STD = 100 \mu sec$. The dashed line represents the optimum situation ($d = 0$). This distribution has been discretized in $1 \mu sec$ steps and jitters between $\pm 400 \mu sec$ have been taken into account (this represents the $erf\left(\frac{4}{\sqrt{2}}\right) \approx 1 - 10^{-5}$ of the set). Thus, the probability of error, as a function of the symbol rate ($R_s = \frac{1}{T'}$), is found as follows:

$$p_{e,T'}(e) = \sum_{jitter=-400\mu sec}^{400\mu sec} p_j(jit) \cdot p_{e,\frac{jit}{T'}}(e) \quad (11)$$

For reduced data rates (i.e. 1000 bps), the splitting of the data into more than two subchannels has little effect in the improvement of the system performance. As long as the data rates increase, a higher number of subcarriers is required in order to maintain the BER low.

D. Cyclic Prefix

In the previous subsection, the superior performance of splitting the high rate single carrier signaling into several low rate MC subchannels has been shown. The longer the symbol is, the better $d = \frac{jitter}{T'}$ ratio, but the ISI between MC symbols is still present with a probability of $p_j(j)$. In order to reduce, even more, the effect of the jitter (ISI), we will add a cyclic prefix (CP^+) and a cyclic postfix (CP^-) at the beginning and at the end of each MC symbol respectively [12]. The objective of the insertion of these pre and postfixes is the cancellation

of the ISI (this will keep the N_{SC} subcarriers orthogonal) as long as the $\pm dT'$ is less than the duration of the cyclic pre and postfix. Since being misaligned $+dT'$ and $-dT'$ is equiprobable, we will set the same duration to the prefix and postfix. We will refer to this duration with the $c = \frac{CP_l}{T'}$ ratio, where CP_l is the CP^+ and CP^- length.

In order to evaluate the impact on the performance of the use of the CP^+ and CP^- , we will redefine the distribution of probability of the jitter ($p'_j(j)$) as can be seen in (12).

$$p'_j(j) = \begin{cases} p_j(0) + 2 \sum_{n=1}^{CP_l} p_j(n) dj & j = 0 \\ 0 & j \in [-CP_l, 0) \cup (0, CP_l] \\ p_j(j) & \text{others} \end{cases} \quad (12)$$

Using this distribution, the probability of error as a function of c , d and T' is shown in (13).

$$p_{e,c,T'}(e) = \sum_{jit=-400\mu sec}^{400\mu sec} p'_j(jit) \cdot p_{e,c,\frac{jit}{T'},T'}(e) \quad (13)$$

where

$$p_{e,c,d,T'}(e) = 0.5 \cdot Q \left(\sqrt{\frac{2E_b \left(1 - \frac{2c}{N_{SC}}\right)^2}{N_0}} \right) + 0.5 \cdot Q \left(\sqrt{\frac{2E_b \left(1 - \frac{c}{N_{SC}} - 2\frac{d-c}{N_{SC}}\right)^2}{N_0}} \right)$$

From (13), we can expect a decrease of the system performance, since the use of cyclic pre and postfixes implies a waste of power that will not be used for signal detection. Fig. 4 depicts this situation. For reduced data rates (i.e. 1000 bps) and a N_{SC} of 8 or 16, the performance degradation due to the reduction of the power available for detection is negligible. Obviously, as the data rates increase while the number of subcarriers remains constant, that waste of power notably reduces the performance of the system.

Although it seems that it is not worth to employ a cyclic prefix, since far away from improving the performance, it is reduced; the advantage of using these CPs is that we are preventing intercarrier interference (ICI). In a MC environment, when ISI occurs, not only the degradation shown in Fig. 3 succeed, moreover, the orthogonality among subcarriers is destroyed [12], causing a higher degradation that the one caused by ISI in a single carrier situation. The use of the cyclic prefix will allow us to keep the subcarriers orthogonal when time misalignment occurs, preventing ISI from causing ICI.

Among other sources of ICI, in this approach we will focus on the different clock frequencies between the transmitter and the receiver. In the next section, a study of the frequency mismatch effect between clocks will be fulfilled.

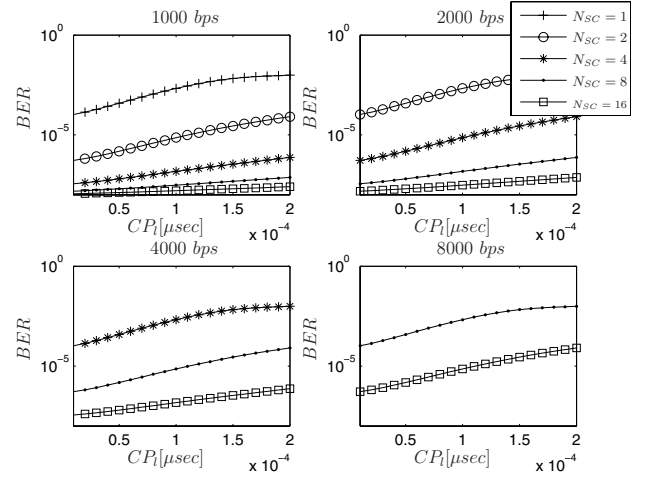


Fig. 4. System Performance ($p_{e,c,T'}(e)$) as a function of c ($\frac{E_b}{N_0} = 12dB$)

III. FREQUENCY SYNCHRONIZATION

Apart from the advantages above mentioned, MC modulations are very sensitive to synchronization errors [12]. The frequency offset correction between transmitter and receiver is a key step in the demodulation process. In our scenario, this frequency offset is caused by a frequency mismatch between the transmitter and the receiver clocks.

If the frequency offset is not corrected before the MC demodulation, two problems arise. First, we are not sampling the subcarriers in the optimum point, so a decrease of the available power that will be used for detection occurs. Second, this deviation from the optimal sampling point will yield to the undesirable sampling of the others subcarriers causing ICI.

From (9), the spectral representation of a MC signal can be expressed as (14), where SC_n is the n -subcarrier spectrum. Let's see the performance degradation caused by a frequency offset of $\xi_f [Hz]$ between the transmitter and receiver clocks (see Fig. 5).

$$\begin{aligned} S(f) &= \sum_{n=0}^{N_{SC}-1} b_n \frac{\text{sinc}\left(\frac{f+nm\Delta f}{\Delta f}\right)}{\Delta f} \\ &= \sum_{n=0}^{N_{SC}-1} b_n \cdot SC_n(f, m, T') \end{aligned} \quad (14)$$

Several studies approach this ICI as a noisy Gaussian process applying the central limit theorem [12], [13]. This is only applicable when the number of subcarriers is high enough. In this work, an exact calculation is derived, useful for a low number of subcarriers. From a given N_{SC} , m , T' and ξ_f , we have to expect a decrease of the signal of interest amplitude and the contribution of the constructive or destructive levels of adjacent subcarriers. If we have N_{SC} subcarriers, we have $N_{SC}-1$ potential interferers and $2^{N_{SC}-1}$ combinations ($c_0, c_1, \dots, c_{2^{N_{SC}-1}-1}$) of this interferers that will contribute to the detected level of the signal of interest.

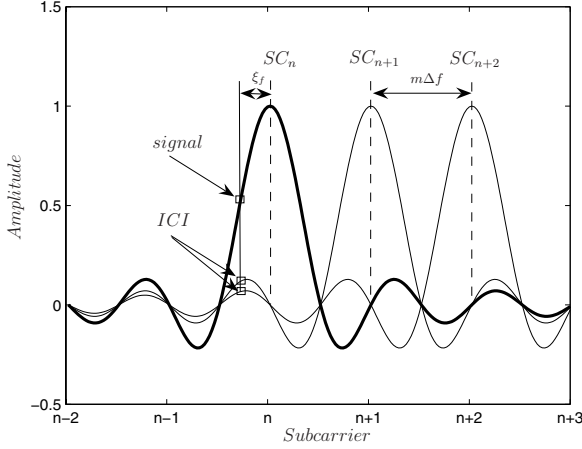


Fig. 5. MC spectrum

The signal level that will be given to the decision stage of the demodulation of the subcarrier n being affected by a combination c of the interferers is $a_{n,c}(\xi_f, m, T') = b_n SC_n(f_n + \xi_f, m, T') + \underbrace{\sum_{i=0, i \neq n}^{N_{SC}-1} b_{i,c} SC_i(f_n + \xi_f, m, T')}_{ICI}$

where $b_{i,c}$ is the BPSK symbol of the subcarrier i of the combination c . In this scenario, with a probability of the combination $p(c) = \frac{1}{2^{N_{SC}-1}}$, we can define the probability of error of the subcarrier n and the overall probability of error as shown in (15) and (16) respectively.

$$p_{e,n,\xi_f,m,T'}(e) = \sum_{c=0}^{2^{N_{SC}-1}-1} p(c) Q_{n,c,\xi_f,m,T'} \quad (15)$$

where

$$Q_{n,c,\xi_f,m,T'} = Q\left(\sqrt{\frac{2 a_{n,c}(\xi_f, m, T')^2 T'}{N_0}}\right)$$

$$p_{e,\xi_f,m,T'}(e) = \frac{1}{N_{SC}} \sum_{n=0}^{N_{SC}-1} p_{e,n,\xi_f,m,T'}(e) \quad (16)$$

The relative frequency offset to the intercarrier spacing can be defined as $\nu = \frac{\xi_f}{\Delta f}$. For a given ξ_f , it is interesting to choose a high enough Δf in order to keep ν as low as possible. If the SC_n are too narrow, the frequency offset will cause a low amplitude sampling of those SC_n . Otherwise, if we set SC_n wide enough, for a fixed ξ_f , we will sample more signal level. From (14) and Fig. 4 a reasonable trade off between SC_n width and robustness against the jitter can be a T' of 1 msec. This symbol rate ($R_s = \frac{1}{T'} = 1 \text{ KSpS}$), can be delivered with several values of N_{SC} . The higher N_{SC} , the more throughput we will get, but more interferers we will have in case of $\xi_f \neq 0$. From (16), for this first proposal, we will choose $N_{SC} = 8$ and $R = 8000$, as well as a cyclic prefix length of 200 μsec and a postfix of the same length, giving in

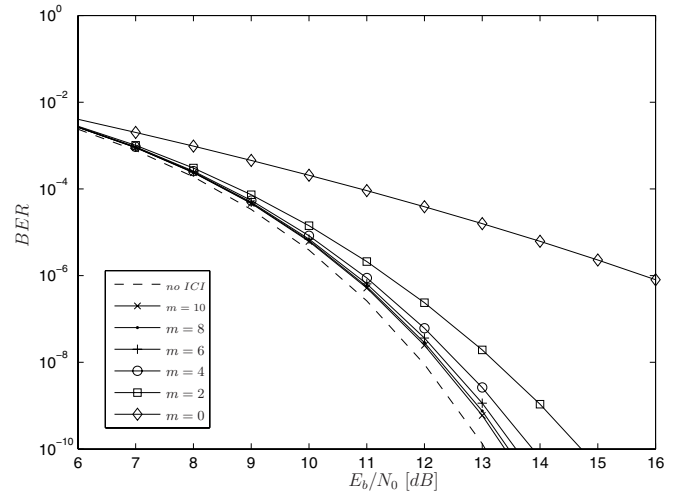


Fig. 6. System performance in front of a $\xi_f = 253 \text{ Hz}$ for a $N_{SC} = 8$ and $R = 8000 \text{ bps}$

a useful symbol time of $T_U = \frac{1}{\Delta f} = 600 \mu\text{sec}$. These values yield to a $\nu = 0.07$ while given a high enough number of subcarriers to deal with the jitter and small enough to allocate them in a friendly frequency range of the CENELEC A Band, as it will be shown later.

In order to avoid the introduced ICI, we will spread the subcarriers $m \cdot \Delta f \text{ Hz}$. Fig. 6 depicts the effect on the system performance of spreading the subcarrier more than what is strictly necessary. The dashed line represents the ICI-free scenario. For $m = 1$, the performance dramatically decreases to an unacceptable levels, for $m = 4$, it approaches the ideal dashed line, occupying a bandwidth of $\Delta f \cdot m \cdot N_{SC} = 53.3 \text{ kHz}$. For $m > 4$, performance is slightly improved.

IV. PHASE ESTIMATION

The last synchronization stage to be faced is the phase detection and compensation in order to correctly detect the BPSK symbols. In our approach, the differential version of the BPSK is proposed instead of the coherent one. The DBPSK receiver is less complex and offers similar performance than its coherent implementation. For $\frac{Eb}{N_0} > 10 \text{ dB}$, the BPSK outperforms the DBPSK by approximately 1 dB only [11].

All the discussion made up to this point is valid for a DBPSK approach by shifting the performance curves 1 dB.

V. CONCLUSION

In order to deploy an AMR network, the cost of the equipment on the customer premises and the added value services that the system provides are two key factors in its business case. If we focus on modulation issues, the synchronization procedures are the most critical points that affect the complexity and cost of the equipment. In this situation, it is mandatory to use the implicit time reference that the power line network offers. Due to the jitter, the mains voltage zero-crossings offer a reliable time reference for reduced symbol rates. There are two options in order to increase the data rate: either increasing

TABLE II
PROBABILITY OF ICI

| $CP[\mu sec]$ $STD[\mu sec]$ | 0 | 40 | 80 | 120 | 160 | 200 |
|---------------------------------|---|-----------|-----------|-----------|-----------|------------|
| 30 | 1 | $2e^{-1}$ | $8e^{-3}$ | $6e^{-5}$ | $1e^{-7}$ | $3e^{-11}$ |
| 44 | 1 | $4e^{-1}$ | $7e^{-2}$ | $6e^{-3}$ | $3e^{-4}$ | $5e^{-6}$ |
| 58 | 1 | $5e^{-1}$ | $3e^{-1}$ | $4e^{-2}$ | $6e^{-3}$ | $6e^{-4}$ |
| 72 | 1 | $6e^{-1}$ | $3e^{-1}$ | $9e^{-2}$ | $2e^{-2}$ | $5e^{-3}$ |
| 86 | 1 | $6e^{-1}$ | $3e^{-1}$ | $1e^{-1}$ | $6e^{-2}$ | $2e^{-2}$ |
| 100 | 1 | $7e^{-1}$ | $4e^{-1}$ | $2e^{-1}$ | $1e^{-1}$ | $4e^{-2}$ |
| Mean | 1 | $5e^{-1}$ | $2e^{-1}$ | $9e^{-2}$ | $3e^{-2}$ | $1e^{-2}$ |

TABLE III
MC MODULATION PARAMETERS

| | |
|----------------------------|---|
| Symbol Time | $T' = 1 msec$ |
| Cyclic Prefix Length | $CP^+ = 200 \mu sec$ |
| Cyclic Postfix Length | $CP^- = 200 \mu sec$ |
| Useful Symbol Time | $T_U = 600 \mu sec$ |
| Number of Subcarriers | $N_{SC} = 8$ |
| Mapping | $DBPSK$ |
| Bit Rate | $R_b = 8000 bps$ |
| Minimum Subcarrier Spacing | $\Delta f = 1.6 \hat{k}Hz$ |
| Real Subcarrier Spacing | $m \cdot \Delta f _{m=4} = 6.6 \hat{k}Hz$ |
| Occupied Bandwidth | $BW = 53.3 \hat{k}Hz$ |
| Central frequency | $f_c = 41.6 \hat{k}Hz$ |

the modulation level or transmitting several low symbol rate parallel streams. Since the channel impairments claim for a robust mapping, only one bit per symbol has to be transmitted and BPSK is used as a reliable modulation scheme. In this paper, we have shown how the zero-crossing jitter effects can be mitigated by means of employing a MC modulation and CPs.

The sensitivity to ICI is one of the main drawbacks of MC modulations. In this scenario, ICI is caused by ISI and by the frequency difference between system clocks. The first source of ICI is attenuated by means of the CPs. This solution covers approximately $1 - 1e^{-2}$ of the occurrences (See Table II for $CP_l = 200 \mu sec$). As far as the second source of ICI is concerned, the separation of the N_{SC} subcarriers along the available frequency range more than what is strictly necessary reduces the effect of the interferers subcarriers into the subcarrier of interest. This subcarrier has to be wide enough to minimize ν as much as possible, thus delivering enough signal level to the demodulator. Coherent MC modulations need a channel estimation stage before signal demapping and detection. This process involves an added complexity to the system, so, the differential version of the BPSK will avoid that cost with a low decrease of the system performance. In Table III, the MC modulation parameters are shown. In order to avoid the noisiest regions of the available A band, the MC spectrum is right shifted, occupying the upper frequency range.

Due to the robustness of the MC modulation in front of the

jitter and the spreading of the subcarriers, the cost of time and frequency synchronization is avoided. The FFT demodulation is the only cost of the data demodulation process. In order to sample the $BW = 53.3 \hat{k}Hz$ in $(N_{SC} - 1) \cdot m + 1 = 29$ points, a 32 FFT has to be executed each symbol time T' leading to a required computational cost of less than 100 *KOperations* per second.

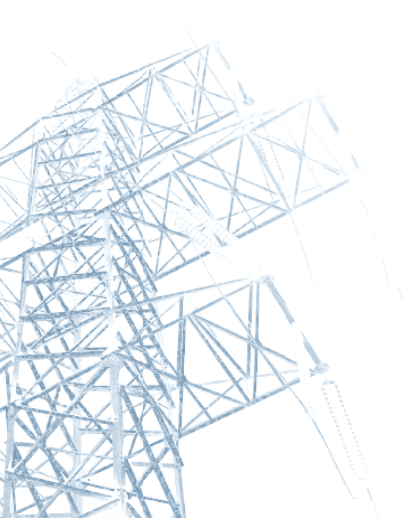
Further research has to be done in order to select the best codes in terms of peak to average power ratio reduction and data protection.

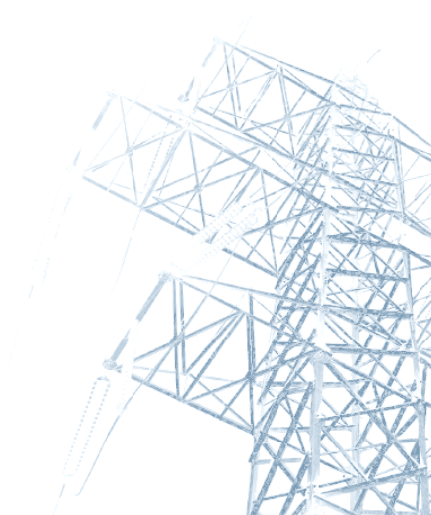
REFERENCES

- [1] L. Weilin, H. Widmer, and P. Raffin, "Broadband plc access systems and field deployment in european power line networks," *IEEE Communications Magazine*, vol. 41, pp. 114–118, May 2003.
- [2] N. Miura, H. Sato, H. Narita, and M. Takaki, "Automatic meter-reading system by power line carrier communications," *Proc. IEE Generation, Transmission and Distribution*, vol. 137, pp. 25–31, Jan. 1990.
- [3] CENELEC, "Signalling on low-voltage electrical installations in the frequency range 3 khz to 148,5 khz – part 1: General requirements, frequency bands and electromagnetic disturbances," EN 50065-1:2001, 2001.
- [4] E. N. Factory, "Medidas ENDESA PLC banda estrecha (Narrowband PLC measurements, ENDESA)," Endesa Network Factory, Barcelona, Tech. Rep., Mar. 2005.
- [5] STMicroelectronics, "ST7538 FSK power line transceiver," STMicroelectronics, Tech. Rep., Nov. 2005.
- [6] Echlon, "PL3120 and PL3150 power line smart transceivers," Tech. Rep.
- [7] AMIS, "AMIS-30585 S-FSK plc modem," AMIS, Tech. Rep., June 2005.
- [8] Y. Communications, "IT800-DS-016-R1.2," Yitran Communications, Tech. Rep.
- [9] T. Instruments, "TMS320C2000 digital signal controller power line communication," Texas Instruments, Tech. Rep., Aug. 2005.
- [10] K. Dostert, *Powerline Communications*. Prentice Hall, 2001.
- [11] J. G. Proakis, *Digital communications*, 4th ed. McGraw-Hill, 2000.
- [12] K. Fazel and S. Kaiser, *Multi-Carrier and Spread Spectrum Systems*. John Wiley & Sons, 2003.
- [13] L. Hanzo, S. Ng, T. Keller, and W. Webb, *Quadrature Amplitude Modulation*. John Wiley & Sons, 2003.

8.3. APPENDIX A.3

R. Aquilué, M. Ribó, J.R. Regué, J.L. Pijoan, G. Sánchez, “Urban Underground Medium Voltage Channel Measurements and Characterization”, in Proc. IEEE Symposium on Power Line Communications and its Applications (ISPLC2008), Jeju, South Korea, 2008.





Urban Underground Medium Voltage Channel Measurements and Characterization

Ricard Aquilué*, Miquel Ribó*, Joan Ramon Regué*, Joan Lluís Pijoan* and Germán Sánchez†

* Department of Communications and Signal Theory, La Salle Engineering,
Ramon Llull University, Barcelona, Spain. Email: {raqilue,joanp}@salle.url.edu

† ENDESA Network Factory, Createc.
Barcelona, Spain.

Abstract—Power line communications (PLC) technologies rely on the power grid for data transmission. Since the communications channel is already deployed, this communication alternative is specially interesting for the power grid owner, i.e., the electrical utility (EU). Focusing on the MV distribution network, located after the last step-down electrical substation, with typical levels from 6 to 25 kV, feeds directly large commercial or industrial consumers and domestic and small commercial consumers through several transformer stations. The growing interest on MV-PLC technology, the natural aggregation point for data coming and going into the LV network, faces the same issue that the LV-PLC technology did (and does): standardization. In this way, a properly implemented channel model will allow the design of suitable modulation and access methods. This paper presents a complete set of measurements done in a MV urban underground ring and proposes a deterministic model for the MV-PLC transfer function.

I. INTRODUCTION

The world of power line communications (PLC) can be divided into three main types: low voltage (LV) PLC, medium voltage (MV) PLC and high voltage (HV) PLC. These last years, LV-PLC has attracted a great expectation. With the telecommunications market liberalization, together with the energy market deregulation, EUs can use their own infrastructure, the power line grid (specially the MV and LV networks), to deliver communications services and increase their control, monitoring and billing capabilities over costumers' behavior.

In conjunction with the LV network, the MV network comprises the distribution stage of the electric power grid. Focusing on MV, the MV-PLC technology can be considered as the natural aggregation point for data coming in and going out the LV network. Located after the last step-down electrical substation (ES), and with typical levels from 6 to 25 kV, the MV network feeds directly large commercial or industrial consumers and domestic and small commercial consumers through several transformer stations (TS). This work will focus in urban networks, where the MV network is fully underground.

A key point in a physical layer design process is channel modeling. If properly implemented, the channel model will allow the design of suitable modulation and access methods. Before modeling, channel characterization has to be carried out. Basically, two different approaches regarding channel characterization can be followed:

Behavioral This is a top-down strategy, followed when dealing with random channel effects, such as the noise scenario [1] or when the channel topology is casuistic is extremely large, e.g., LV networks [2].

Structural This is a bottom-up strategy, where physical parameter estimation is derived from single measurements of the power line network elements. Focusing MV channel characterization, some transmission line model based works can be found, e.g., [3]–[5].

On the other hand, two different approaches can be followed regarding channel modeling:

Stochastic Derived from behavioral characterization, typically employed when modeling noise or complex topologies [6], [7].

Deterministic Derived from structural measurements, without random elements.

The aim of this work is to measure the structural parameters of a MV ring and their devices in order to deterministically model their behavior and then, based on statistic records of European MV networks [8], tune the physical parameters that will make the model valid for several regions. Moreover, statistics regarding the noise scenario and a methodology for channel input impedance measure will be given.

This paper is organized as follows. In Section II a brief description of the network under study will be given, while in Section III, the measurement set-up will be explained. Then, in Section IV the structural and behavioral characterization will be carried out. Finally, the validation of the transfer function characterization and the concluding remarks will be given in Section V.

II. MV NETWORK TOPOLOGY

Regarding the MV distribution power grid, there are basically three topologies: star, ring and mesh. This work is focused on the typical urban ring topology [9]. In urban areas, ENDESA is now mainly deploying 18/30 kV unipolar underground cable, with triple extruded aluminium core and cross linked polyethylene (XLPE) dielectric, compiling the rules EN-50267-2-1, IEC-60502.2 and ENDESA proprietary rules DND001 and SND013. When the MV line enters the TS (Fig. 1) it has to pass through the input and output breaker to follow its way through the ring. If the MV to LV transformer

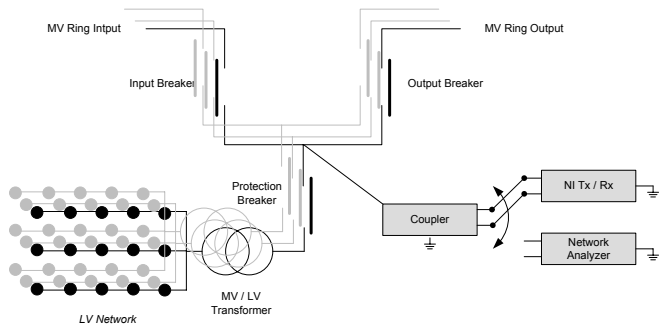


Fig. 1. Transformer Substation Schematic and Field Measurements Set-up

is wanted to be in service, the protection breaker has to be switched on. In this work, the PLCoupling / DIMAT CAMT-1 capacitive coupler has been used [10]. Near the mains frequency, MV channel access impedance varies influenced by the mains level. Otherwise, for frequencies over tens of kilohertz, HV/MV and MV/LV transformers are almost perfect barriers [11].

In this work, different measurements will be carried out in order to characterize the following urban underground MV channel effects [1], [12]:

- Input impedance. Mainly affected by:
 - Characteristic impedance of the MV cable.
 - Connected feeder's loads.
- Noise scenario .
 - Background colored noise: In MV networks, this noise is mainly caused by leakage or discharge events, power converters, transformer non idealities... As well as in HV networks, stationary low-power periodical and synchronous with the mains impulse events can also be considered background noise.
 - Impulse events: The main causes of this noise type are network switching transients, lightning and other discharging events.
 - Narrowband noise: Narrowband interferences.
- Attenuation and frequency selectivity. Caused by power dissipation and reflections in the grid or coupling devices.

III. MEASUREMENT SET-UP

In this Section, two measurement set-ups will be briefly described. The first one, depicted in Fig. 1, shows the set-up for the measurements carried out in the MV ring. A Network analyzer (NA), two National Instruments PXI chassis, one of them carrying an arbitrary generator board [13] and another a high speed digitizer [13], both GPS synchronized, phase-to-ground coupled by means of a PLCoupling / DIMAT CAMT-1 capacitive coupler [10], have been employed. This set-up was used for the *Field measurements*, explained in the next Section. The second one, depicted in Fig. 2, describes the set-up for the MV cable and coupler scattering (S) parameters [14] characterizations, explained in *Laboratory measurements*.

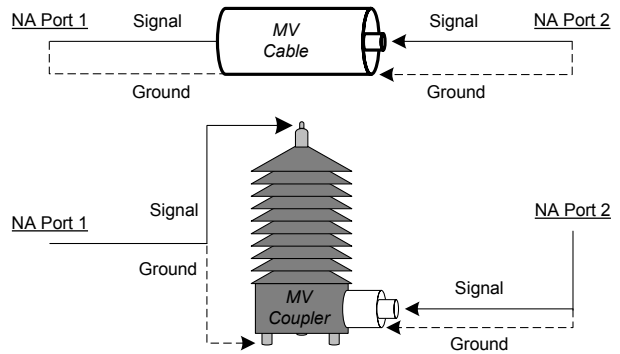


Fig. 2. Network Analyzer Set-up

IV. MEASUREMENTS AND RESULTS

The aim of this work is to provide a set of measurements in order to get the needed behavioral and structural knowledge to define a proper model for MV urban networks. This set of measurements consists of:

- 1) Field measurements (FM). The following measurements have been done in a 324 meters link in Barcelona, Spain, between the FECSA/ENDESA substations BA07460 (transmitter) and BA07155 (receiver):
 - Link attenuation characteristics.
 - Link time and frequency spread.
 - Background noise.
 - Impulsive interferences.
 - Reflection coefficient.
- 2) Laboratory measurements (LM):
 - MV cable S parameters characterization.
 - MV coupler S parameters characterization.
- 3) Joint measurements:
 - Input Impedance.

A. FM: Link Attenuation Characteristics

The link attenuation characteristics have been measured by means of a GPS synchronized sweep transmission from 100 kHz to 30 MHz in 100 kHz steps. The receiver averaged the measured level during one second in order to minimize the impact of noise. In Fig. 3, the attenuation of the link under study is depicted. The dashed line shows the overall link attenuation, i.e., the attenuation due to the cable losses, the reflection and transmission capabilities of the coupler and the input impedance and parallel loads connected to that link. As stated, since there are more parameters than the intrinsic cable attenuation, the continuous line depicts an approximation of the attenuation per hundred meter, showing similar values as the ones in [15]. This measure will be recalled in Section V when validating the channel characterization.

The time behavior of this characteristic is notably constant, with negligible variations over time. The attenuation characteristic band-pass shape is mainly due, on one hand, to the 1 nF coupler capacitor and to the effect of the embedded

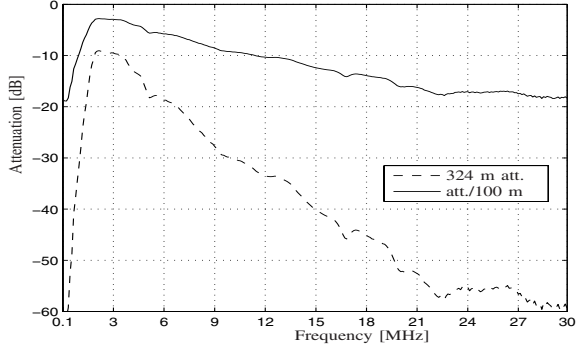


Fig. 3. Measured Link Attenuation

impedance matching network ¹, and, on the other, to the MV cable attenuation.

B. FM: Link Time and Frequency Spread

By means of pseudo-noise (PN) based channel sounding, the channel scattering function will be given, as well as the delay and Doppler spread values.

Equation (1) shows the transmitted signal, $s(t)$, consisting on a modulated maximal length sequence (m-sequence) train with center frequency $f_c = 2.5$ MHz, located at the pass band center of the attenuation characteristic.

$$\begin{aligned}
 s(t) &= \sum_{n=0}^{N_{sq}-1} s_{PN}(t - nT) e^{j2\pi f_c t} \\
 &= \sum_{n=0}^{n=N_{sq}-1} \sum_{i=0}^{N_c-1} b_i p\left(t - i\frac{T}{N_c} - nT\right) e^{j2\pi f_c t}
 \end{aligned} \quad (1)$$

Where $s_{PN}(t)$ is a PN sequence of length N_c chips that have been interpolated by a pulse shaping filter $p(t)$, $b_i \in \{-1, 1\}$ are the sequence chips, N_{sq} is the number of m-sequences per burst, T is the sequence period, $T_c = \frac{T}{N_c}$ is the chip period and $\Delta T_s = TN_{sq}$ is the sounding period. This technique allows an unambiguous sounding when the channel has a impulse response, $h(\tau)$, shorter than T , with a time resolution of T_c , allowing a maximum detectable Doppler of $\frac{1}{2T}$ with an accuracy of $\frac{1}{\Delta T_s}$. Table I shows the sounding parameters.

After downconversion, the base-band received m-sequence train, $r_{PN}(t)$, is correlated with a local PN sequence replica $s_{lPN}(t)$, as shown in Eq. (2).

$$R_{r_{PN}, s_{lPN}}(t) = \int_0^T r_{PN}(t + \tau) s_{lPN}(\tau) d\tau \quad (2)$$

If $t = \eta \frac{T}{N_c N_{ov}} + nT$ where N_{ov} is the oversampling factor, i.e., the number of samples per chip; the discretized channel impulse response matrix $h[n, \eta]$ can be obtained from Eq. (2)

¹The CAMT-1 has an equipment side input impedance of 50 Ω and a line side input impedance of 20 Ω

TABLE I
PN SOUNDING PARAMETERS

| PARAMETER | VALUE |
|---------------------------------|---|
| Sequence type | m-sequence |
| Number of chips | $N_c = 511$ |
| Chip period | $T_c = \frac{1}{1 \cdot 10^6} = 1 \mu s$ |
| Sequence period | $T = T_c \cdot N_c = 511 \mu s$ |
| Number of sequences per burst | $N_{sq} = 200$ |
| Pulse shaping ($p(t)$) filter | Root Raised Cosine Filter ($\alpha = 0.65$) |
| Occupied bandwidth | 1.65 MHz |
| Center frequency | $f_c = 2.5$ MHz |
| Maximum Detectable Delay | 511 μs |
| Delay Resolution | 1 μs |
| Maximum Detectable Doppler | 978 Hz |
| Doppler Resolution | 9.7 Hz |

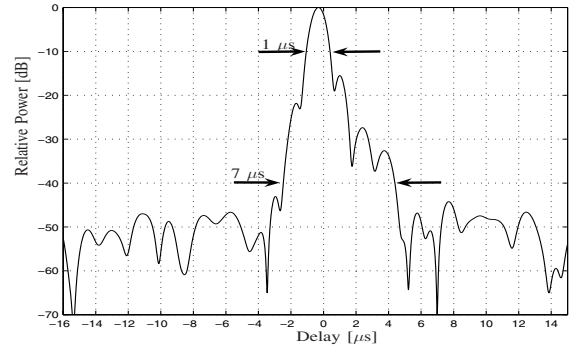


Fig. 4. Delay Power Profile

as shown in Eq. (3), where n and η are the time and delay indexes respectively.

$$h[n, \eta] = R_{r_{PN}, s_{lPN}} \left(\eta \frac{T}{N_c N_{ov}} + nT \right) \quad (3)$$

where

$$\begin{aligned}
 n &\in \mathbb{N} \text{ and } \eta \in [0, N_{sq} - 1] \\
 \eta &\in \mathbb{N} \text{ and } n \in [0, N_c N_{ov} - 1]
 \end{aligned}$$

Fig. 4 shows a single channel delay power profile, e.g., $\eta_{max}|_{10dB} = 1 \mu s$ and $\eta_{max}|_{40dB} = 7 \mu s$.

C. FM: Background Noise

Simplifying the typical noise scenario defined in [6], two kinds of noise analysis will be carried out: background and impulsive noise. Fig. 5 depicts the mean PSD and the standard deviation (STD) in the frequency domain. This noise has been recorded during four days, with an overall observation time of 400 seconds, sampled at 50 Msps.

These statistics reveal a highly colored background noise until 10 MHz, and from that point on, the delta-like spectrum is related to low-power continuous impulsive events. The colored behavior, due to the summation of several noise sources,

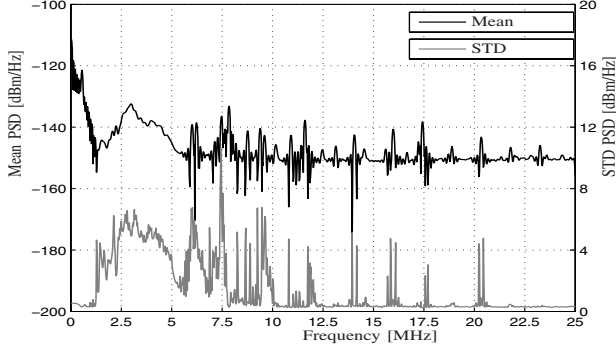


Fig. 5. Background Noise

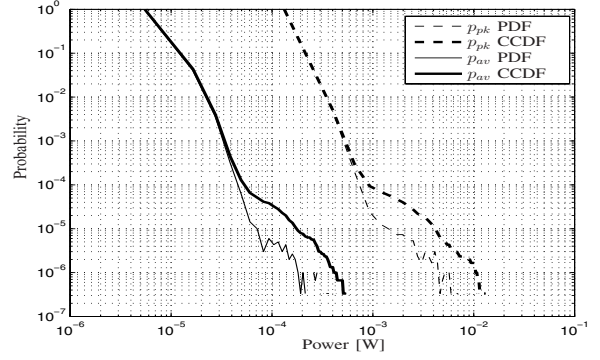


Fig. 7. Peak and Average Impulse Powers

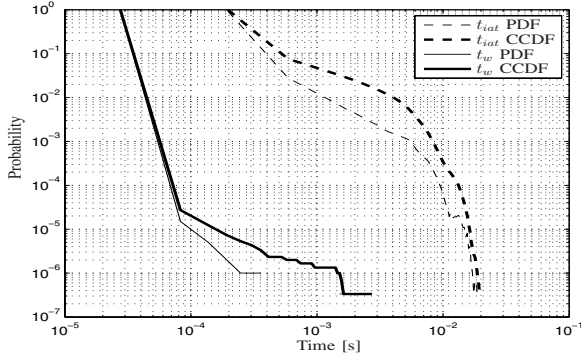


Fig. 6. Time Width and Interarrival Time

remains at low frequencies, where the propagation from those sources to the measurement point is possible. The maximum variability has been observed in that frequency range, while in the highest ranges, only minor changes happened.

D. FM: Impulsive Interferences

More than 18 minutes sampled at 20 Msps have been processed to extract the following statistics. That observation time yields to 7,426,304 analyzed impulses. The horizontal parameters, i.e., random variables (RV), that typically characterize these impulse events [6] are the impulse width (t_w), and the interarrival time (t_{iat}); that is, the time between the rising of the impulse and the end of the same, and the time between two consecutive pulse risings, respectively. Moreover, impulse interferences will be also characterized by two vertical parameters, i.e., impulse peak power (p_{pk}) and impulse average power (p_{av}). Fig. 6 and 7 depict the probability density function (PDF) and complementary cumulative density function (CCDF) for the time and power related RVs, respectively.

On one hand, impulses with durations less than 0.1 ms have an occurrence probability of $1 - 10^{-5}$, showing that almost all impulse durations are in the range of tens of microseconds. On the other, interarrival times of milliseconds, are quite usual ($> 10^{-1}$), undisturbed intervals over tens of milliseconds can

arise with a probability of 10^{-3} . Fig. 7 depicts that p_{pk} CCDF is a shifted version of p_{av} CCDF, showing that impulse energy is uniformly distributed along their duration.

E. FM: Reflection Coefficient

By means of the NA, the MV channel reflection coefficient, measured at the coupler equipment side, namely Γ_{in} , will be used for the network input impedance extraction, as shown in Section IV-H.

F. LM: MV cable S parameters

The objective of this measurement is to obtain the MV cable propagation constant γ , Eq. (4), and characteristic impedance Z_0 .

$$\gamma = \alpha + j\beta \quad \beta = \frac{2\pi f}{c} \quad (4)$$

in

$$V(z) = V^+ e^{-\gamma z} + V^- e^{\gamma z} \quad (5)$$

In Eq. (5), $V(z)$ is the progressive, V^+ , and the regressive voltage wave V^- , in their phasorial representation. In the expression of γ , α , β and c are the attenuation constant, phase constant and propagation velocity, respectively. The extraction of the cable characteristics has been carried out as follows:

- 1) Precise cable length measure.
- 2) Manufacture of the cable to NA connection.
- 3) S parameters measurement. Once the MV cable segment has been properly connected to the NA, the measurement of its 2x2 S parameters matrix, namely S'_{cbl} , is carried out. Note that S'_{cbl} includes both cable and discontinuity behaviors measured by a 50 Ω reference.
- 4) Transitional connection modeling. In order to extract the discontinuity effect from S'_{cbl} at both cable ends, the transition is modeled by a serial anticond (L') and a parallel anticond (C') respectively. When those discontinuity effects are extracted, the resulting S matrix will describe the behavior of the MV cable only, i.e., S_{cbl} .
- 5) Compensation and deembedding of the discontinuity connection geometrical change by means of gradient

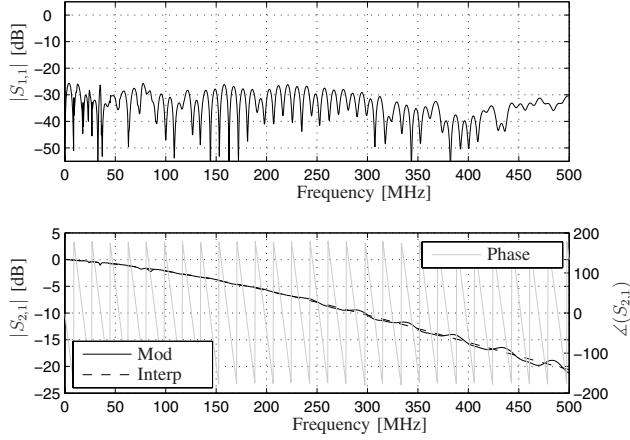


Fig. 8. Transmission and Reflection Parameters (10 m)

based optimization. An impedance matched transmission line has a near zero reflection parameters, i.e., $S_{cbl\ i,i} \approx 0 \forall i$. With the target of achieving such reflection values, an optimization of L' , C' and reference impedance Z_0 is carried out, obtaining a $S'_{cbl\ 1,1}$ and $S'_{cbl\ 2,2}$ less than -25 dB from 10 kHz to 500 MHz. Figure 8 shows the $S'_{cbl\ 1,1}$ and $S'_{cbl\ 2,1}$ after the optimization. At this point, the cable discontinuity parasit behavior can be considered compensated and S'_{cbl} becomes S_{cbl} , where the actual cable parameters are extracted. Equation (6), shows the third order polynomial that fits the $|S_{cbl\ 2,1}|$ [dB/10 m] with a root mean square error less than 0.1.

$$\alpha(f[MHz]) = 9.5 \cdot 10^{-19} \cdot f^3 - 2.3 \cdot 10^{-10} \cdot f^2 - 8 \cdot 10^{-3} \cdot f - 0.029 \quad (6)$$

- 6) Z_0 matching by means of cable reflection coefficient minimization. Since the reflection coefficients are minimized, it means that the reference impedance has the same value that the cable characterized impedance, first order fitted in Eq. (7).

$$Z_0(f[MHz]) = 24.53 + 3.22 \cdot 10^{-2} \cdot f \quad (7)$$

- 7) Finally, from the $\angle(S_{2,1})$ in the 500 MHz frequency range, and taking into account the cable length, the propagation velocity (and β) can be known as shown in Eq. (4): $c = 1.9 \cdot 10^8$.

G. LM: MV coupler S parameters

Measured as depicted in Fig. 2, the PLCoupling / DIMAT CAMT-1 capacitive coupler S parameters are extracted in S_{cplr} . It has been found by simulation that how MV channel access impedance makes the coupler performance vary, as shown in Fig. 9, where transmission and reflection performances are depicted for an access impedance of 10, 20 and 30 Ω .

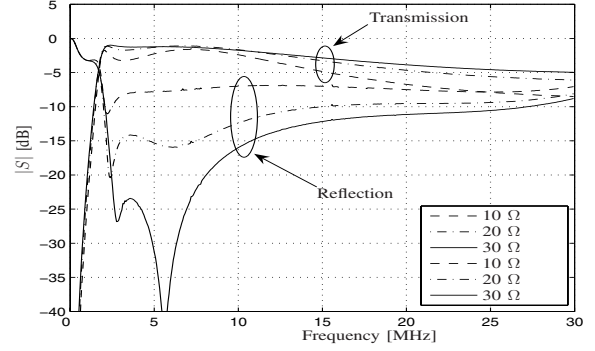


Fig. 9. Coupler Response Variation

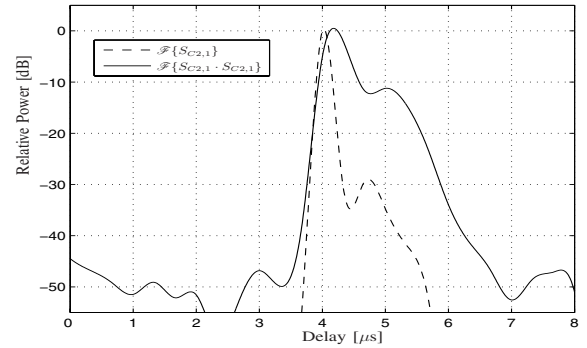


Fig. 10. Coupler Impulse Responses

In Fig. 10 the the $\mathcal{F}\{S_{C2,1}\}$, where $\mathcal{F}\{\cdot\}$ is the square of the Fourier Transform, is shown. Besides, since the signal path goes through two couplers from the transmitter to the receiver, Fig. 10 also shows the delay power profile of two couplers in cascade ($\mathcal{F}\{S_{C2,1} \cdot S_{C2,1}\}$). Taking into account Fig. 4, that measure shows that a large amount of time spreading is due to the coupler.

H. Network Input Impedance

Finally, the MV access impedance is found as follows. If Γ_{in} is the measured channel reflection at the equipment side of the coupler, the MV channel reflection coefficient Γ_L is found as shown in Eq. (8), where $|\cdot|$ is the determinant of the matrix.

$$\Gamma_{in} = S_{cplr\ 2,2} \frac{S_{cplr\ 1,2} \cdot S_{cplr\ 2,1} \cdot \Gamma_L}{1 - S_{cplr\ 1,1} \cdot \Gamma_L} \quad (8)$$

$$\Gamma_L = \frac{\Gamma_{in} \cdot S_{cplr\ 2,2}}{|S_{cplr}| + S_{cplr\ 1,1} \cdot \Gamma_{in}} \quad (9)$$

$$Z_L = Z_0 \frac{1 + \Gamma_L}{1 - \Gamma_L} \quad (9)$$

From Eq. (8), it is straightforward to find the access impedance Z_L , as shown in Eq. (9) and depicted in Fig. 11, where Z_0 is the measurement reference impedance. It shows

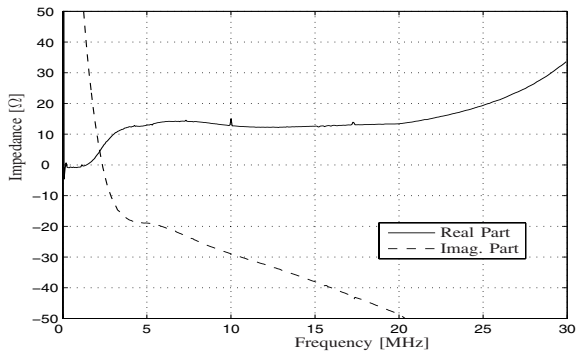


Fig. 11. MV Link Access Impedance

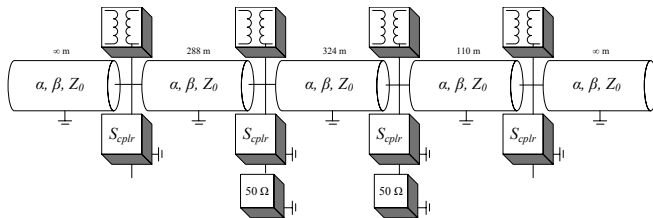


Fig. 12. Simulated Network Topology

that for our measurement scenario, channel input impedance real part ranges from 12 to 20 Ω , with no variations over time.

V. CONCLUDING DISCUSSION

This paper has presented seven measurements, two of them for noise characterization and the others to properly model the transfer function of the urban underground MV distribution network. For this kind of scenario, the approximation that best suits this channel is a combination of deterministic and stochastic modeling.

From structural measurements, the MV distribution cable and coupler have been characterized, in order to deterministically model the MV channel topology. The validation of the characterization has been carried out by modeling the real measured network in ADS², as shown in Fig. 12, and measuring the simulated attenuation characteristic. MV/LV transformers have been modeled as explained in [16]. The MV cable has been modeled by the extracted parameters in Eqs. (6,7, c and the coupler by S_{cplr} . Fig 13 shows a quite good match between simulation and measure. The deviations between the two characteristics are most probably due to the parasite behavior of RMU elements and physical construction issues, e.g., breakers, structure shapes and sections, and so on. Moreover, a methodology for extracting the network input impedance and its value have been presented, based on the coupler deembedding in order to get an actual channel measure.

Due to the noise random nature, it has been characterized in Figs. 6, 7 and 5, revealing its behavior in time width and

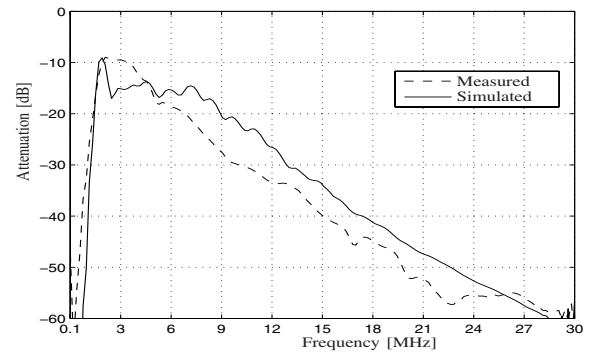


Fig. 13. Measured and Simulated Attenuation Characteristics

interrival impulse times, as well as the mean and variance for the background noise in the frequency domain. Regarding the noise scenario modeling, the several stochastic proposals, e.g., [6], can be easily tuned to met the MV channel background noise and interference characteristics.

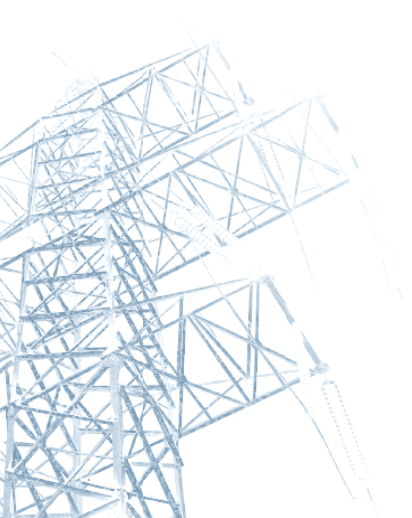
REFERENCES

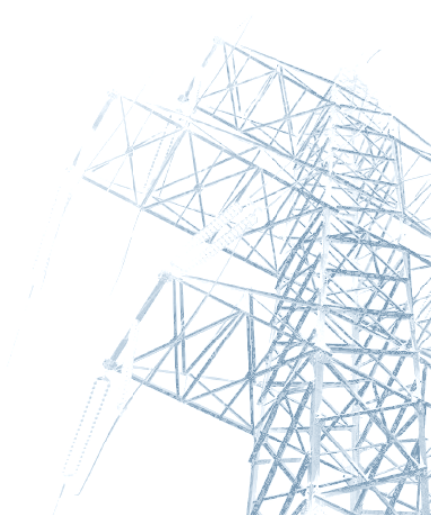
- [1] Z. Tao, Y. Xiaoxian, Z. Bahoui, C. Jian, Y. Zhi, and T. Zhihong, "Research of noise characteristics for 10-kV medium-voltage power lines," *IEEE Transactions on Power Delivery*, vol. 22, pp. 142 – 150, 2006.
- [2] H. Philipps, "Performance measurements of powerline channels at high frequencies," in *IEEE International Symposium on Power Line Communications and Its Applications*, 1998.
- [3] R. Papayzan, P. Petterson, H. Edin, R. Eriksson, and U. Gäfvert, "Extraction of high frequency power cable characteristics from S-parameter measurements," *IEEE Transactions on Dielectrics and Electrical Insulation*, vol. 11, pp. 461 – 470, 2004.
- [4] C. Hensen, W. Schulz, and S. Schwarze, "Characterization, measurement and modeling of medium-voltage power line cables for high data rate communication," in *IEEE International Symposium on Power Line Communications and Its Applications*, 1999.
- [5] Y. Xiaoxian, Z. Tao, Z. Baohui, H. Zonghong, C. Jian, and G. Zhiqiang, "Channel model and measurement methods for 10-kV medium-voltage power lines," *IEEE Transactions on Power Delivery*, vol. 22, pp. 129 – 134, 2007.
- [6] M. Zimmermann and K. Dostert, "Analysis and Modeling of Impulsive Noise in Broad-band Powerline Communications," *IEEE Transactions on Electromagnetic Compatibility*, vol. 44, pp. 249 – 258, 2002.
- [7] —, "A multipath model for powerline channel," *IEEE Transactions on Communications*, vol. 50, pp. 553 – 559, 2002.
- [8] "Report presenting the architecture of PLC system, the electricity network topologies, the operating modes and the equipment over which PLC access system will be installed," OPERA, Tech. Rep. D-44, 2005.
- [9] "Report on MV backbone system," OPERA, Tech. Rep. D-14, 2005.
- [10] Dimat, "Coupling unit for PLC equipment over medium voltage lines," Dimat, Tech. Rep., 2006.
- [11] B. Gustavsen, "Wide band modeling of power transformers," *IEEE Transactions on Power Delivery*, vol. 19, pp. 414 – 422, 2004.
- [12] K. Dostert, *Powerline Communications*. Prentice Hall, 2001.
- [13] N. Instruments, "NI PXI-5441 specifications, 100 msp, 16-bit arbitrary waveform generator with onboard signal processing," National Instruments, Tech. Rep., 2005.
- [14] D. Pozar, *Microwave Engineering*. John Wiley & Sons, 2005.
- [15] "Pathloss as a function of frequency, distance and network topology for various LV and MV European powerline networks," OPERA, Tech. Rep. D-05, 2005.
- [16] T. Tran-Anh, P. Auriol, and T. Tran-Quoc, "High frequency power transformer modeling for Power line Communication applications," in *IEEE Power Systems Conference and Exposition*, July 2006.

²Advanced Design System, from Agilent Technologies, Inc.

8.4. APPENDIX A.4

R. Aquilué, J.L. Pijoan, G. Sánchez, "High Voltage Channel Measurements and Field Test of a Low Power OFDM System", in Proc. IEEE Symposium on Power Line Communications and its Applications (ISPLC2008), Jeju, South Korea, 2008.





High Voltage Channel Measurements and Field Test of a Low Power OFDM System

Ricard Aquilué*, Joan Lluís Pijoan* and Germán Sánchez†

* Department of Communications and Signal Theory, La Salle Engineering, Ramon Llull University, Barcelona, Spain. Email: {raqilue,joanp}@salle.url.edu

† ENDESA Network Factory, Createc, Barcelona, Spain.

Abstract—High voltage (HV) power lines have been used as a communications medium since the 1920s. Those point to point links were typically based on single-sideband amplitude modulation. Nowadays, the state of the art in HV power line carrier (PLC) communications comprises the combination of analog systems, mainly for teleprotection tasks, and digital systems, used for voice and data transmission. Beside traditional core services (monitoring, operation management, and limitation and removal of failures), electrical utilities would like to satisfy the increasing need of new internal applications. In that way, quadrature amplitude modulation and, most recently, multicarrier modulation (MCM) based modems are beginning to play an important role in HV PLC systems. Although the typical 4 kHz bandwidth has been recently increased up to 32 kHz, this paper proposes a low-power 256 kHz bandwidth orthogonal frequency division multiplexing (OFDM) based physical layer. Based on channel measurements, the OFDM symbol has been designed and tested in order to increase the user bit rate while keeping both the power spectral density and bit error rate low.

I. INTRODUCTION

Since the beginning of 20th century, the High Voltage (HV) network has been exploited as a communications medium. Actually, the first ever running communication equipments on power lines were the HV double-sideband amplitude modulation (1920s) and single-sideband amplitude modulation (SSB-AM) modems (1940s). Since no other communications network could offer such a geographic presence, reliability and cost effectiveness, electrical utility (EU) core services, i.e., monitoring, operation management and limitation and removal of failures, were carried out by voice transmission by means of analog power line carrier (PLC) systems [1].

Due to the low reliability, rate and the level of automation that voice transmission provided, digital data transmission shown up by with low speed (50 bps) amplitude shift keying modems. With the increase of the power grid automation level, the required data rate grew to support the communications of such a complex system, yielding to the typical 2400 bps modems and the 4 kHz channelization [2], [3].

Nowadays, PLC systems are usually based on the combination of analog and digital technologies, that presents a higher degree of flexibility for the EU: while it solves the problem of the low reliability of the digital PLC for tasks such as teleprotection, it overcomes the rate limitation of the analog PLC.

Focusing on data transmission PLC state of the art, the digital systems based on quadrature amplitude modulation (QAM) single carrier modulation (SCM) can reach a net bit rate of up to approximately 80 kbps in a 16 kHz bandwidth with bit error rates (BERs) equal or below 10^{-6} [4]. Multi-carrier modulation (MCM) begins to play an important role in HV communications, being orthogonal frequency division multiplexing (OFDM), the most adaptive and frequency efficient MCM version [5], the choice for manufacturer's next generation HV PLC equipment [6].

Based on the channel measurements carried out in this work, an OFDM physical layer will be proposed and tested in a real scenario. Although the licensed band for PLC is located from 40 kHz to 500 kHz [2], [3], in certain situations, the signal propagation can be favorable enough to use the frequency range above that upper limit; so, the study on this paper will go beyond this constraint and will propose, based on the learned experience, the exploitation of that range by MCM adaptive [5] and Cognitive Radio (CR) techniques [7]. Based on the same measurements, while trying to reduce the interference on other PLC equipment in the PLC-licensed band and on the existing broadcast signals on the non-PLC-licensed band, the MCM symbol design will have in mind the minimization of the transmitted power spectral density (PSD).

This paper is organized as follows: In Section II the description of the HV transport line available where the measurements have been carried out, as well as the measurement and test set-up will be described. In Section III, the measurement outcomes will be discussed and then, in Section IV, the OFDM symbol design and the proposed system performance will be shown. Finally, concluding remarks will be summarized in Section V.

II. MEASUREMENT AND TEST SCENARIO

In this Section, the test scenario as well as the measurement set-up will be introduced.

The scenario under test is a 4-circuits, 3-phase 110 kV, 6.35 km line between the “Egara” and the “Mas Figueres” ENDESA substations, in Barcelona, Spain. Both channel measurements and data transmission tests have been carried out by the same equipment: two National Instruments PXI chassis. Each chassis consists on an industrial embedded computer, one high stability reference clock [8] and a special instrumentation card: high speed arbitrary waveform generator

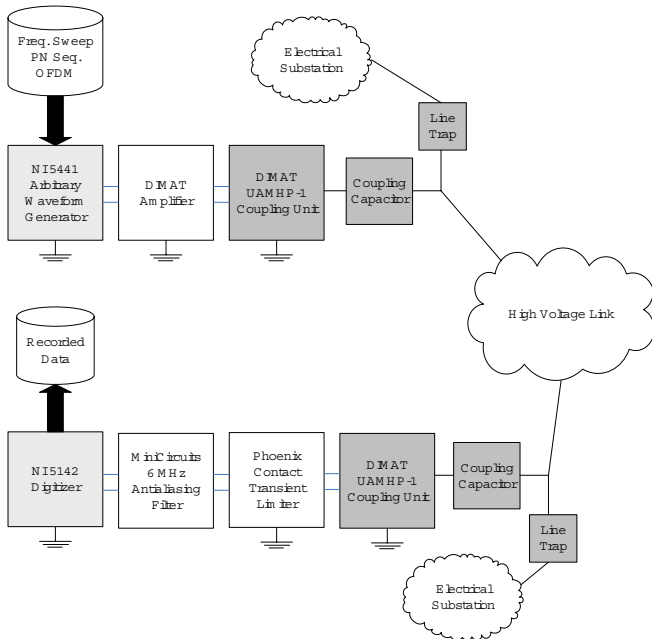


Fig. 1. Measurement and Test Set-Up

at the transmission site [9], high speed digitizer at the reception site [10]. Both chassis are GPS synchronized.

The measurement and test set-up is depicted in Fig. 1. At the transmission site, the digital-to-analog converted signal is immediately fed into a Dimat ad-hoc built amplifier. From 50 kHz to 1.4 MHz, this device offers a gain of 37.5 dB and 160 W of peak envelope power. When amplified, the signal gets the coupling device [11] that matches the 75 Ω amplifier output impedance with the line access impedance.

That matching procedure is carried out manually, i.e., the reflection coefficient at the input of the coupling unit is monitored while switching among coupling unit different configurations. Since the transformers at the line ends can be considered as a perfect barriers for frequencies over a few tenths of kHz [12], the previously found coupling device configuration (and line access impedance) can be considered valid for that time on. The line trap prevents the radio frequency signal from entering the substation premises while it propagates toward the receiver site. When decoupled and before the acquisition, the signal is amplitude limited and noise and antialias low pass filtered at 6 MHz. In the sequel, the channel is considered to be between the amplifier output and the transient limiter input; other devices will be properly compensated.

III. MEASUREMENTS AND RESULTS

In this Section, a complete wideband sounding for the HV-PLC channel will be presented. First, the attenuation characteristic will show the power line transmission capabilities and its long term variations. Then, in order to get knowledge of the short term variations and the channel delay, the pseudo-noise (PN) sequence based sounding will be carried out. Maximal length sequences (or m-sequences) are used because

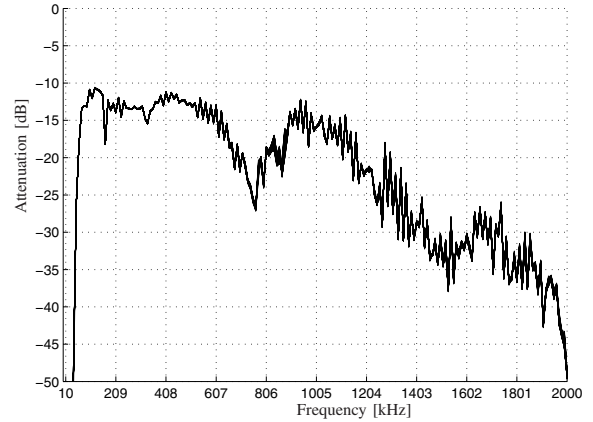


Fig. 2. Link Attenuation

of its well-known good autocorrelation properties [13]. From these measurements, the channel coherence time (Δt_0) and coherence bandwidth (Δf_0) will be deduced in order to properly design the OFDM symbol. Finally, a background noise analysis will be carried out.

A. Attenuation Characteristics

The attenuation characteristic of the link under study has been measured by transmitting one tone sweep every 20 minutes from 10 kHz to 2 MHz in 10 kHz steps. Each step consists on 10 averaged acquisitions during 2 seconds. In Fig. 2 all the measured sweeps can be seen overimposed.

The channel attenuation characteristic shows a pass band behavior. The low cut-off frequency (40 kHz) is due to the coupling capacitor and coupling device combined frequency response, and the high one is due to the same devices plus the line attenuation. The ripple at the pass band is due to the multipath effect, while the null from 610 kHz to 880 kHz is due to the coupling devices impedance mismatching. The perfect match among the 360 sweeps means that both propagation and coupling performances remained constant for one week, so, there is no long term variation in the link transfer function.

B. Time Spread and Frequency Spread

The transmitted pilot signal, $s(t)$ (Eq. (1)), consists on a modulated m-sequence train at center frequency f_c .

$$\begin{aligned}
 s(t) &= \sum_{n=0}^{N_{sq}-1} s_{PN}(t-nT)e^{j2\pi f_c t} \\
 &= \sum_{n=0}^{N_{sq}-1} \sum_{i=0}^{N_c-1} b_i p\left(t - i\frac{T}{N_c} - nT\right) e^{j2\pi f_c t}
 \end{aligned} \tag{1}$$

Where $s_{PN}(t)$ is a PN sequence of length N_c chips that have been interpolated by a pulse shaping filter $p(t)$, $b_i \in \{-1, 1\}$ are the sequence chips, N_{sq} is the number of PN sequences per burst, T is the sequence period, $T_c = \frac{T}{N_c}$ is

TABLE I
PN SOUNDING PARAMETERS

| PARAMETER | VALUE |
|---------------------------------|---|
| Sequency type | m-sequence |
| Number of chips | $N_c = 2047$ |
| Chip period | $T_c = 10^{-3} = 1.66 \mu\text{s}$ |
| Sequence period | $T = T_c N_c = 3.41 \text{ ms}$ |
| Number of sequences per burst | $N_{sq} = 10$ |
| Pulse shaping ($p(t)$) filter | Root Raised Cosine Filter ($\alpha = 0.65$) |
| Occupied bandwidth | 0.99 MHz |
| Center frequency | $f_c = 600 \text{ kHz}$ |

the chip period and $\Delta T_s = TN_{sq}$ is the sounding period. This technique allows an unambiguous sounding when the channel impulse response ($h(\tau)$) is shorter than T , with a time resolution of T_c , allowing a maximum detectable Doppler of $\frac{1}{2T}$ with an accuracy of $\frac{1}{\Delta T_s}$. Table I shows the sounding parameters.

After downconversion, the base-band received m-sequence train, $r_{PN}(t)$, is correlated with a local PN sequence replica $s_{IPN}(t)$, as shown in Eq. (2).

$$R_{r_{PN}s_{IPN}}(t) = \int_0^T r_{PN}(t + \tau), s_{IPN}(\tau) d\tau \quad (2)$$

If $t = \eta \frac{T}{N_c N_{ov}} + nT$ where N_{ov} is the oversampling factor, i.e., the number of samples per chip, and n and η are the time and delay indexes respectively; the discretized channel impulse response matrix $h[n, \eta]$ can be obtained from Eq. (2) as shown in Eq. (3).

$$h[n, \eta] = R_{r_{PN}, s_{IPN}} \left(\eta \frac{T}{N_c N_{ov}} + nT \right) \quad (3)$$

where

$$\begin{aligned} n &\in \mathbb{N} \text{ and } n \in [0, N_{sq} - 1] \\ \eta &\in \mathbb{N} \text{ and } \eta \in [0, N_c N_{ov} - 1] \end{aligned}$$

Fig. 3 shows the relative power of $h[n, \eta] \forall n$, that is, the N_{sq} impulse responses overlapped, revealing no short time channel variations. In the same, the first and most powerful path, which is the direct one, followed by a negative exponential spreading of $20 \mu\text{s}$, can be seen. This decreasing spreading after each path is caused by network devices non idealities (e.g. coupling devices, coupling capacitor, line traps...). That first path is followed by the second one, 17.4 dB attenuated and $47 \mu\text{s}$ after. This second path is due to the reflection of the first incoming signal at the receiving substation, its propagation back again to the transmitter site and its second reflection to the original destination. The same can be told about the third path. It is straightforward to find a propagation speed of $2.7 \cdot 10^8 \frac{\text{m}}{\text{s}}$ or 0.9 times c_0 (speed of light in the vacuum). This decrease on the expected speed is most probably due to the line geometrical and topological characteristics, as well as to the line supports.

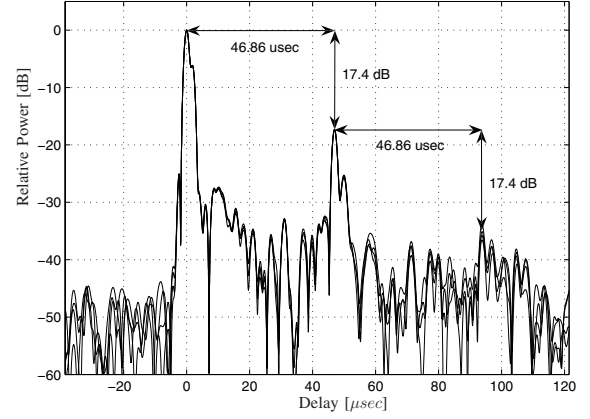


Fig. 3. Channel Impulse Response

The spreading in time calls for a robust modulation in front of frequency selective channels and inter-symbol interference (ISI). OFDM delivers such robustness in this kind of scenario if both subcarrier bandwidth and cyclic prefix length are properly designed, therefore, achieving a flat channel per subcarrier and avoiding ISI, respectively. As expected, no channel variation has been found in time domain, yielding to a zero Doppler scattering and subsequently a $\Delta t_0 \rightarrow \infty$. Adaptive techniques cannot be implemented in real time due to equipment restrictions, however an stationary channel enhances the modulation adaptation performance and OFDM offers the maximum achievable spectral granularity, becoming the best candidate to implement adaptive techniques [5].

Once the time domain variation has been characterized, the frequency domain variation, i.e., the Δf_0 , has to be found. From 3, the channel transfer function, $H(f)$ can be calculated by means of the Fourier Transform. Then, in order to find the Δf_0 , the frequency correlation function, Eq. (4), is depicted in Fig. 4, yielding to a Δf_0 of 70 kHz for a 0.9 correlation factor.

$$R(\Delta f) = \frac{E\{H^*(f)H(f + \Delta f)\}}{E\{H(f)\}} \quad (4)$$

C. Noise Scenario

In this Section, a closer look will be given to the noise scenario, specifically, to background noise. This type of noise is a broadband permanent interference with relatively high level and mainly caused by corona effect and other leakage or discharge events. Background noise PSD is time and frequency variant (colored noise). Due to climatic dependences, corona noise power fluctuations up to tens of dB can be expected. Stationary, low-power periodical and synchronous with the mains impulse events can also be considered background noise. These kinds of impulses are caused by discharges on insulators and other electrical substation devices. Narrowband interferences such a coupled broadcast emissions or other

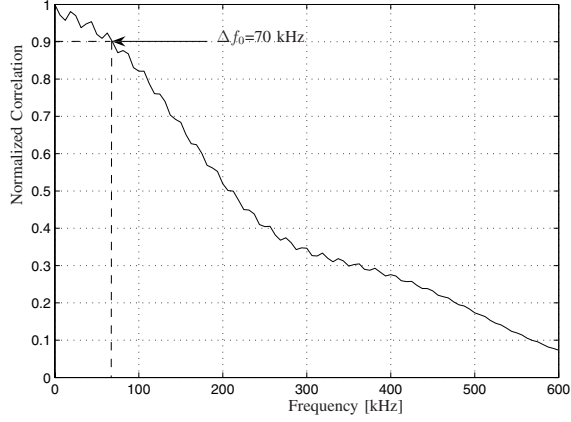


Fig. 4. Frequency Autocorrelation Function $R(\Delta f)$

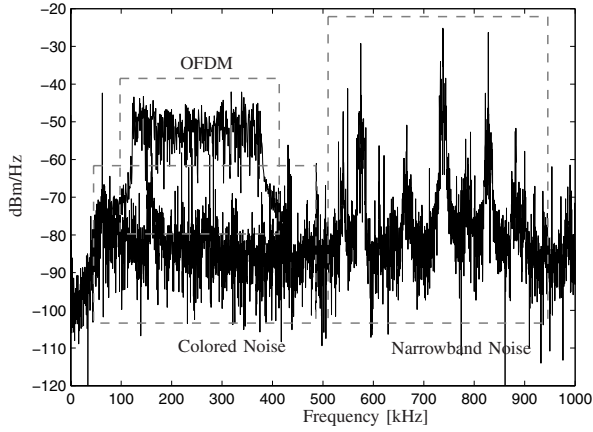


Fig. 5. Background Noise and OFDM PSDs

communications equipment, due to its slow variability, can be considered background noise too [1].

Fig. 5 shows the background noise and OFDM overimposed PSDs at the receiver site. Two noise regions can be clearly identified, i.e., from the lower frequencies up to 500 kHz and from 500 kHz on. The former band is colored noise limited, while the latter is narrowband interference limited.

Fig. 6 depicts the maximum and the minimum PSD values for 10 frequency subbands, from 0 to 1 MHz, 100 kHz each, during a 4 days observation period. Although this behavior can be considered slow variant, this scenario shows a highly dynamic background noise in frequency domain, since variations up to 20 dB have been measured in the lower region. In the background limited band, the noise PSD decreases as frequency increases, showing a friendly range in the upper frequencies, until the end of the licensed range. Since no adaptive scheme will be used, this background noise study will not directly affect the OFDM symbol design, but the obtained results claim again for a power and bit-loading adaptive OFDM physical layer [5].

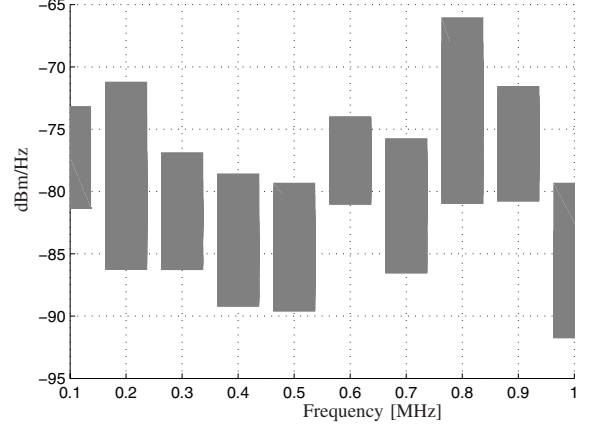


Fig. 6. Background Noise Variability

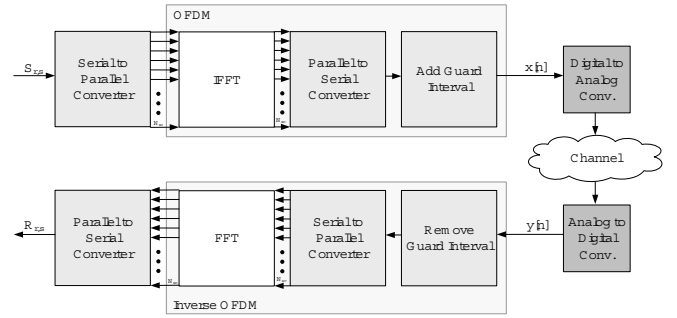


Fig. 7. OFDM Block Diagram

IV. OFDM DESIGN AND TEST

In this Section, based on the measurements previously presented, the MCM symbol design will be introduced, and the performance of the proposed physical layer in a real HV link will be tested.

Fig. 7 shows a typical OFDM transmitter and receiver block diagram where $S_{r,s}$, for $r, s \in \mathbb{N}$, $r \in [0, N_{sym} - 1]$ and $s \in [0, N_{sc} - 1]$, are the complex symbols that will modulate the N_{sc} subcarriers of the N_{sym} symbols per OFDM frame. After the serial to parallel conversion, the OFDM symbol is implemented by means of the inverse Fast Fourier Transform (IFFT), Eq. (5). Then, after a serial to parallel conversion and before the conversion to the analog domain, the N_g samples of guard interval are added in order to avoid ISI in the useful part of the symbol. By means of the received and sampled signal $y[n]$ FFT, the received symbols $R_{r,s}$ are recovered and ready for demapping [5].

$$x_s[n] = \frac{1}{N_{sc}} \sum_{r=0}^{N_{sc}-1} S_{r,s} e^{j2\pi n \frac{r}{N_{sc}}} \quad (5)$$

A. Symbol and Frame Design

Transmitted power will be chosen in order to get a BER of approximately 10^{-2} before decoding. If using 16-QAM as a

mapping scheme, 256 kHz of occupied bandwidth and 0.15 W of transmitted power, around 20 dB of SNR is expected at the receiver site (Fig. 5). Taking into account this ratio and the impulse response in Fig. 3, only the first and the second path (at $\tau_{max}=46.86 \mu\text{s}$) have to be considered. A $T_{cp}=80 \mu\text{s}$ will prevent ISI from occur. The cyclic prefix duration, T_{cp} , is in charge of avoiding ISI, and consequently, inter-carrier interference (ICI). This guard interval has to be greater than the maximum delay spread (τ_{max}) [5].

The 10^{-2} expected BER is the minimum required modulation performance for allowing the channel coding perform correctly. A 1/2 convolutional code with constraint length 7 and trace-back length 35 will be used in order to achieve a BER performance close to the typical performance delivered by other systems: 10^{-6} . Moreover, a 120 depth interleaving will be employed in order to spread the symbols among the whole OFDM lattice [14].

Once T_{cp} has been fixed, the symbol length will be chosen while trying to maximize the cyclic prefix efficiency (6), that is, the ratio between the useful symbol time, T_u , and the symbol time T_s , where $T_s = T_{cp} + T_u$.

$$\rho_{cp} = \frac{T_u}{T_{cp} + T_u} \quad (6)$$

The maximum symbol time is restricted by the Δt_0 , i.e. $\Delta t_0 > T_s$, and by $\Delta f = \frac{1}{T_u}$, since a minimum Δf is needed in order to avoid the effect of ICI for a given uncompensated frequency offset, f_{off} [Hz]. In this way, in order to keep an acceptable performance degradation, a relative uncorrected frequency offset, δ_{off} , of $\delta_{off} = \frac{f_{off}}{\Delta f} \leq 0.01$ has to be fulfilled. A T_u of 1 ms will yield to a relaxed constraint of $f_{off} \leq 10$ Hz, while keeping $\rho_{cp} \geq 0.9$ [5].

Finally, a 1080 μs OFDM symbol of $N_{sc}=256$ subcarriers will be used. With $\Delta f=1$ kHz per subcarrier, an overall symbol bandwidth of 256 kHz is achieved.

Once Δf has been determined, the pilot separation in frequency domain, N_f can be found by satisfying the Nyquist sampling theorem in the frequency domain [15]. There are some rules of thumb that state that a channel oversampling of 2x is recommended [16], so following (7) and (8), where Δf_{N_f} and $\lfloor \cdot \rfloor$ are the frequency separation between pilot subcarriers and the nearest integer towards minus infinity respectively, N_f can be found.

$$\Delta f_{N_f} = \frac{1}{2} \frac{\Delta f_0}{2} = \frac{1}{2} \frac{70 \text{ kHz}}{2} = 17.5 \text{ kHz} \quad (7)$$

$$N_f = \left\lfloor \frac{\Delta f_{N_f}}{\Delta f} \right\rfloor = 17 \quad (8)$$

In order to avoid channel prediction, which is more unreliable than interpolation, instead of using a N_f of 17 subcarriers, a separation of 16 subcarriers will be used.

Although the number of OFDM symbols in one frame is usually constrained by time and frequency acquisition and tracking algorithm accuracy (among others) [5], in our case, this is upper limited by the receiving equipment digitizer

TABLE II
OFDM PARAMETERS

| PARAMETER | VALUE |
|----------------------------------|---|
| Cyclic prefix | $T_{cp} = 80 \mu\text{s}$ |
| Useful symbol time | $T_u = 1 \text{ ms}$ |
| Symbol time | $T_s = 1.08 \text{ ms}$ |
| Subcarrier bandwidth | $\Delta f = 1 \text{ kHz}$ |
| Number of subcarriers | $N_{sc} = 256$ |
| Pilot subcarriers | $N_p = 16$ |
| MCM bandwidth | 256 kHz |
| Pilot frequency spacing | $N_f = 16$ |
| Pilot time spacing | $N_t = 4$ |
| Number of OFDM symbols per frame | $N_{sym} = 16$ |
| Mapping | 16-QAM |
| Channel estimation | Least Squares |
| Channel interpolation | 1-D + 1-D 1 st order |
| Channel coding | 1/2 convolutional code, constraint length 7, trace-back length 35 and 120 of interleaving depth |
| Gross bitrate | $R_{bg} = 930 \text{ kbps}$ |
| User bitrate | $R_{bu} = 465 \text{ kbps}$ |
| Transmission mean power | $P_{tx} = 8.9 \text{ dBm}$ |
| Peak to average power ratio | $PAPR = 12.8 \text{ dB}$ |

memory, a limitation of 16 (+1 pilot symbol) symbols has to be respected. A PN based pilot symbol used for synchronization is inserted at the beginning of each frame.

The channel stationary behavior gives no restriction regarding the pilot separation in time domain, so, since $N_{sym} = 16$, a pilot separation in time domain $N_t = 16$ could be chosen, yielding to a pilot density related efficiency ρ_{pd} of 0.996 (Eq. (9)).

$$\rho_{pd} = \frac{N_f N_t - 1}{N_f N_t} \quad (9)$$

On the other hand, noise effect regarding channel estimation can be reduced if we decrease the pilot distance down to $N_t = 4$, the efficiency is reduced only by a 1.2 %, yielding to the overall system performance shown in Eq. (10).

$$\rho_{cp} \cdot \rho_{pd} = 0.911 \quad (10)$$

The design parameters of the OFDM symbol and frame are summarized in Table II. While trying to simplify the receiver complexity, least squares channel estimation and 1D+1D lineal channel interpolation have been carried out before equalization [17].

B. Performance

The BER performance of the proposed OFDM is depicted in Fig. 8. The continuous line represent the modulation or gross BER and the dashed one represents the BER after decoding,

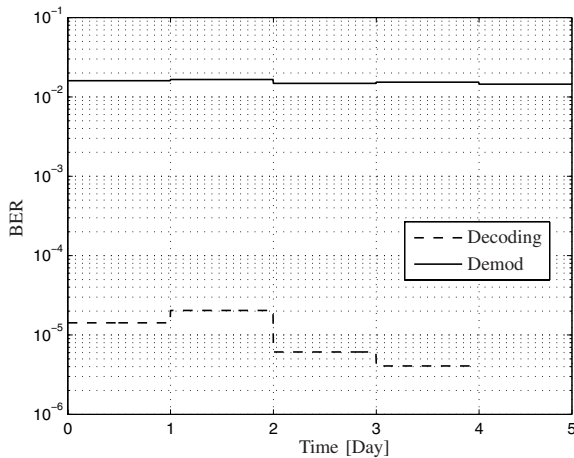


Fig. 8. System Performance

for a user bit rate of 465 kbps. Those lines show the day-by-day averaged performance.

The modulation BER showed a constant behavior, around $2 \cdot 10^{-2}$, while the performance after decoding yielded to a BER of $4 \cdot 10^{-6}$. The fifth day shows no line for the BER after decoding, so a BER better than 10^{-7} was observed in the last day.

V. CONCLUSION AND FUTURE WORK

In this work, a first step towards a new wideband physical layer on HV lines has been presented. The needed channel measurements to carry out an OFDM symbol design have been fulfilled, and the performance of the proposed system has been tested in a real scenario.

A properly designed OFDM allows an easy equalization and detection while avoiding ISI. OFDM splits the selective signal bandwidth into several flat subchannels, however, an efficiency loss has to be paid due to the cyclic prefix. In order to minimize that loss, a short cyclic prefix is desired, so, if received SNR is low enough, less channel spreading will have to be considered. In this work, only the first reflected path was needed to be avoided. Moreover, it has been shown that high rates can be achieved by increasing bandwidth instead of signal power. This low-PSD minimizes undesired emissions and signal coupling into other systems or other MV-PLC links. The spectral granularity delivered by MCM can be also exploited in terms of spectral notching. Spectral notching is a desirable characteristic in PLC modulations when trying to completely avoid the emission in certain frequencies.

Regarding channel time domain behavior, it has been found that channel transfer function and access impedance can be considered constant, revealing neither short time nor long time variations. This friendly behavior in time domain suggests the use of an adaptive modulation for an efficient channel capacity exploitation. Thus, without wasting power or increasing BER, a higher link spectral efficiency can be achieved by taking advantage of the OFDM subbands flat fading through

adaptation [18]. On the other hand, background noise does vary in time domain (up to 20 dB in certain bands), but its slow variability does not present a serious impairment for an adaptive approach.

Moreover, measurements have revealed that transmission is possible beyond the licensed HV-PLC band. The next spectrum band is licensed to broadcast systems, but, as it has been shown, an easily exploitable narrowband interference limited noise region characterizes the spectrum from 500 kHz and on. MCM access methods and CR techniques offer a good possibility to increase HV-PLC channel bandwidth and minimize interferences between HV-PLC neighboring equipment [7].

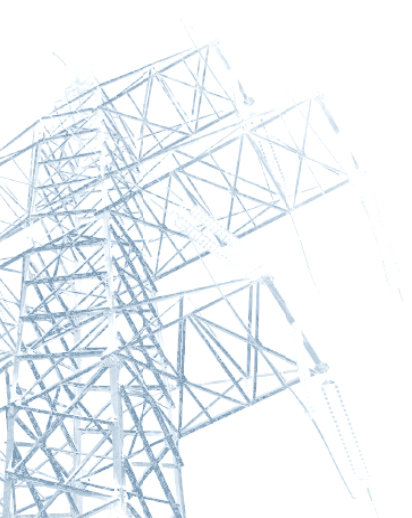
Future work points to the test of OFDM signals with different detectors, and MCM and spread spectrum (SS) combinations, e.g., multicarrier - code division multiple access (MC-CDMA, MCM with spreading in frequency), multicarrier - direct sequence - code division multiple access (MC-DS-CDMA, MCM with spreading in time) and variable spreading factor - orthogonal frequency and code division multiplexing (VSF-OFCDM, MCM with variable spreading in both dimensions) [5]; as well as the performance of previous systems with large bandwidths and low PSDs in longer links, up to hundreds of km.

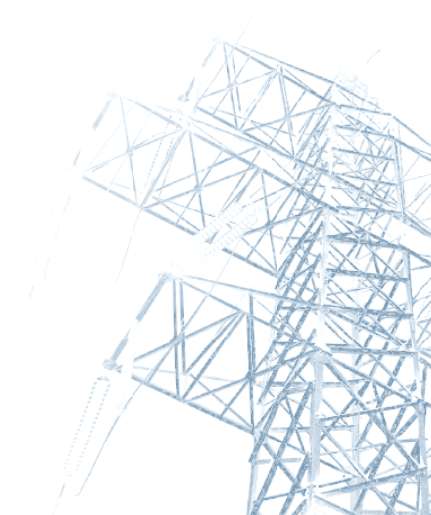
REFERENCES

- [1] K. Dostert, *Powerline Communications*. Prentice Hall, 2001.
- [2] IEC, "Planning of (single-sideband) power line carrier systems," IEC 60633, 1980.
- [3] —, "Single sideband power-line carrier terminals," IEC 60495, 1993.
- [4] Dimat, "OPD-1 digital power-line carrier terminal," Dimat, Tech. Rep., 2004.
- [5] K. Fazel and S. Kaiser, *Multi-Carrier and Spread Spectrum Systems*. John Wiley & Sons, 2003.
- [6] ABB, "ETL-600 universal digital power line carrier," ABB, Tech. Rep., 2006.
- [7] S. Srinivasa and S. A. Jafar, "The throughput potential of cognitive radio a theoretical perspective," *IEEE Communications Magazine*, vol. 45, pp. 75–79, May 2007.
- [8] N. Instruments, "NI-660x specifications," National Instruments, Tech. Rep., 2006.
- [9] —, "NI PXI-5441 specifications, 100 msp/s, 16-bit arbitrary waveform generator with onboard signal processing," National Instruments, Tech. Rep., 2005.
- [10] —, "NI PXI-5142 specifications, 14-bit 100 ms/s digitizer with onboard signal processing," National Instruments, Tech. Rep., 2006.
- [11] Dimat, "UAMHP-1 high voltage coupling unit," Dimat, Tech. Rep., 2006.
- [12] B. Gustavsen, "Wide band modeling of power transformers," *IEEE Transactions on Power Delivery*, vol. 19, pp. 414 – 422, 2004.
- [13] D. V. Sarwate and M. B. Pursley, "Crosscorrelation Properties of Pseudorandom and Related Sequences," *Proceedings of IEEE*, vol. 68, p. 593–619, May 1980.
- [14] J. G. Proakis, *Digital communications*, 4th ed. McGraw-Hill, 2000.
- [15] P. Hoeher, D. Kaiser, and P. Robertson, "Two-dimensional pilot-symbol-aided channel estimation by wiener filtering," in *Proc. IEEE International Conference on Acoustics, Speech and Signal Processing*, vol. 3, Apr. 1997, pp. 1845 – 1848.
- [16] M. Morelli and U. Mengali, "A comparison of pilot-aided channel estimation methods for OFDM systems," in *IEEE Transactions on Signal Processing*, vol. 49, 2001, pp. 3065 – 3073.
- [17] L. Hanzo, S. Ng, T. Keller, and W. Webb, *Quadrature Amplitude Modulation*. John Wiley & Sons, 2003.
- [18] S. Taek and A. J. Goldsmith, "Degrees of freedom in adaptive modulation: an unified view," *IEEE Transactions on Communications*, vol. 49, pp. 1561–1571, 2001.

8.5. APPENDIX A.5

R. Aquilué, M. Ribó, J.R. Regué, J.L. Pijoan, G. Sánchez, “Scattering Parameters Based Underground Medium Voltage Power Line Communications Channel Measurements, Characterization and Modeling”, accepted for publication in IEEE Transactions on Power Delivery, June 2008.





Scattering Parameters Based Channel Characterization and Modeling for Underground Medium Voltage Power Line Communications

Ricard Aquilué*, Miquel Ribó*, Joan Ramon Regué*, Joan Lluís Pijoan* and Germán Sánchez†

* Department of Communications and Signal Theory, La Salle Engineering, Ramon Llull University, Barcelona, Spain. Email: raquilue@salle.url.edu

† ENDESA Network Factory, Createc, Barcelona, Spain.

Abstract—Power line communications (PLC) technologies rely on the power grid for data transmission. Since the communication channel is already deployed, this communication alternative is specially interesting for the power grid owner, i.e., the electrical utility (EU). The medium voltage (MV) distribution network, located after the last step-down electrical substation with typical levels from 6 to 25 kV, feeds directly large consumers and small ones through several transform stations. The growing interest on MV-PLC technology, the natural aggregation point for data coming and going into the low voltage (LV) network, faces the same issue that the LV-PLC technology did (and does): standardization. In this way, a properly implemented channel model will allow the design of suitable modulation and access methods. This paper proposes a deterministic channel model for the MV underground network transfer function, based on a complete set of measurements done in a MV urban ring. Moreover, the characterization of the MV-PLC channel elements, as well as the noise scenario and access impedance has been carried out.

I. INTRODUCTION

The world of power line communications (PLC) can be divided, regarding the network topology, into three main types: low voltage (LV) PLC, medium voltage (MV) PLC and high voltage (HV) PLC. These last years, LV-PLC has attracted a great expectation since its wideband capabilities have made this technology a suitable choice for last-mile access and in-home communications. Moreover, LV-PLC also includes a utility oriented low frequency and low speed applications, such as automatic meter reading (AMR), load distribution, dynamic billing and so on. On the other hand, MV-PLC and HV-PLC, historically oriented to teleprotection and telecontrol tasks, are being considered as a reliable communication channel. With the telecommunications market liberalization, together with the energy market deregulation, EUs can use their own infrastructure, the power line grid (specially the MV and LV networks), to deliver communications services and increase their control and monitoring capabilities over costumers' behavior.

In conjunction with the LV network, the MV network comprises the distribution stage of the electric power grid. Focusing on MV, the MV-PLC technology can be considered as the natural aggregation point for data coming in and going

out the LV network. Located after the last step-down electrical substation (ES), and with typical levels from 6 to 25 kV, the MV network feeds directly large commercial or industrial consumers and domestic and small commercial consumers through several transform stations (TS).

Although this work will focus in urban networks, where the MV network is fully underground, in rural areas, both overhead and underground topologies can be found. The MV networks can transport power in a single or double three phase circuit basis. Single circuit consists on one line per phase, while double circuit transports power in two lines per phase. The former structure can be found in low density and rural areas, while the latter, in high density areas or areas with special requirements. One line acts as a service line while the second acts as a backup [1].

A key point in a physical layer design process is channel modeling. If properly implemented, the channel model will allow the design of suitable modulation and access methods. Before modeling, channel characterization has to be carried out. Basically, two different approaches regarding channel characterization can be followed:

Behavioral This is a top-down strategy, where the statistical characterization of the system is based on exhaustive channel measurements. It is not straightforward to define reference models, since even more exhaustive measurements are needed to cover power networks worldwide casuistic. This is the followed approach when dealing with random channel effects, such as the noise scenario [2] or when the channel topology casuistic is extremely large, e.g., LV networks [3].

Structural This is a bottom-up strategy, where physical parameter estimation is more intuitive and derived from single measurements of the power line network elements. Model adaptation to power grid features worldwide is easier. Focusing MV channel characterization, some transmission line model based works can be found [4]–[8]

On the other hand, two different approaches can be followed regarding channel modeling:

Stochastic Derived from behavioral characterization, the-

se channels models simulate channel conditions based on statistics. As stated, they are typically employed when modeling noise or complex topologies [9], [10].

Deterministic Derived from structural measurements and their structural devices definition, deterministic models are restricted to simulate the modeled structure, without random elements.

The best choice is the use of structural modeling with statistical values for the structural parameters [11]. The aim of this work is to measure the structural parameters of a MV ring (see Section II) and their devices in order to deterministically model their behavior and then, based on statistic records of European MV networks [12], tune the physical parameters that will make the model valid for several regions. Moreover, statistics regarding the noise scenario and a methodology for channel input impedance measure will be given.

This paper is organized as follows. In Section II a brief description of the network under study will be given, while in Section III, the measurement set-up will be explained. Then, in Section IV the structural and behavioral characterization will be carried out. Finally, the validation of the transfer function characterization and the proposed model will be explained in Section V and the concluding remarks will be given in Section VI.

II. MV NETWORK TOPOLOGY

Regarding the MV distribution power grid, there are basically three topologies: star, ring and mesh. The star topology joins the ES with the TSs by means of one or several radial lines departing from the center of the star (the ES). These lines (or feeders) can be exclusive for one transformer substation or cross several transformer substations. Moreover, these lines can be even branched.

In mesh topologies, where ES are joined by several MV lines, the power can be delivered by several routes: in case of a MV line failure, the power can be rerouted. Complexity is the main drawback of this kind of architectures. On the other hand, star topologies have several advantages over the meshed ones, like easier fault protection, voltage control and lower cost; but if one segment of the MV line fails, it means interrupting the service beyond the point of failure. Although MV networks are mainly meshed, EUs operate them as star or ring topology, configuring the mesh into several star or ring networks.

In order to overcome the problem of star networks, an improved star topology named ring topology, consisting of two MV feeders departing from the ES that share a common point named the border of the ring. This border is an open circuit between the two radial MV lines. This border can be moved in order to limit the impact of a failure into the network, minimizing the length of the segment (and the number of TS) affected by the failure [1].

Focusing in the ring topology, when the MV line enters the TS (Fig. 1) it has to pass through the input breaker and the output breaker to follow its way through the ring. In case of a failure in some TS, both the input and output breakers will be

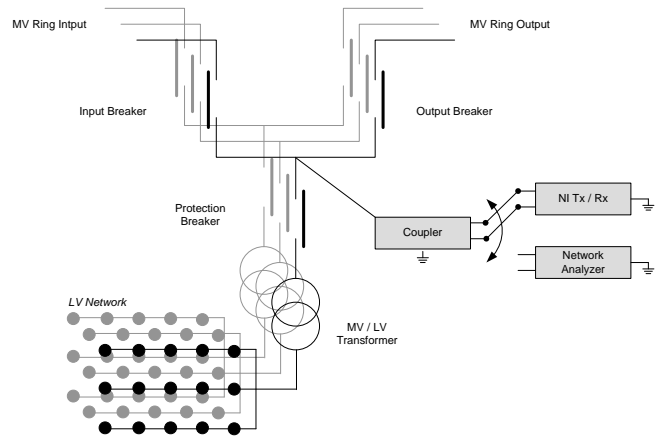


Fig. 1. Transformer Substation Schematic and Field Measurements Set-up

opened in order to move the ring border to the faulty point. In conjunction with the protection breaker, the input and output breaker are the typical topology configuration in TS called ring main unit (RMU). If the MV to LV transformer is wanted to be in service, the RMU protection breaker has to be switched on. PLC signal is transmitted and received through the MV channel by means of capacitive (or inductive) couplers. Typical coupling scheme is phase-to-ground.

Near the mains frequency, MV channel access impedance varies influenced by the mains level, directly connected loads to the MV grid (large consumers), the connection and disconnection of other meshed MV feeders and the consumer loads connected to them. Otherwise, for frequencies over tens of kilohertz, HV/MV and MV/LV transformers are almost perfect barriers, so, high frequency signals are naturally confined within the MV network. Typically, high frequency signal attenuations from 60 to 80 dB can be expected from the transformer HV or LV side to the MV network [13]. On the other hand, if some kind of high frequency coupling between MV and LV or HV networks is needed, the MV properties will be determined by the LV network, in terms of interference and impedance [14], [15].

III. MEASUREMENT SET-UP

In this Section, two measurement set-ups will be briefly described. The first one, depicted in Fig. 1, shows the set-up for the measurements carried out in the MV ring. A microwave network analyzer (MNA), two National Instruments PXI chassis, one of them carrying an arbitrary generator board [16] and another a high speed digitizer [16], both GPS synchronized [17], phase-to-ground coupled by means of a PLCoupling / DIMAT CAMT-1 capacitive coupler [18], have been employed. This set-up was used for the *Field measurements*, explained in the next Section.

The second one, depicted in Fig. 2, describes the set-up for the MV cable and coupler scattering (S) parameters [19] characterizations, explained in *Laboratory measurements*.

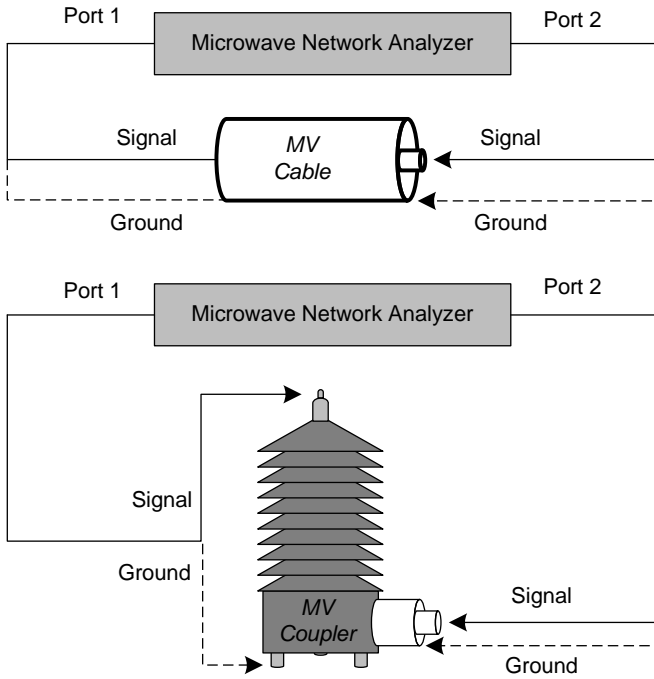


Fig. 2. Network Analyzer Set-up

IV. MEASUREMENTS AND CHARACTERIZATION

In this work, different measurements will be carried out in order to characterize the following urban underground MV channel effects [2], [14]:

- Input impedance. Mainly affected by:
 - Characteristic impedance of the MV cable.
 - Connected feeder's loads.
- Noise scenario .
 - Background colored noise: In MV networks, this noise is mainly caused by leakage or discharge events, power converters, transformer non idealities... As well as in HV networks, stationary low-power periodical and synchronous with the mains impulse events can also be considered background noise. These kinds of impulses are caused by discharges on insulators and other ES or TS devices.
 - Impulse events: The main causes of this noise type are network switching transients (isolator switching or breaker operation), lightning and other discharging events.
 - Narrowband noise: Narrowband interferences such as coupled broadcast emissions or other communications equipment are considered background noise.
- Attenuation and frequency selectivity. Caused by power dissipation and reflections in the grid or coupling devices. These two effects are included in the channel transfer function.

The aim of this work is to provide a set of measurements in order to get the needed behavioral and structural knowledge

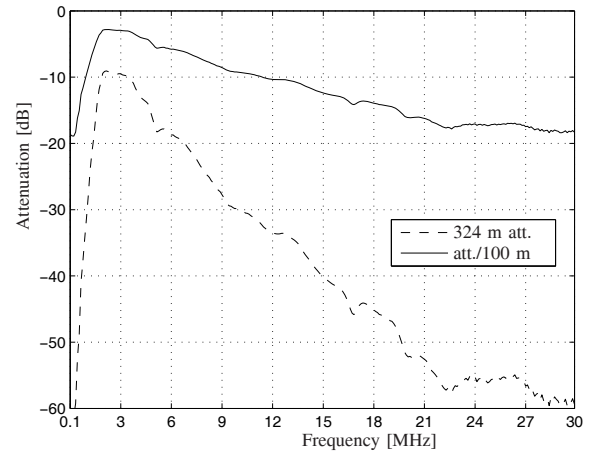


Fig. 3. Measured Link Attenuation

to define a proper model for MV urban networks. This set of measurements consists of:

- 1) Field measurements (FM). The following measurements have been done in a 324 meters link in Barcelona, Spain, between the Endesa (the main spanish electrical utility) substations BA07460 (transmitter) and BA07155 (receiver):
 - Link attenuation characteristics.
 - Link time and frequency spread.
 - Background noise.
 - Impulsive interferences.
 - Reflection coefficient.
- 2) Laboratory measurements (LM):
 - MV cable S parameters characterization.
 - MV coupler S parameters characterization.
- 3) Joint measurements:
 - Input Impedance.

A. FM: Link Attenuation Characteristics

The link attenuation characteristics have been measured by means of a GPS synchronized sweep transmission from 100 kHz to 30 MHz in 100 kHz steps.

In Fig. 3, the attenuation of the link under study is depicted. The dashed line shows the overall link attenuation, i.e., the attenuation due to the cable losses, the reflection and transmission capabilities of the coupler and the input impedance and parallel loads connected to that link. As stated, since there are more parameters than the intrinsic cable attenuation, the continuous line depicts an approximation of the attenuation per hundred meter, showing similar values as the ones in [13]. This measure will be recalled in Section VI when validating the channel characterization.

The time behavior of this attenuation characteristic is notably constant, with negligible variations over time. The attenuation characteristic band-pass shape is mainly due, on one hand, to the 1 nF coupler capacitor and to the effect of

TABLE I
PN SOUNDING PARAMETERS

| PARAMETER | VALUE |
|---------------------------------|---|
| Sequency type | m-sequence |
| Number of chips | $N_c = 511$ |
| Chip period | $T_c = \frac{1}{1.10^8} = 1 \mu\text{s}$ |
| Sequence period | $T = T_c \cdot N_c = 511 \mu\text{s}$ |
| Number of sequences per burst | $N_{sq} = 200$ |
| Pulse shaping ($p(t)$) filter | Root Raised Cosine Filter ($\alpha = 0.65$) |
| Occupied bandwidth | 1.65 MHz |
| Center frequency | $f_c = 2.5 \text{ MHz}$ |
| Maximum Detectable Delay | $511 \mu\text{s}$ |
| Delay Resolution | $1 \mu\text{s}$ |
| Maximum Detectable Doppler | 978 Hz |
| Doppler Resolution | 9.7 Hz |

the embedded impedance matching network, and, on the other, to the MV cable attenuation.

B. FM: Link Time and Frequency Spread

By means of pseudo-noise (PN) based channel sounding [20], the channel scattering function will be given, as well as the delay and Doppler spread values.

Equation (1) shows the transmitted signal, $s(t)$, consisting on a modulated maximal length sequence (m-sequence) train with center frequency $f_c = 2.5 \text{ MHz}$, located at the pass band center of the attenuation characteristic.

$$\begin{aligned}
 s(t) &= \sum_{n=0}^{N_{sq}-1} s_{PN}(t - nT) e^{j2\pi f_c t} \\
 &= \sum_{n=0}^{N_{sq}-1} \sum_{i=0}^{N_c-1} b_i p\left(t - i\frac{T}{N_c} - nT\right) e^{j2\pi f_c t}
 \end{aligned} \quad (1)$$

Where $s_{PN}(t)$ is a PN sequence of length N_c chips that have been interpolated by a pulse shaping filter $p(t)$, $b_i \in \{-1, 1\}$ are the sequence chips, N_{sq} is the number of m-sequences per burst, T is the sequence period, $T_c = \frac{T}{N_c}$ is the chip period and $\Delta T_s = TN_{sq}$ is the sounding period. This technique allows an unambiguous sounding when the channel has a impulse response, $h(\tau)$, shorter than T , with a time resolution of T_c , allowing a maximum detectable Doppler of $\frac{1}{2T}$ with an accuracy of $\frac{1}{\Delta T_s}$. Table I shows the sounding parameters.

After downconversion, the base-band received m-sequence train, $r_{PN}(t)$, is correlated with a local PN sequence replica $s_{lPN}(t)$, as shown in Eq. (2).

$$R_{r_{PN}, s_{lPN}}(t) = \int_0^T r_{PN}(t + \tau) s_{lPN}(\tau) d\tau \quad (2)$$

If $t = \eta \frac{T}{N_c N_{ov}} + nT$ where N_{ov} is the oversampling factor, i.e., the number of samples per chip; the discretized channel impulse response matrix $h[n, \eta]$ can be obtained from Eq. (2)

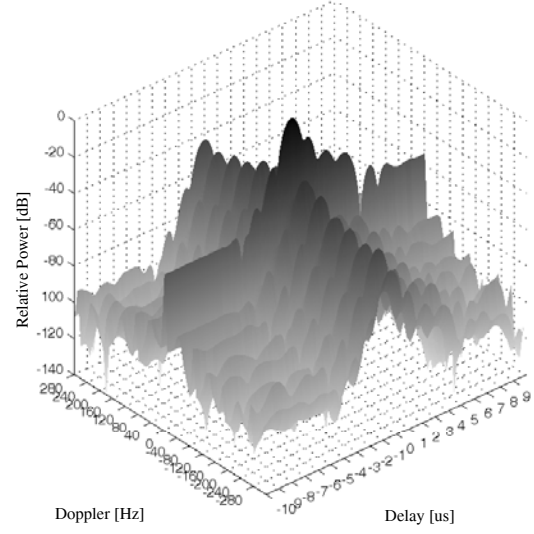


Fig. 4. Scattering Function

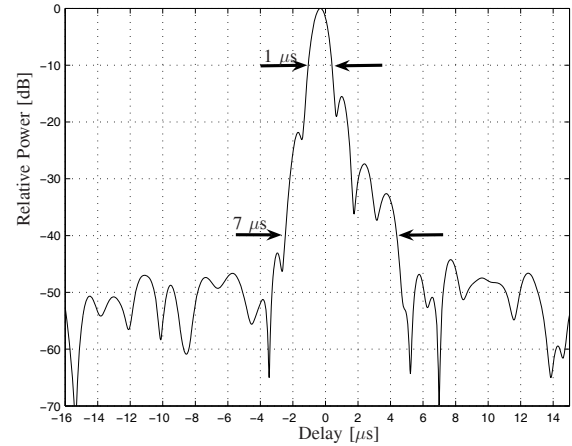


Fig. 5. Delay Power Profile

as shown in Eq. (3), where n and η are the time and delay indexes respectively.

$$h[n, \eta] = R_{r_{PN}, s_{lPN}} \left(\eta \frac{T}{N_c N_{ov}} + nT \right) \quad (3)$$

where

$$\begin{aligned}
 n &\in \mathbb{N} \text{ and } n \in [0, N_{sq} - 1] \\
 \eta &\in \mathbb{N} \text{ and } \eta \in [0, N_c N_{ov} - 1]
 \end{aligned}$$

Fig. 4 depicts the Discret Fourier Transform of $h[n, \eta]$ in the time domain, yielding to $h[k, \eta]$, i.e., the scattering function, where k is the Doppler index; and Fig. 5 shows the channel delay power profile.

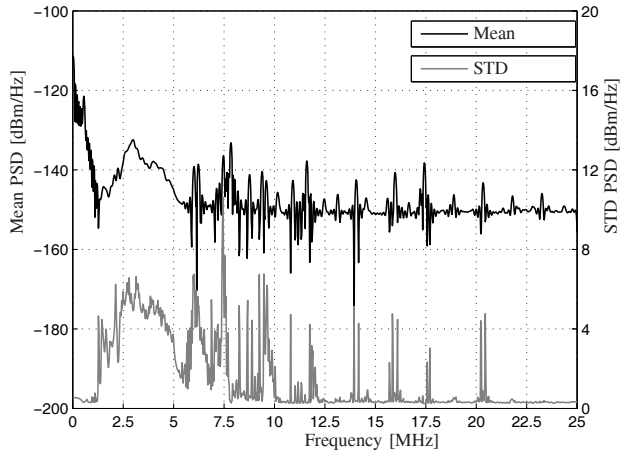


Fig. 6. Background Noise

The former (Fig. 4) depicts the power spreading in both time and frequency domain, showing the obvious invariant channel behavior, and the delay spread, detailed in Fig. 5, e.g., $\eta_{max}|_{10dB} = 1 \mu s$ and $\eta_{max}|_{40dB} = 7 \mu s$.

C. FM: Background Noise

One of the most characteristic aspect of PLC channels is their noise scenario. Simplifying the typical noise scenario defined in [9], two kinds of noise analysis will be carried out:

- 1) Background Noise. Including several low power spectral density (PSD) noise sources, narrowband interferences (mostly very slow variant sinusoidal signals) and low power periodic impulsive noise: some impulsive events also remain stationary, so, in this work, impulses with a continuous repetition and with a peak power less than 6 dB than the background noise mean power will be considered background noise too.
- 2) Impulsive Interferences. Those impulses not considered background noise, i.e., impulses with a peak power more than 6 dB than the background noise mean power.

Fig. 6 depicts the mean PSD and the standard deviation (STD) in the frequency domain. This noise has been recorded during four days, with an overall observation time of 400 seconds, sampled at 50 Msps.

These statistics reveal a highly colored background noise until 10 MHz, and from that point on, the delta-like spectrum is related to low-power continuous impulsive events. The colored behavior, due to the summation of several noise sources, remains at low frequencies, where the propagation from those sources to the measurement point is possible. The maximum variability has been observed in that frequency range, while in the highest ranges, only minor changes happened.

D. FM: Impulsive Interferences

While some noisy events remain stationary during time with a relatively low power, several impulsive interferences are characterized by their high amplitude. During five days, more

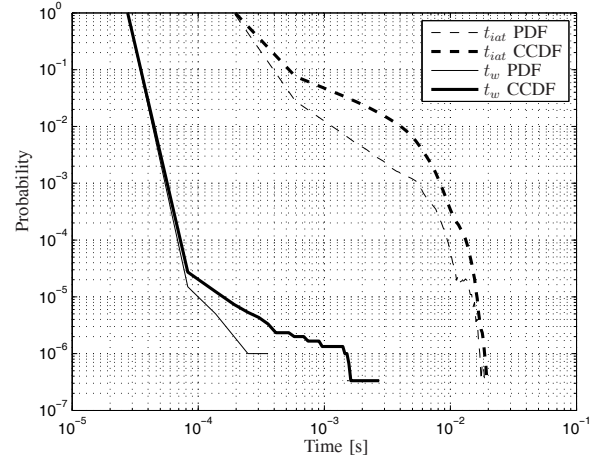


Fig. 7. Time Width and Interarrival Time

than 18 minutes sampled at 20 Msps have been processed to extract the following statistics. That observation time yields to 7,426,304 analyzed impulses.

The horizontal parameters, i.e., random variables (RV), that typically characterize these impulse events [9] are the impulse width (t_w), and the interarrival time (t_{iat}); that is, the time between the rising of the impulse and the end of the same, and the time between two consecutive pulse risings, respectively. Moreover, impulse interferences will be also characterized by two vertical parameters, i.e., impulse peak power (p_{pk}) and impulse average power (p_{av}). Fig. 7 and 8 depict the probability density function (PDF) and complementary cumulative density function (CCDF) for the time and power related RVs, respectively.

On one hand, impulses with durations less than 0.1 ms have an occurrence probability of $1 - 10^{-5}$, showing that almost all impulse durations are in the range of tens of microseconds. On the other, interarrival times of milliseconds, are quite usual ($> 10^{-1}$), undisturbed intervals over tens of milliseconds can arise with a probability of 10^{-3} .

Fig. 8 depicts that p_{pk} CCDF is a shifted version of p_{av} CCDF, showing that almost all impulses have the same shape or damping factor. Almost all impulsive events, about 99.9 %, have an average power lower than $50 \mu W$, on the other hand, there is one per million occurrences that reach the mW of average power. Also one impulse per million approximately, reaches $10 \mu W$ of peak power.

E. FM: Reflection Coefficient

Input impedance, specially when dealing with power line networks, is a key characteristic of the transmission channel, since it is different for different topologies and rules the power that the transmission and reception devices will be able to inject and recover from the network, respectively.

By means of the MWNA, the MV channel reflection coefficient, measured at the coupler equipment side, namely Γ_{in} , will be used for the network input impedance extraction,

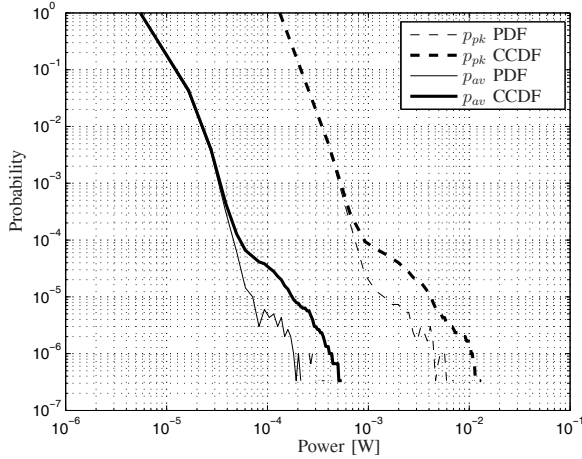


Fig. 8. Peak and Average Impulse Powers

as shown in Section IV-H, where the coupler behavior will be compensated in order to get the actual channel reflection coefficient and input impedance, thus.

F. LM: MV cable S parameters

In urban areas, Endesa is now mainly deploying 18/30 kV unipolar underground cable, with triple extruded aluminium core and cross linked polyethylene (XLPE) dielectric, compiling the rules EN-50267-2-1, IEC-60502.2 and Endesa proprietary rules DND001 and SND013.

The objective of this measurement is to obtain the MV cable propagation constant γ , Eq. (4), and characteristic impedance Z_0 .

$$\gamma = \alpha + j\beta \quad (4)$$

where

$$\beta = \frac{2\pi f}{c}$$

in

$$V(z) = V^+ e^{-\gamma z} + V^- e^{\gamma z} \quad (5)$$

In Eq. (5), $V(z)$ is the progressive, V^+ , and the regressive voltage wave V^- , in their phasorial representation. In the expression of γ , α , β and c are the attenuation constant, phase constant and propagation velocity, respectively. The extraction of the cable characteristics has been carried out as follows:

- 1) Precise cable length measure.
- 2) Manufacture of the cable to MWNA connection. The MV cable to the MWNA measurement port connections (Fig. 2) need an ad-hoc transition manufacture. These discontinuities involve geometrical changes in the cable structure, modifying its behavior, specially, at high frequencies; so special attention has been paid in their construction: short distance between the cable end and the connector (about 2 mm), single direct path between the cable aluminium conductor and the N connector core

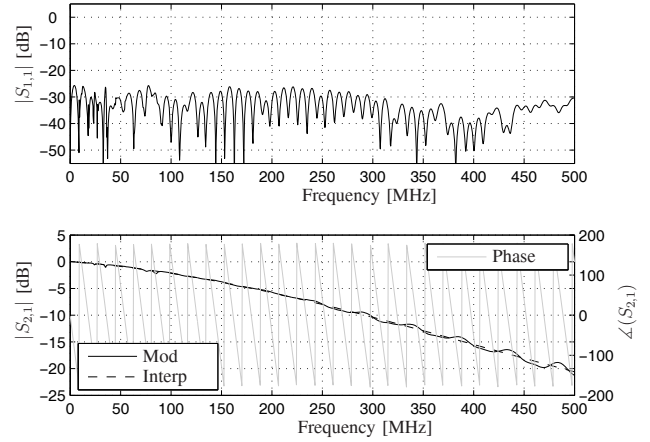


Fig. 9. Transmission and Reflection Parameters

and several paths between cable and N connector shields (trying to not to change the shield propagation modes).

- 3) S parameters measurement. Once the MV cable segment has been properly connected to the MWNA, the measurement of its 2x2 S parameters matrix, namely S'_{cbl} , is carried out. Note that S'_{cbl} includes both cable and discontinuity behaviors measured by a 50 Ω reference.
- 4) Transitional connection modeling. Taking into account the transition shapes and signal paths, and, in order to extract the discontinuity effect from S'_{cbl} at both cable ends, the transition is modeled by a serial anticond (L') and a parallel anticapacitor (C'), i.e., a coil and a capacitor with negative inductance and capacitance, respectively. When those discontinuity effects are extracted, the resulting S matrix will describe the behavior of the MV cable only, i.e., S_{cbl} .
- 5) Compensation and deembedding of the discontinuity connection geometrical change by means of gradient based optimization. An impedance matched transmission line has a near zero reflection parameters, i.e., $S_{cbl i,i} \approx 0 \forall i$. With the target of achieving such reflection values, an optimization of L' , C' and reference impedance Z_0 is carried out, obtaining a $S'_{cbl 1,1}$ and $S'_{cbl 2,2}$ less than -25 dB from 10 kHz to 500 MHz. Figure 9 shows the $S'_{cbl 1,1}$ and $S'_{cbl 2,1}$ after the optimization. At this point, the cable discontinuity parasit behavior can be considered compensated and S'_{cbl} becomes S_{cbl} , where the actual cable parameters are extracted. Equation (6), shows the third order polynomial that fits the $|S_{cbl 2,1}|$ [dB/10 m] with a root mean square error less than 0.1.

$$\alpha(f[MHz]) = 8.1 \cdot 10^{-8} \cdot f^3 - 9.8 \cdot 10^{-10} \cdot f^2 - 1.3 \cdot 10^{-2} \cdot f - 0.029 \quad (6)$$

- 6) Z_0 matching by means of cable reflection coefficient minimization. By the same methodology and target

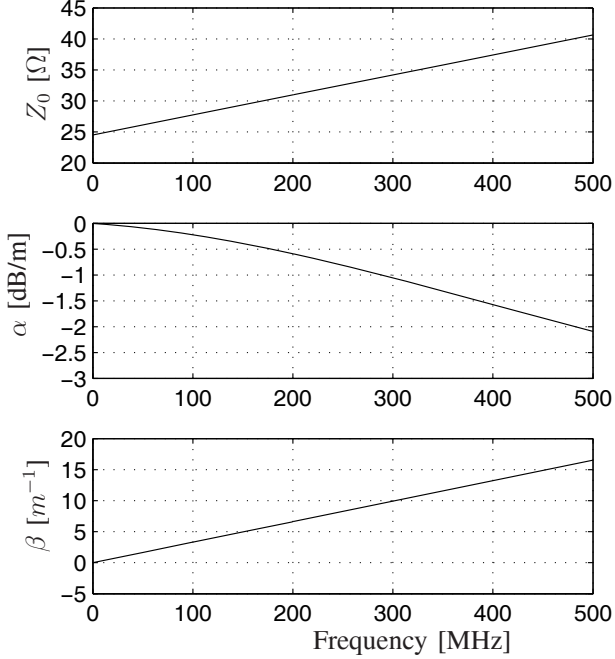


Fig. 10. MV Cable Propagation Constant

of the reflection coefficient minimization, the optimum reference impedance has been found. Since the reflection coefficients are minimized, it means that the reference impedance has the same value that the cable characterized impedance, first order fitted in Eq. (7).

$$Z_0(f[\text{MHz}]) = 24.53 + 3.22 \cdot 10^{-2} \cdot f \quad (7)$$

- 7) Finally, from the $\angle(S_{2,1})$ in the 500 MHz frequency range, and taking into account the cable length, the propagation velocity (and β) can be known as shown in Eq. (8), where l and ϕ are the cable length and the phase rotation respectively.

$$c = \frac{2\pi \cdot f \cdot l}{\phi} = 1.9 \cdot 10^8 \quad (8)$$

Fig. 10 summarizes the extracted MV cable parameters, yielding to the complete definition of the characteristic impedance and propagation constant, i.e., attenuation and phase coefficients.

G. LM: MV coupler S parameters

In this work, the measurement devices have been connected to the MV channel by means of phase-to-ground capacitive coupling. Measured as depicted in Fig. 2, the PLCoupling / DIMAT CAMT-1 capacitive coupler S parameters are extracted in S_{cplr} . This device is intended to adapt a communications equipment impedance of 50 Ω to an expected line access impedance of 20 Ω . If this requirement is met, the performance

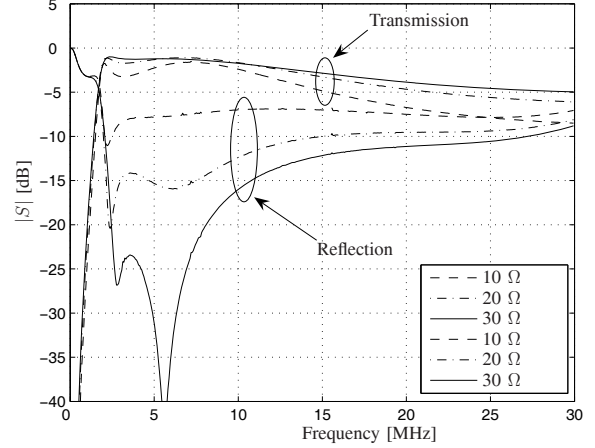


Fig. 11. Coupler Response Variation

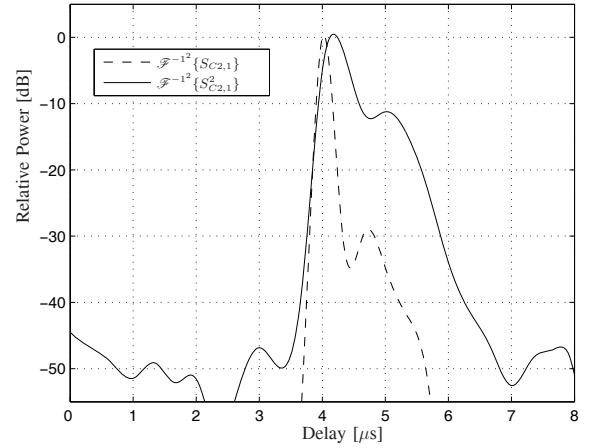


Fig. 12. Coupler Impulse Responses

of the coupler is the one shown in [18]. It has been found by simulation that if MV channel access impedance is different from the expected, the coupler performance varies, as shown in Fig. 11, where transmission and reflection performances are depicted for an access impedance of 10, 20 and 30 Ω .

In Fig. 12 the $S_{cplr_{2,1}}$ is shown in time domain, i.e., the $\mathcal{F}^{-1}\{S_{C2,1}\}$, where $\mathcal{F}^{-1}\{\cdot\}$ is the square of the inverse Fourier Transform. Besides, since the signal path goes through two couplers from the transmitter to the receiver, Fig. 12 also shows the delay power profile of two couplers in cascade ($\mathcal{F}^{-1}\{S_{C2,1} \cdot S_{C2,1}\}$). Taking into account Fig. 5, that measure shows that a most of the time spreading is due to the coupler.

H. Network Input Impedance

Finally, the MV access impedance is found as follows. If Γ_{in} is the measured channel reflection at the equipment side of the coupler, the MV channel reflection coefficient Γ_L is

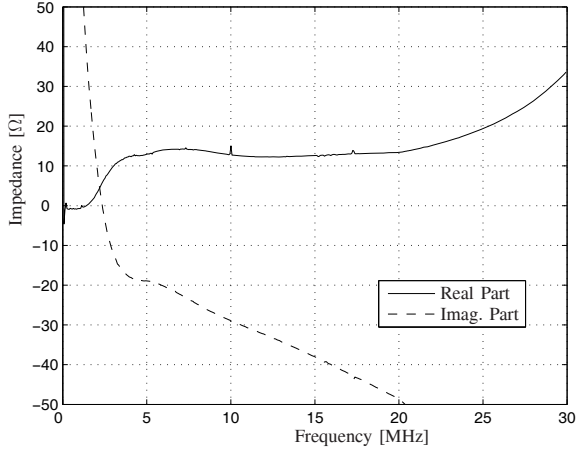


Fig. 13. MV Link Access Impedance

found as shown in Eq. (9), where $|\cdot|$ is the determinant of the matrix.

$$\begin{aligned}\Gamma_{in} &= S_{cplr\ 2,2} \frac{S_{cplr\ 1,2} \cdot S_{cplr\ 2,1} \cdot \Gamma_L}{1 - S_{cplr\ 1,1} \cdot \Gamma_L} \\ \Gamma_L &= \frac{\Gamma_{in} \cdot S_{cplr\ 2,2}}{|S_{cplr}| + S_{cplr\ 1,1} \cdot \Gamma_{in}}\end{aligned}\quad (9)$$

From the expression of Γ_L in Eq. (9), it is straightforward to find the access impedance Z_L , as shown in Eq. (10), where Z_0 is the measurement reference impedance, and depicted in Fig. 13. It shows that for our measurement scenario, channel input impedance real part ranges from 12 to 20 Ω , with no variations over time; while the reactance behaves capacitive.

$$Z_L = Z_0 \frac{1 + \Gamma_L}{1 - \Gamma_L} \quad (10)$$

V. MV CHANNEL TOPOLOGY MODELING AND VALIDATION

In some channels, like the LV grid, the network topology is complex, very branched, and often, unknown. This kind of environment calls for a stochastic modeling, usually based on multipath models. This is not the case for the MV network, where:

- 1) The topology is known.
- 2) The network device characteristics are known.

In this scenario, another kind of modeling can be carried out, i.e., deterministic modeling. This work proposes an ad-hoc modeling for every kind of MV network based on previous S parameter characterization of network devices.

With this approach, given a network topology and the easily measured device S parameters, the transfer function can be easily obtained from and to any two points of the network. This approach is very versatile, since the model can be exported to different regions where different topologies and/or network

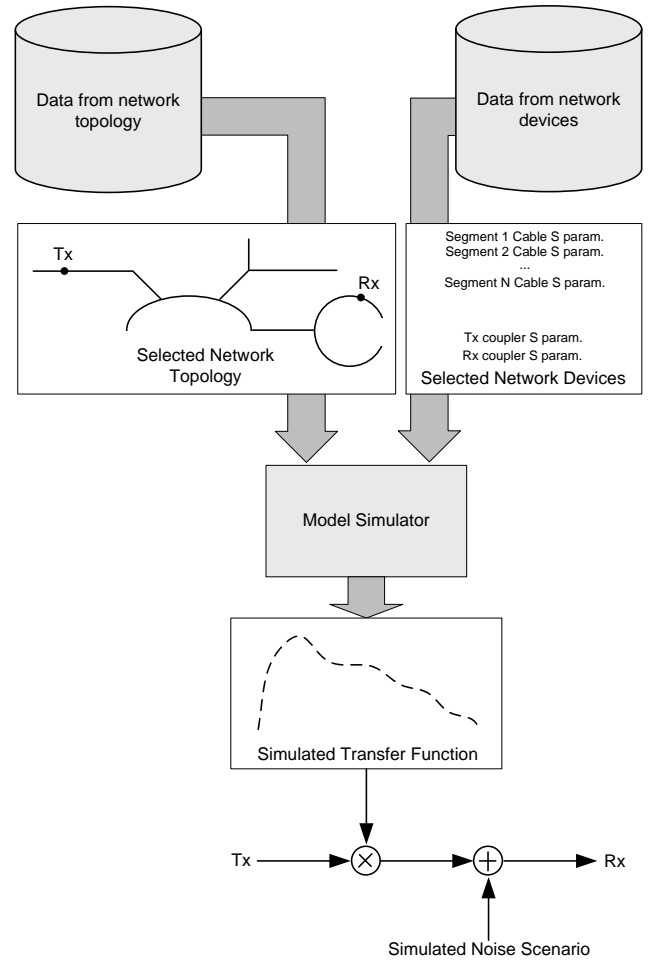


Fig. 14. MV Channel Model

devices are used. Once the channel transfer function has been found, the noise scenario can be added by easily tuning some noise model, e.g. [9], by the noise characterization presented in this work (Fig. 14).

In order to deterministically model the MV channel topology, the MV distribution cable and coupler have been characterized from structural measurements. The validation of the characterization and the model has been carried out by modeling the real measured network in a circuitual simulator, as shown in Fig. 15, and measuring the simulated attenuation characteristic. The modeled network consists of five MV cable segments and four joints between them. These joints are the points where the RMUs are located. In each joint the MV/LV transformer and the coupler can be found, as well as the 50 Ω impedance of the measurement devices. Although MV/LV transformers are considered perfect barriers for the high frequency signals, they have been circuitual modeled and included in the simulated topology as explained in [21]. The MV cable has been modeled by the extracted parameters in Eqs. (6,7,8) and the coupler by S_{cplr} .

Fig 16 shows a quite good match between simulation and measure. The deviations between the two characteristics are

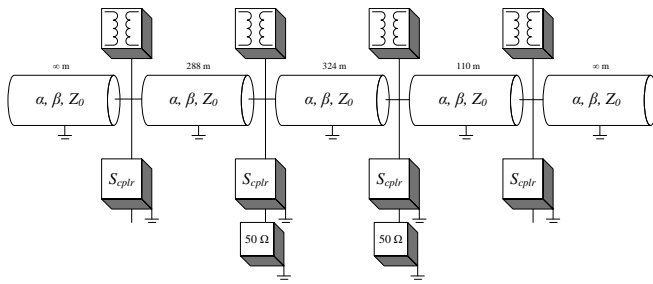


Fig. 15. Simulated Network Topology

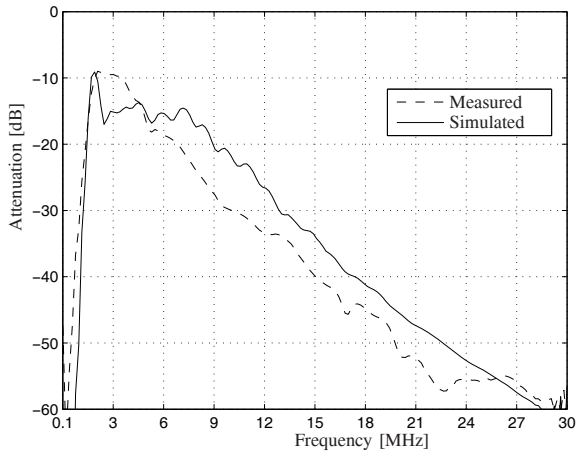


Fig. 16. Measured and Simulated Attenuation Characteristics

most probably due to the parasite behavior of RMU elements and physical construction issues, e.g., breakers, structure shapes and sections, and so on.

VI. CONCLUDING DISCUSSION

This paper has presented a S parameters based MV channel model for underground power lines. For this kind of scenario, the approximation that best suits this channel is a combination of deterministic and stochastic modeling for the channel transfer function and the noise scenario, respectively.

Previous to the model, this work has presented seven measurements, two of them for noise characterization and the others to properly model the transfer function of the urban underground MV distribution network.

The scattering parameters based structural characterization of network devices easily yields to the deterministic modeling of an arbitrary network topology, i.e., any kind of topology with any type of components. Moreover, also scattering parameters based, a methodology for extracting the network input impedance and its value have been presented, based on the coupler deembedding in order to get an actual channel measure.

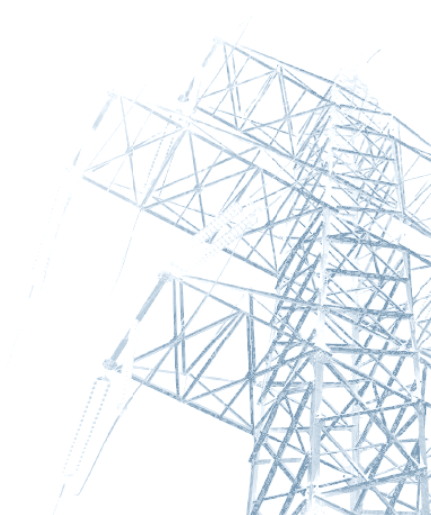
The noise random nature has been characterized in Figs. 7, 8 and 6, revealing its behavior in time width and interarrival impulse times, as well as the mean and variance for the

background noise in the frequency domain. Regarding the noise scenario modeling, the several stochastic proposals, e.g., [9], can be easily tuned to meet the MV channel background noise and interference characteristics.

This is a very powerful approach, since the model can be exported to different regions where different topologies and/or network devices are used while obtaining precise channel transfer functions. Moreover, the structural parameters can be set by a statistical values, in order to get the channel behavior for a certain network topology subset or group.

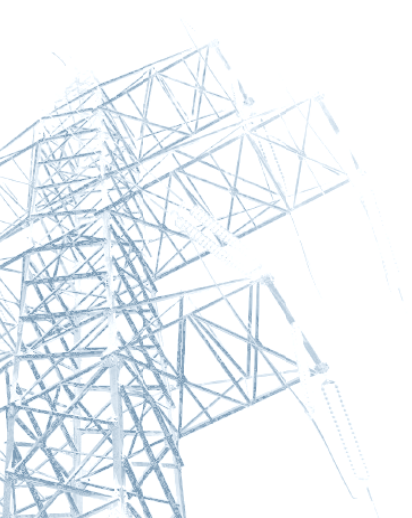
REFERENCES

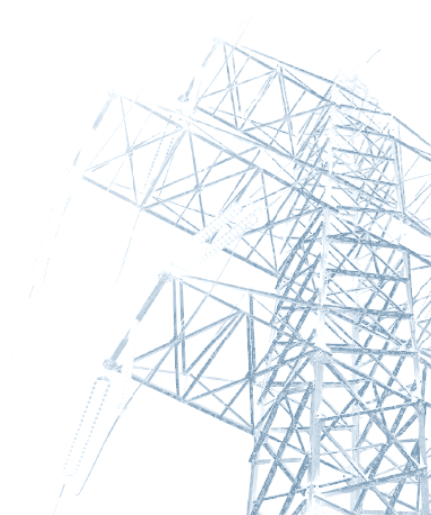
- [1] "Report on MV backbone system," OPERA, Tech. Rep. D-14, 2005.
- [2] Z. Tao, Y. Xiaoxian, Z. Bahoui, C. Jian, Y. Zhi, and T. Zhihong, "Research of noise characteristics for 10-kV medium-voltage power lines," *IEEE Transactions on Power Delivery*, vol. 22, pp. 142 – 150, 2006.
- [3] H. Philipps, "Performance measurements of powerline channels at high frequencies," in *IEEE International Symposium on Power Line Communications and Its Applications*, 1998.
- [4] R. Papayzan, P. Petterson, H. Edin, R. Eriksson, and U. Gäfvert, "Extraction of high frequency power cable characteristics from S-parameter measurements," *IEEE Transactions on Dielectrics and Electrical Insulation*, vol. 11, pp. 461 – 470, 2004.
- [5] R. Papayzan and R. Eriksson, "Calibration for time domain propagation constant measurements on power cables," *IEEE Transactions on Instrumentation and Measurement*, vol. 52, pp. 415 – 418, 2003.
- [6] C. Hensen, W. Schulz, and S. Schwarze, "Characterization, measurement and modeling of medium-voltage power line cables for high data rate communication," in *IEEE International Symposium on Power Line Communications and Its Applications*, 1999.
- [7] Y. Xiaoxian, Z. Tao, Z. Baohui, H. Zonghong, C. Jian, and G. Zhiqiang, "Channel model and measurement methods for 10-kV medium-voltage power lines," *IEEE Transactions on Power Delivery*, vol. 22, pp. 129 – 134, 2007.
- [8] Y. Xiaoxian, Z. Tao, Z. Baohui, Y. Fengchun, D. Jiandong, and S. Minghui, "Research of impedance characteristics for medium-voltage power networks," *IEEE Transactions on Power Delivery*, vol. 22, pp. 129 – 134, 2007.
- [9] M. Zimmermann and K. Dostert, "Analysis and Modeling of Impulsive Noise in Broad-band Powerline Communications," *IEEE Transactions on Electromagnetic Compatibility*, vol. 44, pp. 249 – 258, 2002.
- [10] —, "A multipath model for powerline channel," *IEEE Transactions on Communications*, vol. 50, pp. 553 – 559, 2002.
- [11] F. J. Cañete, "Power line channels: frequency and time selective part 1," in *IEEE International Symposium on Power Line Communications and Its Applications*, 2007.
- [12] "Report presenting the architecture of PLC system, the electricity network topologies, the operating modes and the equipment over which PLC access system will be installed," OPERA, Tech. Rep. D-44, 2005.
- [13] "Pathloss as a function of frequency, distance and network topology for various LV and MV European powerline networks," OPERA, Tech. Rep. D-05, 2005.
- [14] K. Dostert, *Powerline Communications*. Prentice Hall, 2001.
- [15] B. Gustavsen, "Wide band modeling of power transformers," *IEEE Transactions on Power Delivery*, vol. 19, pp. 414 – 422, 2004.
- [16] N. Instruments, "NI PXI-5441 specifications, 100 msp/s, 16-bit arbitrary waveform generator with onboard signal processing," National Instruments, Tech. Rep., 2005.
- [17] —, "NI-660x specifications," National Instruments, Tech. Rep., 2006.
- [18] Dimat, "Coupling unit for PLC equipment over medium voltage lines," Dimat, Tech. Rep., 2006.
- [19] D. Pozar, *Microwave Engineering*. John Wiley & Sons, 2005.
- [20] D. V. Sarwate and M. B. Pursley, "Crosscorrelation Properties of Pseudorandom and Related Sequences," *Proceedings of IEEE*, vol. 68, p. 593–619, May 1980.
- [21] T. Tran-Anh, P. Auriol, and T. Tran-Quoc, "High frequency power transformer modeling for Power line Communication applications," in *IEEE Power Systems Conference and Exposition*, July 2006.



8.6. APPENDIX A.6

R. Aquilué, I. Gutiérrez, J.L. Pijoan, G. Sánchez, "High Voltage Multicarrier Spread Spectrum Field Test", accepted for publication in IEEE Transactions on Power Delivery, May 2008.





High Voltage Multicarrier Spread Spectrum System Field Test

Ricard Aquilué*, Ismael Gutierrez*, Joan Lluís Pijoan* and Germán Sánchez†

* Department of Communications and Signal Theory, La Salle Engineering, Ramon Llull University. Barcelona, Spain. Email: raquilue@salle.url.edu

† Endesa Network Factory, Centro Referencia Aplicaciones Tecnológicas. Barcelona, Spain.

Abstract—High voltage (HV) power lines have been used as a communications medium since the 1920s. Those point to point links were typically based on single-sideband amplitude modulation. Nowadays, the state of the art in HV power line carrier (PLC) communications comprises the combination of analog systems, mainly for teleprotection tasks, and digital systems, used for voice and data transmission. Beside traditional core services (monitoring, operation management, and limitation and removal of failures), electrical utilities would like to satisfy the increasing need of new internal applications. In that way, quadrature amplitude modulation and, most recently, multicarrier modulation (MCM) based modems are beginning to play an important role in HV PLC systems. Although the typical 4 kHz bandwidth has been recently increased up to 32 kHz, this paper proposes a low-power 256 kHz bandwidth multicarrier spread spectrum (MC-SS) based physical layer. Based on channel measurements, the MC-SS symbol has been designed and tested in order to increase the user bit rate while delivering a reduced power spectral density and bit error rate.

I. INTRODUCTION

Since the beginning of 20th century, the High Voltage (HV) network has been exploited as a communications medium. Actually, the first ever running communication equipments on power lines were the HV double-sideband amplitude modulation (1920s) and single-sideband amplitude modulation (SSB-AM) modems (1940s). Since no other communications network could offer such a geographic presence, reliability and cost effectiveness, electrical utility (EU) core services, i.e., monitoring, operation management and limitation and removal of failures, were carried out by voice transmission by means of analog power line carrier (PLC) systems [1].

In the course of time, voice transmission could not achieve the reliability, rate and the level of automation that the EUs deserved for their applications, therefore, a rapid development of PLC systems towards digital implementations shown up.

At the beginning, the digital data transmission was carried out by means of low speed (50 bps) amplitude shift keying modems. With the increase of the power grid automation level, the required data rate grew to support the communications of such a complex system, yielding to the typical 2400 bps modems and the 4 kHz channelization [2], [3].

Nowadays, PLC systems are usually based on the combination of analog and digital technologies, that presents a higher degree of flexibility for the EU: while it solves the problem of the low reliability of the digital PLC for tasks such as

teleprotection, it overcomes the rate limitation of the analog PLC.

Focusing on data transmission PLC state of the art, the digital systems based on quadrature amplitude modulation (QAM) single carrier modulation (SCM) can reach a net bit rate of up to approximately 80 kbps in a 16 kHz bandwidth with bit error rate (BER) equal or below 10^{-6} [4]. Multicarrier modulation (MCM) begins to play an important role in HV communications due to its inherent robustness against multipath effects and narrowband interferers, in addition to a high spectral efficiency. This is making orthogonal frequency division multiplexing (OFDM), the most adaptive and frequency efficient MCM version [5], the choice for manufacturer's next generation HV PLC equipment, delivering a data rate of 256 kbps available to the user in a bandwidth up to 32 kHz, extending the usable carrier frequency range up to 1 MHz [6].

Beside the traditional core services mentioned before, EUs would like to satisfy the increasing need of new internal services (support for advanced grid control and automation, audio and video security related communication, etc), taking benefit from the use of their own power grids. Current standards regarding HV communications are obsolete and unaligned with supporting HV PLC new technology deployment. IEC-TC57 Workgroup 20 recently started to work on a new standard including HV Digital PLC (DPLC) [7].

Based on the channel measurements carried out in this work, a multicarrier spread spectrum (MC-SS) physical layer will be proposed and tested in a real scenario. Although the licensed band for PLC is located from 40 kHz to 500 kHz [2], [3], in certain situations, the signal propagation can be favorable enough to use the frequency range above that upper limit; so, the study on this paper will go beyond this constraint and will propose, based on the learned experience, the exploitation of that range by MCM adaptive [5] and Cognitive Radio (CR) techniques [8]. Based on the same measurements, while trying to reduce the interference on other PLC equipment in the PLC-licensed band and on the existing broadcast signals on the non-PLC-licensed band, the MCM symbol design is performed in order to minimize of the transmitted power spectral density (PSD).

This paper is organized as follows: In Section II the description of the HV transport lines where the measurements have

been carried out, as well as the measurement and test set-up will be described. Two scenarios have been tested: first, a 6.85 km long link, and another 27 km long. In Section III, the measurement outcomes regarding the 6.85 km link will be discussed and then, in Section IV, the MC-SS symbol design and the proposed system performance will be shown for the same link. In the next Section, Section V, a short briefing of the 27 km link measurement and MC-SS data transmission results will be given. Finally, concluding remarks will be summarized in Section VI.

II. MEASUREMENT AND TEST SCENARIO

In this Section, the test scenario as well as the measurement set-up will be introduced.

The scenarios under test are, in one hand, a 4-circuits, 3-phase 110 kV line between the “Egara” and the “Mas Figueres” ENDESA substations, in Barcelona, Spain, both substations separated by 6.85 km; and on the other, a similar 27 km line between the “Sant Celoni” and the “Tordera” ENDESA substations, also in Barcelona. In the sequel, the former will be named the “short” and the latter the “long” link.

Both channel measurements and data transmission tests have been carried out using the same equipment: two National Instruments PXI chassis. Each chassis consists on an industrial embedded computer, one high stability reference clock [9] and a special instrumentation card. At the transmission site, this instrumentation card is a high speed arbitrary waveform generator, capable of output data at 100 Msps at 16 bits of vertical resolution [10]; while the receiver chassis has an analogous 14 bits high speed digitizer [11]. Both chassis are GPS synchronized.

The measurement and test set-up is depicted in Fig. 1. At the transmission site, the digital-to-analog converted signal is immediately fed into an ad-hoc built amplifier¹. From 50 kHz to 1.4 MHz, this device offers a gain of 37.5 dB and 160 W of peak envelope power (PEP). When amplified, the signal gets the coupling device [12] that, taking into account the coupler capacitor, matches the 75 Ω amplifier output impedance with the line access impedance.

That matching procedure is carried out manually, i.e., the reflection coefficient at the input of the coupling unit is monitored while switching among coupling unit different configurations. Since the transformers at the line ends can be considered as a perfect barriers for frequencies over a few tenths of kHz [13], the previously found coupling device configuration (and line access impedance) can be considered valid for that time on.

The line trap prevents the radio frequency signal from entering the substation premises while it propagates toward the receiver site. When decoupled and before the acquisition, the signal is amplitude limited and noise and antialias low pass filtered at 6 MHz. In the sequel, the channel is considered to

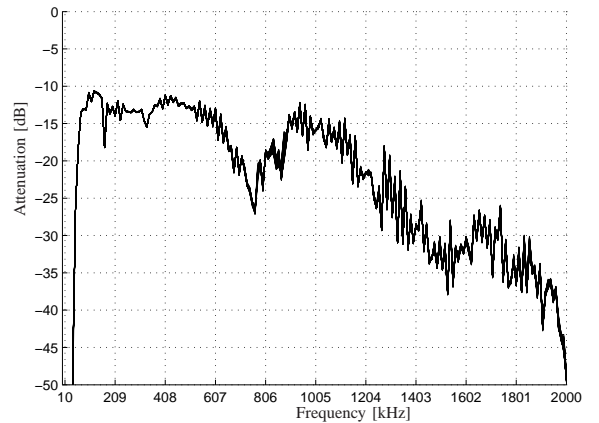


Fig. 2. Link Attenuation

be between the amplifier output and the transient limiter input; other devices will be properly compensated.

In the next two Sections, III and IV, the channel measurements as well as the symbol design and test concerning the short link will be given. Since the same procedure has been followed for the long link study, the most important details concerning that link will be given in Section V.

III. CHANNEL MEASUREMENTS, SHORT LINK

In this Section, a complete wideband sounding for the HV-PLC channel will be presented. First, the attenuation characteristic will show the power line transmission capabilities and its long term variations. Then, in order to get knowledge of the short term variations, i.e., the channel delay and Doppler spreads, the pseudo-noise (PN) sequence based sounding will be carried out. Maximal length sequences (m-sequences) are used because of its well-known good autocorrelation properties [14]. From these measurements, the channel coherence time (Δt_0) and coherence bandwidth (Δf_0) will be deduced in order to properly design the MCM symbol. Finally, a background noise analysis will be carried out.

A. Attenuation Characteristics

The attenuation characteristic of the link under study has been measured by transmitting one tone sweep every 20 minutes from 10 kHz to 2 MHz in 10 kHz steps. Each step consists on 10 averaged acquisitions during 2 seconds. In Fig. 2 all the measured sweeps can be seen overimposed.

The channel attenuation characteristic shows a pass band behavior. The low cut-off frequency (40 kHz) is due to the coupling capacitor and coupling device combined frequency response, and the high one is due to the same devices plus the line attenuation. The ripple at the pass band is due to the multipath effect, as it will be shown later, whereas the null from 610 kHz to 880 kHz is due to the coupling devices impedance mismatching. The perfect match among the 360 sweeps (5 days) means that both propagation and coupling

¹Manufactured by DIMAT S.A., a ZIV Group Company

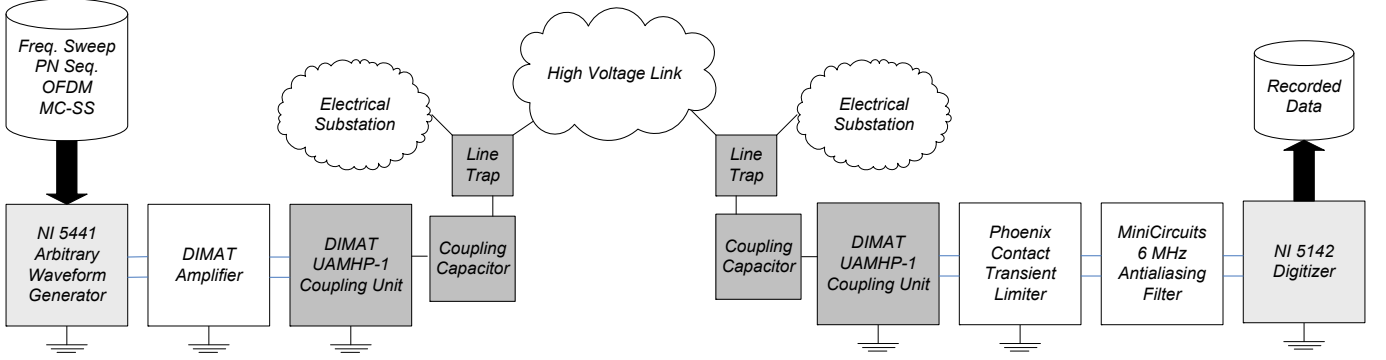


Fig. 1. Measurement and Test Set-Up

TABLE I
PN SOUNDING PARAMETERS

| PARAMETER | VALUE |
|---------------------------------|---|
| Sequency type | m-sequence |
| Number of chips | $N_c = 2047$ |
| Chip period | $T_c = 1.66 \mu\text{s}$ |
| Sequence period | $T = T_c N_c = 3.41 \text{ ms}$ |
| Number of sequences per burst | $N_{sq} = 10$ |
| Pulse shaping ($p(t)$) filter | Root Raised Cosine Filter ($\alpha = 0.65$) |
| Occupied bandwidth | 0.99 MHz |
| Center frequency | $f_c = 600 \text{ kHz}$ |

performances remained constant for one week, so, there is no long term variation in the link transfer function.

B. Time Spread and Frequency Spread

In this Section, by means of PN sequences, the short term channel variation as well as time spreading will be studied.

The transmitted pilot signal, $s(t)$ (Eq. (1)), consists on a modulated m-sequence train at center frequency f_c .

$$\begin{aligned}
 s(t) &= \sum_{n=0}^{N_{sq}-1} s_{PN}(t - nT) e^{j2\pi f_c t} \\
 &= \sum_{n=0}^{N_{sq}-1} \sum_{i=0}^{N_c-1} b_i p\left(t - i \frac{T}{N_c} - nT\right) e^{j2\pi f_c t}
 \end{aligned} \quad (1)$$

Where $s_{PN}(t)$ is a PN sequence of length N_c chips that have been interpolated by a pulse shaping filter $p(t)$, $b_i \in \{-1, 1\}$ are the sequence chips, N_{sq} is the number of PN sequences per burst, T is the sequence period, $T_c = \frac{T}{N_c}$ is the chip period and $\Delta T_s = TN_{sq}$ is the sounding period. This technique allows an unambiguous sounding when the channel impulse response ($h(\tau)$) is shorter than T , with a time resolution of T_c , allowing a maximum detectable Doppler of $\frac{1}{2T}$ with an accuracy of $\frac{1}{\Delta T_s}$. Table I shows the sounding parameters.

After downconversion, the base-band received m-sequence train, $r_{PN}(t)$, is correlated with a local PN sequence replica $s_{IPN}(t)$, as shown in Eq. (2).

$$R_{r_{PN}, s_{IPN}}(t) = \int_0^T r_{PN}(t + \tau) s_{IPN}(\tau) d\tau \quad (2)$$

The discretized channel impulse response matrix $h[n, \eta]$ can be obtained from Eq. (2) as shown in Eq. (3), where $t = \eta \frac{T}{N_c N_{ov}} + nT$ where N_{ov} is the oversampling factor, i.e., the number of samples per chip, and n and η are the time and delay indexes respectively.

$$h[n, \eta] = R_{r_{PN}, s_{IPN}}\left(\eta \frac{T}{N_c N_{ov}} + nT\right) \quad (3)$$

where

$$\begin{aligned}
 n &\in \mathbb{N} \text{ and } n \in [0, N_{sq} - 1] \\
 \eta &\in \mathbb{N} \text{ and } \eta \in [0, N_c N_{ov} - 1]
 \end{aligned}$$

Fig. 3 shows the normalized power of $h[n, \eta] \forall n$, that is, the N_{sq} impulse responses overlapped, revealing no short time channel variations. In the same figure, the first and most powerful path, which is the direct one, followed by an exponential energy decrease of $20 \mu\text{s}$, can be seen. This decreasing spreading after each path is caused by network devices (e.g. coupling devices, coupling capacitor and line traps, etc) non idealities. That first path is followed by the second one, 17.4 dB attenuated and $47 \mu\text{s}$ after. This second path is due to the reflection of the first incoming signal at the receiving substation, its propagation back again to the transmitter site and its second reflection to the original destination. The same can be told about the third path. Taking into account a distance of 6.85 km between transmitter and receiver, it is straightforward to find a propagation speed of $2.92 \cdot 10^8 \frac{\text{m}}{\text{s}}$ or 0.97 times c_0 (speed of light in the vacuum), a little less than the expected for a transversal electromagnetic propagation, probably due to the topological and structural line characteristics, e.g. path, supports, direction changes, etc.

The spreading in time calls for a robust modulation in front of frequency selective channels and inter-symbol interference (ISI). OFDM delivers such robustness in this kind of scenario if both subcarrier bandwidth and cyclic prefix length are properly designed, therefore, achieving a flat channel per subcarrier and avoiding ISI, respectively. As expected, no

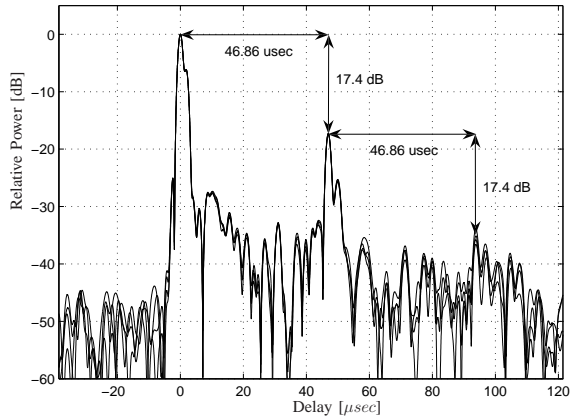


Fig. 3. Channel Impulse Response

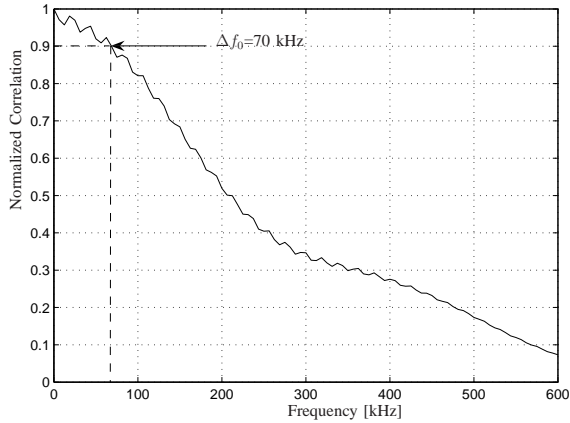


Fig. 4. Frequency Autocorrelation Function $R(\Delta f)$

channel variation has been found in time domain, yielding to a zero Doppler scattering and subsequently a large value for the coherence time of the channel, i.e., $\Delta t_0 \rightarrow \infty$. Adaptive techniques cannot be implemented in real time due to current equipment restrictions, however an stationary channel enhances the modulation adaptation performance and OFDM offers the maximum achievable spectral granularity, becoming the best candidate to implement adaptive techniques [5].

Once the time domain variation has been characterized, the frequency domain variation, i.e., the Δf_0 , has to be found. From Eq. (3), the channel transfer function, $H(f)$ can be calculated by means of the Fourier Transform. Then, in order to find the Δf_0 , the frequency correlation function, Eq. (4), is depicted in Fig. 4.

$$R(\Delta f) = \frac{E\{H^*(f)H(f + \Delta f)\}}{E\{H(f)\}} \quad (4)$$

In this work, a Δf_0 of 70 kHz for a 0.9 correlation is considered (Fig. 4). Taking this frequency correlation measure

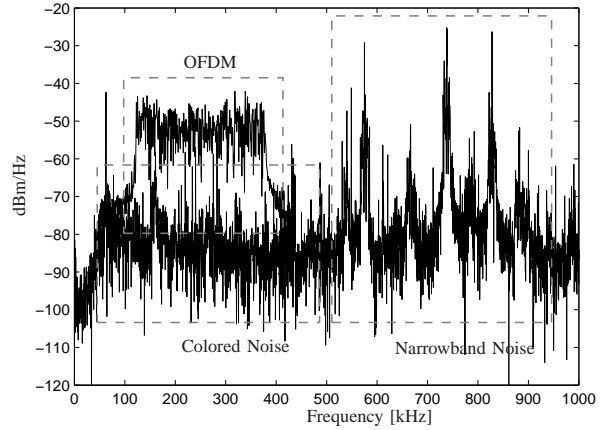


Fig. 5. Background Noise and OFDM PSDs

into account, the channel sampling theorem has to be fulfilled in the frequency domain [15] for channel estimation purposes. This issue will be deeply studied in Section IV-A.

C. Noise Scenario

In this Section, a closer look will be given to the noise scenario, specifically, to background noise. This type of noise is a broadband permanent interference with relatively high level and mainly caused by corona effect and other leakage or discharge events. Background noise PSD is time and frequency variant (colored noise). Due to climatic dependences, corona noise power fluctuations up to tens of dB may be expected. Moreover, stationary, low-power periodical and synchronous with the mains power frequency impulse events can also be considered background noise. These kinds of impulses are caused by discharges on insulators and other electrical substation devices. Narrowband interferences such a coupled broadcast emissions or other communications equipment, due to its slow variability, can be considered background noise too [1].

Fig. 5 shows the background noise and the received OFDM overimposed PSDs at the receiver site. Two noise regions can be clearly identified, i.e., from the lower frequencies up to 500 kHz and from 500 kHz on. The former band is colored noise limited, while the latter is narrowband interference limited.

Fig. 6 depicts the maximum, the minimum and the mean PSD values (three upper black lines) from 40 kHz to 1 MHz, during a 4 days observation period. Although this behavior can be considered slow variant, large differences in time show up. This scenario shows a highly dynamic background noise in frequency domain, since maximum variations up to 40 dB have been measured, with standard deviations (STD) around 10 dBm/Hz, in the whole frequency range. Larger differences between maximum and minimum, as well as larger STD values, can be found in the frequencies where coupled signals from other equipment are located, e.g., around 160 kHz and 320 kHz. Since no adaptive scheme will be used, this background noise study will not directly affect the MCM

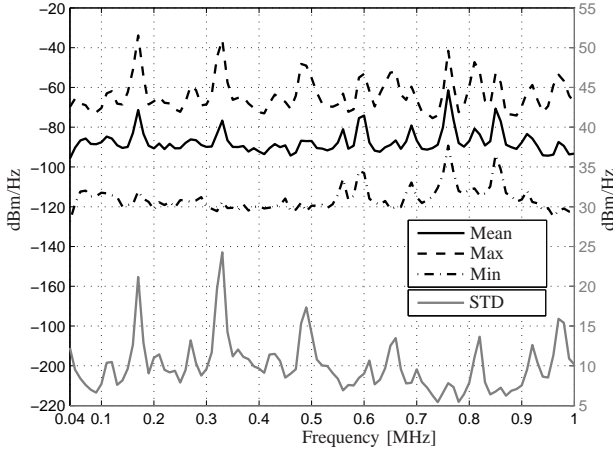


Fig. 6. Background Noise Statistics

symbol design, but the obtained results claim again for a power and bit-loading adaptive MCM physical layer [5].

IV. MCM DESIGN AND TEST, SHORT LINK

In this section, based on the measurements previously presented, the MCM symbol design will be presented, as well as the delivered performance for the three tested physical layer schemes: OFDM (Fig. 7) and two combinations of OFDM and code division multiple access (CDMA), generally known as MC-SS techniques. According how different streams share the spectrum, two typical schemes arise under the concept of MC-SS: multicarrier- code division multiple access (MC-CDMA) and multicarrier - direct sequence - code division multiple access (MC-DS-CDMA) [16], [17].

Fig. 7 shows the typical OFDM transmitter and receiver block diagram where $S_{r,s}$, for $r, s \in \mathbb{N}$, $r \in [0, N_{sym} - 1]$ and $s \in [0, N_{sc} - 1]$, are the complex symbols that will modulate the N_{sc} subcarriers of the N_{sym} symbols per OFDM frame. After the serial to parallel conversion, the OFDM symbol is modulated in the frequency domain by means of the inverse Fast Fourier Transform (IFFT). Then, after a serial to parallel conversion and before the conversion to the analog domain, the N_g samples of the guard interval are added in order to avoid inter-symbol interference (ISI) in the useful part of the symbol (5). By means of the received and sampled signal $y[n]$ FFT (IFFT), the received symbols R_k are recovered and ready for demapping.

$$x_s[n] = \frac{1}{N_{sc}} \sum_{r=0}^{N_{sc}-1} S_{r,s} e^{j2\pi n \frac{r}{N_{sc}}} \quad (5)$$

Although two-dimensional spreading methods exists, e.g., Variable Spreading Factor - Orthogonal Frequency and Code Division Multiplexing (VSF-OFCDM) [18], this work is focused on the two typical one-dimension spreading in frequency and time, MC-CDMA and MC-DS-CDMA, respectively.

The MC-CDMA (Fig. 8) scheme, also known as OFDM-CDMA, can be considered a classical OFDM system where the information applied to each L_f subcarriers belongs to the same spread symbol, where L_f is the spreading factor (SF) in frequency domain. The choose of the L_f determines how much the information is spread and, thus, the degree of frequency diversity. Moreover, the L_f determines the number of streams ($K_f \leq L_f$) that will share the same bandwidth. In case of full-loading $K_f = L_f$. When L_f becomes smaller than N_{sc} , different groups of subcarriers can be established ($G_f = \frac{N_{sc}}{L_f}$). In MC-DS-CDMA, the information applied to each L_t OFDM symbols in the same subcarrier belongs to the same spread symbol, where L_t is the SF in time domain. The choose of the L_t determines how much the information is spread and, thus, the amount of time diversity. In the same way, the L_t determines the number of streams ($K_t \leq L_t$) that will share the same OFDM symbols. In case of full-loading, the number of streams equals the SF again, $K_t = L_t$. When L_t becomes smaller than the number of OFDM symbols per frame N_{sym} , different groups can be established ($G_t = \frac{N_{sym}}{L_t}$).

After the initial serial to parallel conversion, if channel state information (CSI) is available at the transmitter, the signal goes through a power and bit-loading algorithm in order to adapt the power allocation and constellation scheme for each subcarrier or subcarrier groups [19]. Due to technical real time restrictions of the test equipment, the CSI is not available and the power and bit allocation matrix equals the identity. Then, $X_{n,m}^{i,j}$ designates the symbol that will be spreaded in frequency domain by the spreading code $c_f^i \in \mathbb{C}^{L_f \times 1}$ and in time domain by the spreading code $c_t^j \in \mathbb{C}^{L_t \times 1}$, where $c^H c = 1$ and $(\cdot)^H$ represents the Hermitic transpose and $i, j \in \mathbb{N}$, where $i \in [1, K_f]$ and $j \in [1, K_t]$. The indexes $n, m \in \mathbb{N}$, where $n \in [1, G_f]$ and $m \in [1, G_t]$, denote the frequency and time group where $X_{n,m}^{j,k}$ belongs to.

Regarding MC-CDMA, $L_t = 1$ and $c_t^j = [1] \forall j$, while $L_f > 1$ and $c_f^i = [\beta_f^{0,i}, \dots, \beta_f^{L_f-1,i}]$ yielding to G_f groups in frequency domain (6). Then $X_{n,m}^{i,j}$ can be redefined as $X_{g,s}^i$, where i, g and s are the spreading code, frequency group and OFDM symbol indexes, respectively.

$$x_s[n] = \frac{1}{N_{sc}} \sum_{g=0}^{G_f-1} \sum_{k=0}^{K_f-1} X_{g,s}^k \sum_{l=0}^{L_f-1} \beta_f^{l,k} e^{j2\pi n \frac{g L_f + l}{N_{sc}}} \quad (6)$$

On the other hand, MC-DS-CDMA is characterized by spreading in time, not in frequency, then $L_f = 1$ and $c_f^i = [1] \forall i$, while $L_t > 1$ and $c_t^j = [\beta_t^{0,j}, \dots, \beta_t^{L_t-1,j}]$ yielding to G_t groups in time domain (7). In (7), $X_{mod(d)}$ is the remainder of the quotient $\frac{X}{d}$ and $\lfloor \cdot \rfloor$ means the nearest integers towards minus infinity. In this case, $X_{n,m}^{i,j}$ can be redefined as $X_{r,g'}^j$, where j, r and g' are the spreading code, subcarrier and time group.

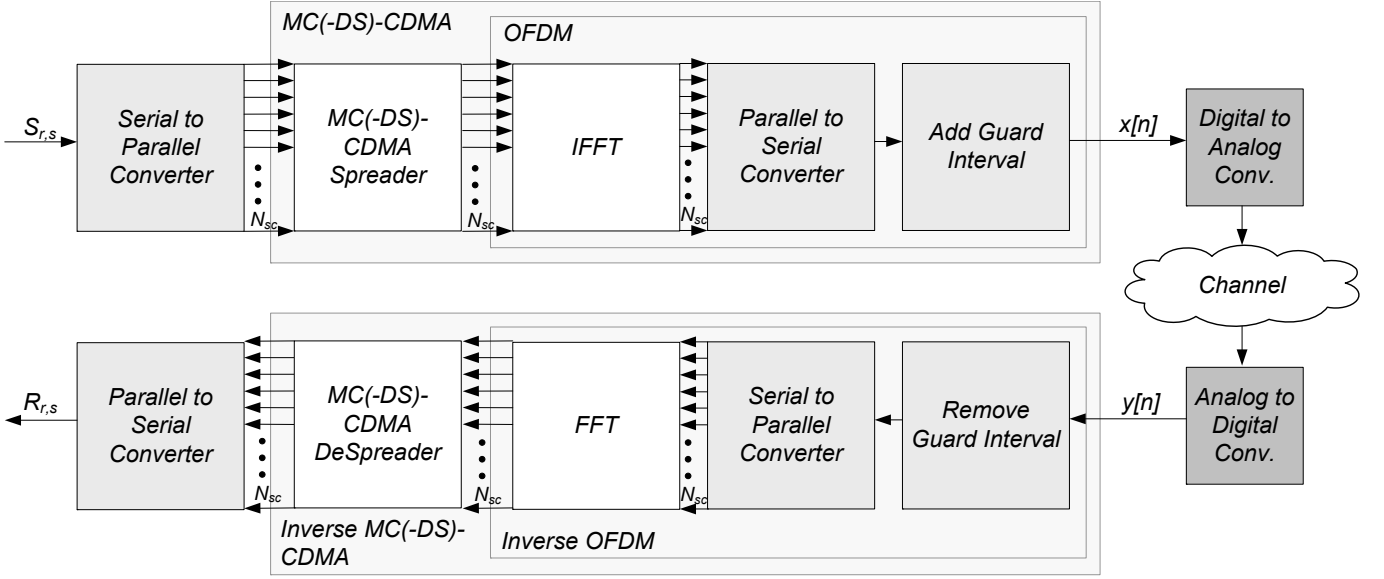


Fig. 7. OFDM, MC-CDMA and MC-DS-CDMA Block Diagram

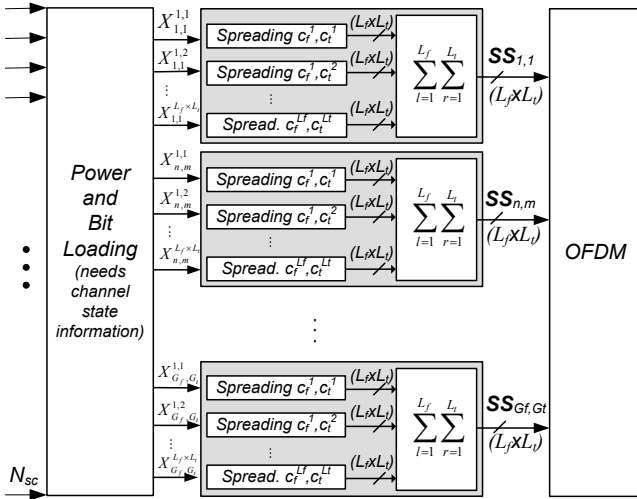


Fig. 8. Detail of MC-CDMA and MC-DS-CDMA Spreading Stage

$$x_s[n] = \frac{1}{N_{sc}} \sum_{k=0}^{K_t-1} \sum_{r=0}^{N_{sc}-1} X_{r,g'}^k \beta_t^{l',k} e^{j2\pi n \frac{r}{N_{sc}}} \quad (7)$$

where

$$g' = \lfloor s_{mod}(G_t) \rfloor$$

$$l' = s_{mod}(L_t)$$

As will be shown in the next Section, the three schemes, i.e., OFDM (5), MC-CDMA (6) and MC-DS-CDMA (7) are fairly compared in this paper, since the same signal to noise ratio (SNR) and the same user data rate will be used for testing, i.e., the same $\frac{E_b}{N_0}$ (bit energy to noise spectral density ratio).

A. Symbol Design

In this Section, the MCM symbol design will be carried out. First, the OFDM symbol parameters as well as the frame parameters will be given. Then, since the OFDM parameters will be used as a starting point for the MC-SS modulations design, only the spreading sequences, spreading factor and number of active streams need to be determined.

Transmitted power will be chosen in order to get a BER of approximately 10^{-2} before decoding. If using 16-QAM as a mapping scheme, 256 kHz of occupied bandwidth and 9 dBm of transmitted average power, around 20 dB of SNR is expected at the receiver site (Fig. 5). Taking into account this ratio and the impulse response in Fig. 3, only the first and the second path (at $\tau_{max}=46.86 \mu s$) have to be considered. A $T_{cp}=80 \mu s$ will prevent ISI from occur. The cyclic prefix duration, T_{cp} , is in charge of avoiding ISI, and consequently, inter-carrier interference (ICI). This guard interval has to be greater than the maximum delay spread (τ_{max}) [5].

The 10^{-2} expected BER is the minimum required modulation performance for allowing the channel coding perform correctly. A 1/2 convolutional code with constraint length 7 and trace-back length 35 will be used in order to achieve a BER performance close to the typical performance delivered by other systems: 10^{-6} . Moreover, a 120 depth interleaving will be employed in order to spread the symbols among the whole OFDM lattice [20].

Once T_{cp} has been fixed, the symbol length will be chosen while trying to maximize the cyclic prefix efficiency (8), that is, the ratio between the useful symbol time, T_u , and the symbol time T_s , where $T_s = T_{cp} + T_u$.

$$\rho_{cp} = \frac{T_u}{T_{cp} + T_u} \quad (8)$$

The maximum symbol time is restricted by the Δt_0 , i.e. $\Delta t_0 > T_s$, and by $\Delta f = \frac{1}{T_u}$, since a minimum Δf is needed in order to avoid the effect of ICI for a given uncompensated frequency offset, f_{off} [Hz]. In this way, in order to keep an acceptable performance degradation, a relative uncorrected frequency offset, δ_{off} , of $\delta_{off} = \frac{f_{off}}{\Delta f} \leq 0.01$ has to be fulfilled. A T_u of 1 ms will yield to a relaxed constraint of $f_{off} \leq 10$ Hz, while keeping $\rho_{cp} \geq 0.9$ [5].

Finally, a 1080 μs OFDM symbol of $N_{sc}=256$ subcarriers will be used. With $\Delta f=1$ kHz per subcarrier, an overall symbol bandwidth of 256 kHz is achieved.

Once Δf has been determined, the pilot separation in frequency domain, N_f can be found by satisfying the Nyquist sampling theorem in the frequency domain [15]. There are some rules of thumb that state that a channel oversampling of twice the Nyquist frequency is recommended [21], so following (9) and (10), where Δf_{N_f} and $\lfloor \cdot \rfloor$ are the frequency separation between pilot subcarriers and the nearest integer towards minus infinity respectively, N_f can be found.

$$\Delta f_{N_f} = \frac{1}{2} \frac{\Delta f_0}{2} = \frac{1}{2} \frac{70 \text{ kHz}}{2} = 17.5 \text{ kHz} \quad (9)$$

$$N_f = \lfloor \frac{\Delta f_{N_f}}{\Delta f} \rfloor = 17 \quad (10)$$

In order to avoid channel prediction at the OFDM lattice edges, which is more unreliable than interpolation, instead of using a N_f of 17 subcarriers, a separation of 16 subcarriers will be used.

Although the number of OFDM symbols in one frame is usually constrained by time and frequency acquisition and tracking algorithm accuracy (among others) [5], in our case, this is upper limited by the receiving equipment digitizer memory, a limitation of 16 (+1 pilot symbol) symbols has to be respected. A PN based pilot symbol used for synchronization is inserted at the beginning of each frame.

The channel stationary behavior gives no restriction regarding the pilot separation in time domain, so, since $N_{sym} = 16$, a pilot separation in time domain $N_t = 16$ could be chosen, yielding to a pilot density related efficiency ρ_{pd} of 0.996 (Eq. (11)).

$$\rho_{pd} = \frac{N_f N_t - 1}{N_f N_t} \quad (11)$$

On the other hand, noise effect regarding channel estimation can be reduced if we decrease the pilot distance down to $N_t = 4$, the efficiency is reduced only by a 1.2 %, yielding to the overall system performance shown in Eq. (12).

$$\rho_{cp} \cdot \rho_{pd} = 0.911 \quad (12)$$

Finally, the MCM parameters can be seen in Table II. While trying to simplify the receiver complexity, least squares channel estimation and 1D+1D lineal channel interpolation have been carried out before equalization [22].

TABLE II
MCM PARAMETERS

| PARAMETER | VALUE |
|----------------------------------|---|
| OFDM | |
| Cyclic prefix | $T_{cp} = 80 \mu s$ |
| Useful symbol time | $T_u = 1 \text{ ms}$ |
| Symbol time | $T_s = 1.08 \text{ ms}$ |
| Subcarrier bandwidth | $\Delta f = 1 \text{ kHz}$ |
| Number of subcarriers | $N_{sc} = 256$ |
| Pilot subcarriers | $N_p = 16$ |
| MCM bandwidth | 256 kHz |
| Pilot frequency spacing | $N_f = 16$ |
| Pilot time spacing | $N_t = 4$ |
| Number of OFDM symbols per frame | $N_{sym} = 16$ |
| Mapping | 16-QAM |
| Channel estimation | Least Squares and Minimum Mean Square Error |
| Channel interpolation | 1-D + 1-D 1 st order |
| Channel coding | 1/2 convolutional code, constraint length 7, trace-back length 35 and 120 of interleaving depth |
| Gross bitrate | $R_{bg} = 930 \text{ kbps}$ |
| User bitrate | $R_{bu} = 465 \text{ kbps}$ |
| Transmission peak power | $P'_{tx} = 150 \text{ mW}$ or 21.7 dBm |
| Transmission mean power | $P_{tx} = 7.7 \text{ mW}$ or 8.9 dBm |
| Peak to average power ratio | $PAPR = 12.8 \text{ dB}$ |
| MC-CDMA² | |
| Spreading sequence | Walsh-Hadamard |
| Spreading factor | $L_f = 8$, chip inteleaving depth 8 |
| Detection | Single User |
| Number of streams | $K_f = 8$ (Fully loaded) |
| MC-DS-CDMA² | |
| Spreading sequence | Walsh-Hadamard |
| Spreading factor | $L_t = 8$, chip inteleaving depth 2 |
| Detection | Single User |
| Number of streams | $K_t = 8$ (Fully loaded) |

In order to have a fair comparison between the OFDM and the MC-SS schemes, a Walsh-Hadamard $L_f=L_t=8$ fully loaded MC-CDMA and MC-DS-CDMA will be considered. The interleaving carried out in OFDM yields to an increase of both frequency and time diversity at symbol level. In the MC-SS modulations, a chip level interleaving in frequency and time will be carried out in MC-CDMA and MC-DS-CDMA, respectively. A single user detection scheme will be used for despreading [5].

²OFDM parameters apply to MC-CDMA and MC-DS-CDMA

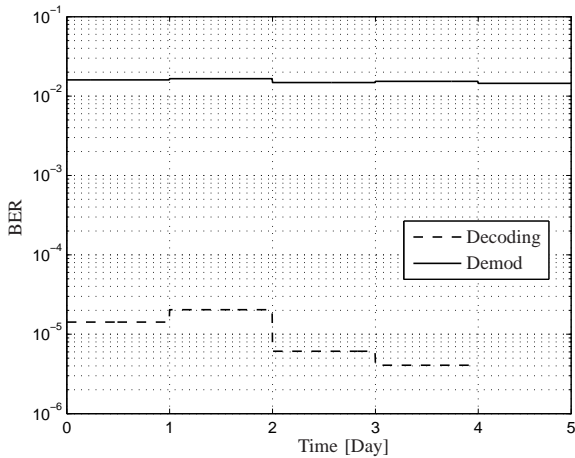


Fig. 9. OFDM Performance

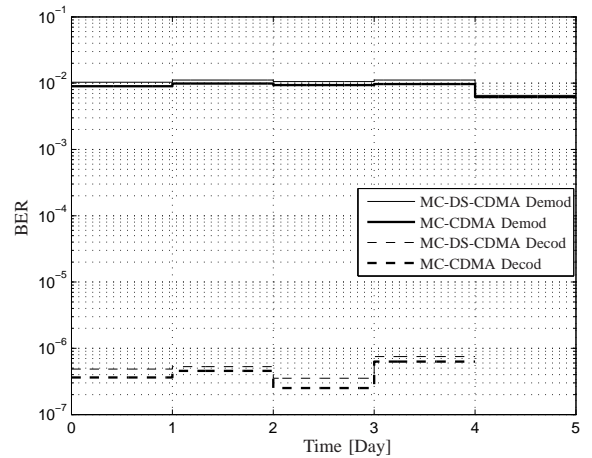


Fig. 10. MC-SS Performance

B. System Performance

The BER performance of the pure OFDM scheme is depicted in Fig. 9. The continuous line represents the modulation BER, i.e., without decoding, and the dashed line represents the BER after decoding, for a user bit rate of 465 kbps. Those lines show the day-by-day averaged performance.

The modulation BER showed a constant behavior, around $2 \cdot 10^{-2}$, while the performance after decoding yielded to a BER of $4.4 \cdot 10^{-6}$. The fifth day shows no line for the BER after decoding. During this interval, all the modulation errors were successfully corrected by the code, so a BER better than 10^{-7} was observed.

The MC-SS scheme performance is depicted in Fig. 10. Again, the continuous lines represent the modulation BER and the dashed lines represent the BER after decoding, for a user bit rate of 465 kbps. Since a higher level of channel diversity is obtained with spreading, both MC-SS schemes outperform the pure OFDM approach. Specifically, the MC-CDMA scheme delivers the best performance, i.e., $3.1 \cdot 10^{-7}$ of decoded BER (again, no errors during the fifth day). This is due to the fact that the channel we are dealing with presents a higher level of frequency selectivity rather than time selectivity. This selective behavior is most probably due to the noise scenario (colored spectrum in frequency domain and asynchronous impulses in time domain) rather than to the multipath effect.

Table III summarizes the performance of the three tested schemes.

V. LONG LINK

Previous sections have been focused on the channel study and symbol design for a low power MCM symbol. Only 7.7 mW of average power have been used in order to deliver the system performance shown in Table III.

In this Section, by means of the same channel study and symbol design methodologies, both MC-CDMA and MC-DS-CDMA schemes have been tested. In this scenario, the system performance has been measured by using a similar

TABLE III
SYSTEM PERFORMANCE

| Gross bitrate = 930 kbps | |
|--------------------------|---------------------|
| SCHEME | GROSS BER |
| OFDM | $2 \cdot 10^{-2}$ |
| MC-DS-CDMA | $9.9 \cdot 10^{-3}$ |
| MC-CDMA | $8.7 \cdot 10^{-3}$ |
| User bitrate = 465 kbps | |
| SCHEME | USER BER |
| OFDM | $4.4 \cdot 10^{-6}$ |
| MC-DS-CDMA | $4.2 \cdot 10^{-7}$ |
| MC-CDMA | $3.1 \cdot 10^{-7}$ |

peak envelope power (PEP) that other commercial systems use: 40 W, in a 27 km link.

With illustrative purposes only, Fig. 11 and Fig. 12 show the link attenuation and the delay spread, respectively. In the former, the lowest cut-off frequency is again caused by the coupling devices and the ripple in the pass band region by the multipath shown in the latter.

As expected, the attenuation characteristic is more severe and the channel delay is longer than the ones found in the 6.85 km link, Fig. 12 shows the first path followed by two reflected paths 19.8 dB below and 188 μ s after their predecessor. As the link length increases, the time distance between reflections increases, as well as their relative power. In order to be efficient in terms of cyclic prefix duration, an adaptive guard interval length is also welcomed in this channel invariant scenario.

From the obtained results in the short link, only the MC-SS schemes, not the pure OFDM, have been tested. In this scenario, taking into account a PEP of 40 W and 12 dB of peak to average power ratio (PAPR), since no PAPR reduction technique has been implemented, an average power of 2.5 W will be injected into the channel. The test results are

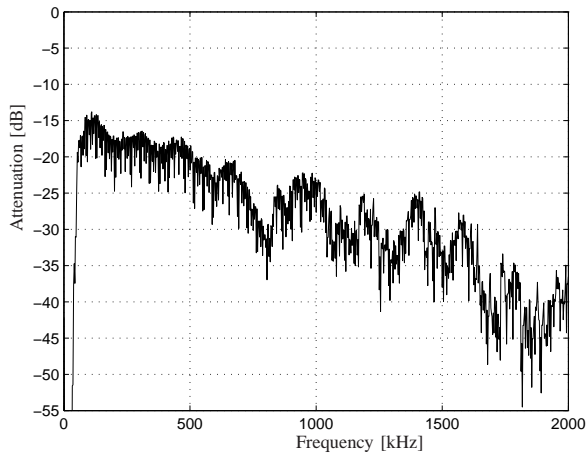


Fig. 11. Link Attenuation

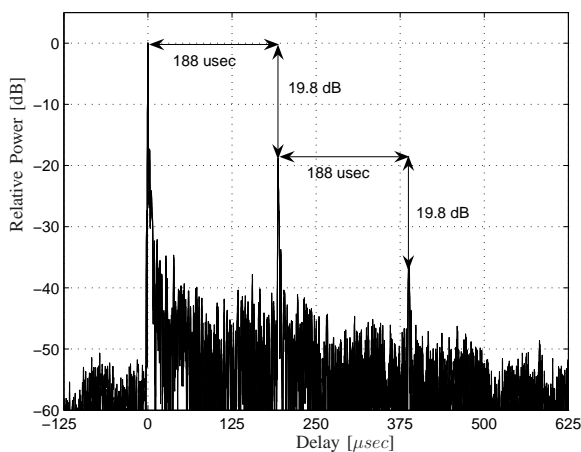


Fig. 12. Channel Impulse Response

shown in Table IV. Again, taking profit of the noise scenario frequency selectivity, the spreading in frequency outperforms the spreading in time. In some situations, by means of power and bit-loading techniques, the achieved performance (465 kbps with $8 \cdot 10^{-8}$ BER) may be desired to be converted into a less demanding figure (less bit rate and/or higher BER) by reducing the average power and transmitted PSD. Moreover, it is also possible that for some applications a BER of, e.g., $1 \cdot 10^{-3}$, can be enough, so higher bit rates could be achieved using the same transmitted power.

VI. CONCLUSION AND FUTURE WORK

In this work, a first step towards a new wideband physical layer on HV lines has been presented. The needed channel measurements to carry out a MCM symbol design have been fulfilled, and the performance of the proposed system has been tested in a real scenario.

A properly designed OFDM allows an easy equalization

TABLE IV
SYSTEM PERFORMANCE

| Gross bitrate = 930 kbps | |
|--------------------------|-------------------|
| SCHEME | GROSS BER |
| MC-DS-CDMA | $4 \cdot 10^{-3}$ |
| MC-CDMA | $3 \cdot 10^{-3}$ |
| User bitrate = 465 kbps | |
| SCHEME | USER BER |
| MC-DS-CDMA | $1 \cdot 10^{-7}$ |
| MC-CDMA | $8 \cdot 10^{-8}$ |

and detection while avoiding ISI. OFDM splits the selective signal bandwidth into several flat subchannels, however, an efficiency loss has to be paid due to the cyclic prefix. In order to minimize that loss, a short cyclic prefix is desired, so, if received SNR is low enough, less channel delay spread will have to be considered. In this work, only the first reflected path was needed to be avoided. Moreover, it has been shown that high rates can be achieved by increasing bandwidth instead of signal power. This low-PSD minimizes undesired emissions and signal coupling into other systems or other MV-PLC links. The spectral granularity delivered by MCM can be also exploited in terms of spectral notching, that is a desirable characteristic in PLC modulations when trying to completely avoid the emission in certain frequencies.

Regarding channel time domain behavior, it has been found that channel transfer function and access impedance can be considered constant, revealing neither short time nor long time variations. This friendly behavior in time domain suggests the use of an adaptive modulation for efficient channel capacity exploitation. Thus, without wasting power or increasing BER, a higher link spectral efficiency can be achieved by taking advantage of the OFDM subbands flat fading through adaptation [19]. On the other hand, background noise does vary in time domain (up to 40 dB in certain bands), but its slow variability does not present a serious impairment for an adaptive approach. Moreover, special attention should be given to this particular noise scenario: variable and colored background noise regarding frequency domain selectivity, and asynchronous impulse events regarding both frequency and time domain selectivity; when designing noise aware adaptive schemes.

Although channel diversity is exploited at bit level by means of coding and interleaving, it has been shown that better performance can be obtained by exploiting diversity at chip level when using MC-SS schemes. Specifically, the MC-CDMA scheme is able to take profit of the noise scenario frequency selective behavior (colored spectrum) delivering the best performance of the three tested schemes, i.e., 465 kbps with $8 \cdot 10^{-8}$ of BER with 2.5 W of average power in a 27 km link.

Moreover, measurements have revealed that transmission is possible beyond the licensed HV-PLC band. The next spectrum band is licensed to broadcast systems, but, as it has been

shown, an easily exploitable narrowband interference limited noise region characterizes the spectrum from 500 kHz and on. MCM access methods and CR techniques offer a good possibility to increase HV-PLC channel bandwidth and minimize interferences between HV-PLC neighboring equipment [8].

Future work points to the test of MC-SS signals with PAPR reduction techniques, different detectors, and hybrid MC-SS approaches like orthogonal frequency and code division multiplexing (VSF-OFCDM, MCM with variable spreading in both dimensions) [5], [18]. This kind of hybrid schemes offer a great level of granularity and adaptation capabilities, being able to offer several quality of service levels in one single frame architecture simultaneously.

REFERENCES

- [1] K. Dostert, *Powerline Communications*. Prentice Hall, 2001.
- [2] IEC, "Planning of (single-sideband) power line carrier systems," IEC 60633, 1980.
- [3] —, "Single sideband power-line carrier terminals," IEC 60495, 1993.
- [4] Dimat, "OPD-1 digital power-line carrier terminal," Dimat, Tech. Rep., 2004.
- [5] K. Fazel and S. Kaiser, *Multi-Carrier and Spread Spectrum Systems*. John Wiley & Sons, 2003.
- [6] ABB, "ETL-600 universal digital power line carrier," ABB, Tech. Rep., 2006.
- [7] R. Napolitano, "Communications over HV-MV-LV power lines: Europe standards and regulations overview," in *IEEE International Symposium on Power Line Communications and Its Applications*, Mar. 2006.
- [8] S. Srinivasa and S. A. Jafar, "The throughput potential of cognitive radio a theoretical perspective," *IEEE Communications Magazine*, vol. 45, pp. 75–79, May 2007.
- [9] N. Instruments, "NI-660x specifications," National Instruments, Tech. Rep., 2006.
- [10] —, "NI PXI-5441 specifications, 100 msp/s, 16-bit arbitrary waveform generator with onboard signal processing," National Instruments, Tech. Rep., 2005.
- [11] —, "NI PXI-5142 specifications, 14-bit 100 ms/s digitizer with onboard signal processing," National Instruments, Tech. Rep., 2006.
- [12] Dimat, "UAMHP-1 high voltage coupling unit," Dimat, Tech. Rep., 2006.
- [13] B. Gustavsen, "The Effect of Distribution Transformers on Distribution Line Carrier Signals," *IEEE Transactions on Power Delivery*, vol. 19, pp. 414 – 422, 2004.
- [14] D. V. Sarwate and M. B. Pursley, "Crosscorrelation Properties of Pseudorandom and Related Sequences," *Proceedings of IEEE*, vol. 68, p. 593–619, May 1980.
- [15] P. Hoehner, D. Kaiser, and P. Robertson, "Two-dimensional pilot-symbol-aided channel estimation by wiener filtering," in *Proc. IEEE International Conference on Acoustics, Speech and Signal Processing*, vol. 3, Apr. 1997, pp. 1845 – 1848.
- [16] S. Kondo and L. B. Milstein, "On the use of multicarrier direct sequence spread spectrum systems," in *Proc. IEEE Military Communications Conference*, Oct. 1993.
- [17] A. Chouly, A. Brajal, and S. Jourdan, "Orthogonal multicarrier techniques applied to direct sequence spread spectrum CDMA systems," in *Proc. IEEE Global Telecommunications Conference*, Oct. 1993.
- [18] N. Maeda, Y. Kishiyama, K. Higuchi, H. Atarashi, and M. Sawahashi, "Experimental evaluation of throughput performance in broadband packet wireless access based on VSF-OFCDM and VSF-CDMA," in *Proc. IEEE International Symposium on Personal, Indoor and Mobile Radio Communications*, Sept. 2003.
- [19] S. Taek and A. J. Goldsmith, "Degrees of freedom in adaptive modulation: an unified view," *IEEE Transactions on Communications*, vol. 49, pp. 1561–1571, 2001.
- [20] J. G. Proakis, *Digital communications*, 4th ed. McGraw-Hill, 2000.
- [21] Morelli and Mengalli, "A comparison of pilot-aided channel estimation methods for OFDM systems," in *IEEE Transactions on Signal Processing*, vol. 49, 2001, pp. 3065 – 3073.
- [22] L. Hanzo, S. Ng, T. Keller, and W. Webb, *Quadrature Amplitude Modulation*. John Wiley & Sons, 2003.

9. APPENDIX B. AUTHOR'S PUBLICATION LIST

9.1. CONFERENCE CONTRIBUTIONS

C. Vilella, D. Miralles, J.C. Socoró, J.L. Pijoan, R. Aquilué, "A new sounding system for HF digital communications from Antarctica", in Proc. 2005 International Symposium on Antennas and Propagation (ISAP2005), Seoul, Republic of Korea, 2005

P. Bergadà, C. Vilella, J.L. Pijoan, M. Ribó, J.R. Regué, R. Aquilué, "Sondeador ionosférico para un enlace entre la Base Antártica Juan Carlos I y el Observatorio del Ebro", in Proc. URSI 2005, Gandía, Spain, 2005

R. Aquilué, P. Bergadà, I. Gutiérrez, J.L. Pijoan, "Channel Estimation for Long Distance HF Communications based on OFDM Pilot Symbols", in Proc. IET Ionospheric Radio Systems and Techniques (IRST 2006), London, England, 2006

P. Bergadà, R. Aquilué, I. Gutiérrez, J.L. Pijoan, "Estimación del canal ionosférico entre la Antártida y el Observatorio del Ebro basada en símbolos OFDM", in Proc. URSI 2006, Oviedo, Spain, 2006

I. Gutierrez, J.L. Pijoan, F. Bader, R. Aquilué, "New Channel Interpolation Method for OFDM Systems by Nearest Pilot Padding", in Proc. European Wireless 2006 (EW2006), Athens, Greece, 2006

C. Vilella, P. Bergadà, M. Deumal, J.L. Pijoan, R. Aquilué, "Transceiver Architecture and Digital Down Converter Design for a Long Distance, Low Power HF Ionospheric Link", in Proc. IET Ionospheric Radio Systems and Techniques (IRST 2006), London, England, 2006

R. Aquilué, P. Bergadà, M. Deumal, J.L. Pijoan, "Multicarrier Symbol Design for HF Transmissions from Antarctica Based on Real Channel Measurements", in Proc. IEEE Military Communications Conference (MILCOM2006), Washington, United States, 2006

J.L. Pijoan, C. Vilella, M. Deumal, P. Bergadà, I. Gutiérrez, R. Aquilué, D. Badia, S. Graells, D. Miralles, J.M. Torta, D. Altadill, "Actividades y resultados de Ingeniería La Salle en la Antártida (2003-2006)", in Proc. VII Simposio Español de Estudios Polares, Granada, Spain, 2006

R. Aquilué, M. Deumal, J.L. Pijoan, L. Corbeira, "A Low Complexity Multicarrier Proposal for Medium Rate Demanding Automatic Meter Reading Systems", in Proc. IEEE Symposium on Power Line Communications and its Applications (ISPLC2007), Pisa, Italy, 2007

R. Aquilué, M. Ribó, J.R. Regué, J.L. Pijoan, G. Sánchez, "Urban Underground Medium Voltage Channel Measurements and Characterization", in Proc. IEEE Symposium on Power Line Communications and its Applications (ISPLC2008), Jeju, South Korea, 2008

R. Aquilué, J.L. Pijoan, G. Sánchez, "High Voltage Channel Measurements and Field Test of a Low Power OFDM System", in Proc. IEEE Symposium on Power Line Communications and its Applications (ISPLC2008), Jeju, South Korea, 2008

9.2. JOURNAL CONTRIBUTIONS

R. Aquilué, M. Ribó, J.R. Regué, J.L. Pijoan, G. Sánchez, "Scattering Parameters Based Underground Medium Voltage Power Line Communications Channel Measurements, Characterization and Modeling", accepted for publication in IEEE Transactions on Power Delivery, June 2008

R. Aquilué, I. Gutiérrez, J.L. Pijoan, G. Sánchez, "High Voltage Multicarrier Spread Spectrum Field Test", accepted for publication in IEEE Transactions on Power Delivery, May 2008